MOLECULAR ROTATION AND DYNAMICS IN SUPERFLUID ^{4}He NANODROPLETS

Carlo Callegari

A DISSERTATION
PRESENTED TO THE FACULTY
OF PRINCETON UNIVERSITY
IN CANDIDACY FOR THE DEGREE
OF DOCTOR OF PHILOSOPHY

RECOMMENDED FOR ACCEPTANCE
BY THE DEPARTMENT OF
CHEMISTRY

May 2000

First reprint, with corrections.
This version slightly differs in pagination from the original archived at Princeton University.
Cover artwork by Iris Scheele, 2000.

Abstract

Cavity-enhanced laser radiation, coupled to molecular-beam bolometric detection has been used to study the spectroscopy of acetylenic molecules embedded in helium nanodroplets. The $2\nu_1$ transition (CH stretch overtone) of HCN, DCCH NCCCH, CH_3CCH, CF_3CCH, $(CH_3)_3CCCH$, $(CH_3)_3SiCCH$, has been investigated in the $1.5\,\mu$m spectral region by means of a color center laser coupled to a resonant buildup cavity, which enhances the laser power experienced by the molecules in the beam by up to a factor of 400, thus overcoming the weakness of the (dipole forbidden) transitions. All molecules are observed to rotate freely in the liquid cluster environment, with strongly enhanced moments of inertia, but with negligible matrix induced shifts (less than $1\,\mathrm{cm}^{-1}$). We show that this enhancement is largely accounted for by hydrodynamic effects, which we have modeled and numerically calculated.

While in the gas phase the rotational lines have instrument-limited widths (a few MHz), in the droplets we have observed linewidths ranging from 600 MHz for $(CH_3)_3SiCCH$ to 2.8 GHz for $(CH_3)_3CCCH$. To investigate the nature of the broadening (which was widely believed to be homogeneous), we have performed a series of infrared (IR) saturation experiments on the $2\nu_1$ transition. We have also thoroughly investigated NCCCH by means of microwave (MW) single-resonance experiments (on rotational transitions) and double-resonance (MW-MW and MW-

IR) experiments. The results demonstrate that the spectral features of molecules in He droplets are inhomogeneously broadened, and allow an estimate of the importance of the different broadening contributions. In particular, MW-IR measurements show that the size of the cluster greatly affects the way rotational energy is relaxed. Large clusters seem to follow a "strong collision model" where memory of the initial rotational state is completely lost after each "relaxation" event, while for smaller clusters relaxation rates are probably affected by the lower density of states available for the dissipation of energy.

Acknowledgments

There are simply too many people that should be thanked in this thesis either for their direct contribution to it, or for making my experience in Princeton truly memorable. Many actually deserve credit for both.

Ilse, your desk is a treasure chest filled with candies, stamps, Band-Aid, and whatever can help make life "in the dungeon" more comfortable. More important: it is but a pale reflection of your good heart. Thank you for always having a smile for everybody. Larry and Werner, how many times did I come to you with impossible requests! You have always been skilled enough (and quite patient indeed) to help me out. Many pages in this thesis would be white if it weren't for your talents. Lou, our office and our lab are better places to live in, thanks to you.

Thanks to Prof. Warren Warren, Norm Jarosik, and Jerry Fraser, who in several occasions lent us equipment to perform many of the experiments that are part of this thesis. It is inspiring to know that so many people around are ready to help and trust for the sake of good science—well, I hope it's good. Thanks to Paul who always had a piece of equipment or a word of advice, according to my necessity.

Thanks to all the members of the Scoles group, for being co-workers and friends, and for putting up with my idiosyncrasies. Frank, my first instructor in

the Scoles lab: you always made everything look easy; John, you patiently guided me through the science of helium droplets; James it's been fun having you as a peer in my early "Bigsur" years, as well as discussing on politics, philosophy, flamenco... With the three of you I went through a lot of beautiful science. My deepest thanks. Dave, it was a lot of fun to have you around; this place is missing someone like you. Thanks in particular for entertainment during the infamous KC trip. Thanks to Udo and Peter, for sharing (junk) food during many experiment nights, and for providing good company all the time. Thanks to Matt for movie nights on the small screen, and to Raul for my limited Spanish vocabulary. Thanks to Becky, Burkhard, Dan, Daniele, Frank (the other one), Gianni, Jörg, Joe, Mike, Pete, Sean, Susan, Terri, Ying for being part of my life at Princeton. A special one to Wolfgang, a true gentleman, and a source of encouragement in my early days of cluster science. Iris, thank you for the artwork on the cover of this revised edition; obviously I take responsibility for requesting the subject.

Thanks to all those who made life outside of the lab possible...I mean pleasant. Erik, Rita, Vojtek, you treated me like a long time friend from the moment I met you, and remained good friends ever after. Thank you for that. Alessandra, Gianfranco, Matteo...italian food, long chats at night in front of a bottle of grappa, about the past or the future. The world feels a small place, with friends like you scattered around it. Many thanks to Nino, Valeria and Sara for being my "family away from home" on Christmas Day, and to the many who did the same on "normal" (but not less special) days. Thank you Giacinto and Giok-Lam for occasionally rescuing a "ghost". Thanks to Peter, Surita and all their crowd for many late nights in good company.

Tony, sharing the house with you has been quite an experience. Thank you for all the insight that—knowingly or not—you gave me on life as well as science.

Many thanks, Denise, for doing the same over a phone line, and of course for your close friendship. Emily, you introduced me to so many new and exciting things. Your friendship is the deepest experience of my Princeton years. Thank you for enriching my spirit.

Thanks to Prof. Zoltan Soos, who took the time to read my thesis (and on such a short notice!). Thanks to Karen, who helped keeping it on schedule.

Thanks to the many who collaborated "from the outside". Franco Dalfovo, who hosted me in Trento while teaching me about Density Functional calculations. My thesis owes you a lot. The UNC group: Lukas, Martin, Andy and Dave for relaxed atmosphere and countless cups of coffee. Klaas, it was a pleasure to run experiments with you; keep up the good work. Prof. Roger Miller, whose hospitality made the double resonance experiment possible. Thank you for believing we could do it.

Those who made it possible: Irene, for days (and often nights) spent putting the machine together for the next experiment, and for her patience at taking care of the details that I would have overlooked. Hemant, co-worker, friend, and computer guru. Thank you for giving so much in all three fields; my Princeton experience would not have been as good without you around. My brother Andrea, who ultimately has the responsability for having dragged me to Princeton (and many more), who shared, helped, supported, and taught, in and out of the lab. *Grazie*. André, laser wizard and comrade of many relaxed moments. Thank you for your (indispensable, need to say?) help and for trying so hard to improve my skills on food, wine, bicycle repair...

Giacinto, Kevin. Nothing of this would have happened without you, who tried your best, and far beyond, to make me a good scientist. Thank you for your enthusiasm and availability.

And thanks to my family, whose constant support gave me the strength never to give up in bad times, and whose love made good times much more joyful. This thesis is dedicated to you all.

Contents

List of Tables

List of Figures

"Ma voi," gridai quasi in un impeto di ribellione, "perché non prendete posizione, perché non mi dite dove sta la verità?"

Guglielmo stette alquanto in silenzio, sollevando verso la luce la lente alla quale stava lavorando. Poi la abbassò sul tavolo e mi mostrò, attraverso la lente, un ferro da lavoro:

"Guarda," mi disse, "cosa vedi?"

"Il ferro, un poco più grande,"

"Ecco, il massimo che si può fare è guardare meglio."

Umberto Eco, Il nome della rosa

When you collect marine animals there are certain flat worms so delicate that they are almost impossible to capture whole, for they break and tatter under the touch. You must let them ooze and crawl of their own will onto a knife blade and then lift them gently into your bottle of sea water. And perhaps that might be the way to write this book—to open the page and to let the stories crawl in by themselves.

John Steinbeck, Cannery Row

Chapter 1

Introduction

1.1 Historical background

When dealing with the condensed phases of light, weakly interacting particles (rare gas atoms, H_2, D_2), one usually refers to de Boer's quantum parameter λ, defined as $\lambda = \hbar/(\sigma\sqrt{m\epsilon})$, where m is the mass of the particle, and σ, ϵ the length and energy scale of its binary interaction potential. By loosely interpreting $\hbar/\sqrt{m\epsilon}$ as a de Broglie wavelength and σ as the interparticle separation we can see that when $\lambda \to 1$, we can expect the quantum nature of the particles to become relevant. As one of the consequences, the particles may be delocalized, even at zero temperature. Among atoms and molecules, the largest values of λ pertain to the two stable isotopes of helium: ^{3}He (0.491) and ^{4}He (0.427) [1], and are high enough that liquid helium (unlike any other substance) will not solidify, under standard pressure conditions, even at 0 K.

Since ^{3}He is a fermion and ^{4}He a boson, it should not be a surprise that their condensates exhibit different properties. In particular ^{4}He exhibits the property of superfluidity at temperatures 10^3 times higher than ^{3}He. In what follows we will always be concerned with the superfluid phase of ^{4}He (He II) and will only

refer to its normal phase (He I) and/or to ^{3}He to remark the differences between a superfluid and a very cold normal fluid.

At atmospheric pressure ^{4}He liquifies at 4.215 K and behaves as a normal liquid; it is only upon further cooling that a phase transition occurs and helium becomes superfluid. The early history of superfluidity starts in 1908, when Kammerling-Onnes successfully liquified helium, and consists in the exploration of the several anomalous properties that were later to be rationalized as manifestations of superfluidity. In 1911 an anomalous behavior of the density as a function of temperature was observed, suggesting the existence of a phase transition which was later named "λ transition", after the peculiar shape of the specific-heat curve. The transition temperature (2.18 K) is conventionally known as T_λ (often "λ point").

Discovery of the then mysterious "creeping" of films of superfluid helium dates back to 1922, but it is not until 1938 that superfluidity was finally discovered as the frictionless flow of He II through narrow capillaries. A contradiction arose with the observation that the viscosity of liquid helium, as measured by the damping of rotation of bodies immersed in the liquid, is quite finite.

During the same years, the first theoretical models, whose concepts are still in use today, were devised: London [2] proposed that there was a connection between the "λ transition" and Bose-Einstein condensation of He atoms into the zero momentum state; along the same line of thought, Tisza [3] proposed the two fluid model, which could actually rationalize the "viscosity contradiction". It was thereby assumed that liquid He II is actually composed of two fluids: a "normal fraction" (of density ρ_n) having finite viscosity and entropy, and a "superfluid fraction" (of density ρ_s) having zero viscosity and entropy. Although it is tempting to associate the superfluid fraction with the Bose-Einstein condensate fraction of helium atoms in the zero momentum state, the two values are numerically very

different (except at 0 K and at T_λ [4]). Moreover the distinction between the two components is fictitious, since individual He atoms cannot be tagged as belonging to the normal or to the superfluid fraction.

Landau justified the two fluid model in terms of a weakly interacting gas of excitations in a strongly interacting fluid of bosons. Superfluidity is then a consequence of the peculiar shape of the excitations' dispersion-curve, which forbids creation of excitations below a critical velocity v_c. The viscosity is then due to scattering of thermally populated excitations. With this approach, ρ_n as a function of temperature can actually be calculated from the density of excitations. Experimental confirmation of Landau's prediction was to come much later, in 1959 when the excitations' dispersion-curve of He II was measured by neutron scattering; it was Cohen and Feynman who first pointed out the feasibility of the experiment, against the common misbelief that multiple scattering of neutrons would have washed out the diffraction peak [4].

Introduction of impurities[1] in liquid helium as a probe of its superfluid phase, had been attempted many years before: starting in 1943, positively and negatively charged impurities were generated by irradiation of liquid He with X-rays and radioactive sources [5]; it should be mentioned here that in dense He gas the negative charge carrier is a free electron [6], and the predominant positive carrier a He_2^+ ion [7].

The "golden age" of charged impurities is often considered to start in the late 50s. The main findings were that in liquid He, atoms cluster around a positive ion and form a large ($\approx$12 Å diam) solid structure commonly called a "snowball"; an electron becomes instead confined inside a cavity in the liquid ($\approx$35 Å diam,

[1]The terms "impurity", "dopant", and "foreign species" will be used in this work as synonyms.

commonly called a "bubble" [8]) formed by repulsive exclusion forces. Perhaps the most intriguing outcome of that research stems from the fact that an electron bubble is a simple object whose effective mass is entirely due to hydrodynamic effects; the excellent agreement between experimental measurements and theoretical predictions of the latter quantity, confirms that ideal fluid equations correctly describe the superfluid down to the angstrom scale [9]. The fact is particularly relevant to this thesis because the model presented in Chapter 4 does require the validity of hydrodynamics on the atomic scale, which we infer by quantum mechanical arguments. Excited neutral impurities (He^*, He_2^*, generated e.g., by electron bombardment) have also been studied, and the body of literature is prohibitively large; reviews can be found in Refs. [9–11]. It is relevant to this thesis to point out a study where the rotationally resolved spectrum of He_2^* in He II was observed [12], and yielded the same rotational constants as in the gas phase. No differences, however, were reported between He I and He II [13]; we shall see that for heavier and more strongly interacting molecules, free rotation is unique to the superfluid phase.

We have so far discussed the so called "intrinsic" impurities, a term implying that they are *generated* rather than *injected* in liquid He (electrons are historically included in this class). Injection of "extrinsic" impurities (foreign atoms or molecules) is an experimental challenge: 1.4 ppm of ^{3}He are normally present in liquid ^{4}He; any other atoms or molecules would quickly diffuse through the liquid and freeze solid on the walls of the container. Doping of bulk liquid helium with "extrinsic" impurities is therefore based on a continuous supply of the atom/molecule to be studied. Alkali, and alkali-earth, ions were generated by evaporation from a hot filament and drawn into the liquid by an electric field [14, 15]. Gaseous atoms and molecules have been introduced in superfluid

helium by directing a supersonic beam into the liquid; this method is viable for rare gases [16], light molecules (H_2, D_2, N_2) [17], and, in combination with a standard microwave discharge, for reactive atomic species (such as nitrogen) [16]. A similar procedure has been used for metal atoms, either generated in an oven or laser-sputtered from a surface. It essential in this case that the atoms be ionized to be accelerated into the liquid; neutrals can be obtained by recombination with electrons, inside the liquid. Laser ablation of the target material directly immersed in the liquid (and addition of a second laser to fragment the larger aggregates) allows greater densities of neutral atoms, and it is by this technique that most if not all of the spectroscopic investigations of atoms in He II have been performed [10]. As impressive as the record of investigated species is—covering about 20 elements of the periodic table—it mostly consists of metal atoms. Other than a few metal dimers/trimers, no molecules have ever been investigated. The reason for this is that laser ablation is a rather specific process; in particular, molecules would not survive the intense laser fields involved, without fragmenting.

A valid alternative to dispersing the species of interest in bulk liquid helium is the use of a helium nanodroplet[2] beam, where each droplet is doped with one (or a few) foreign atom(s)/molecule(s). With this approach, the effects of high mobility in liquid helium are counteracted by confining each impurity in an isolated environment where neither aggregation with other impurities, nor condensation onto the walls of the container, can take place. The main technical requisite is the ability to efficiently attach impurities to a droplet in a controlled way; as we

[2]The more generic term *cluster*, originally used in the literature to identify aggregates of 10^2–10^4 He atoms, is being superseded by *nanodroplet* which emphasizes two fundamental features of these objects: their nanometer scale (as opposed to smaller aggregates of a few atoms only or to larger macroscopic drops), and their liquid state (as opposed to other, solid, rare gas clusters).

are going to see soon, this makes the technique suitable for a vast class of species, ranging in size and complexity from simple electrons to large molecules such as amino acids and fullerenes.

Production of He droplets dates back to 1961 [18], as a curiosity, the main investigation focusing on production and use of hydrogen droplets as fuel pellets for nuclear fusion reactions. Collisions of He droplets, both with surfaces [19] and foreign atoms [20, 21], have been thoroughly investigated by Gspann, who also demonstrated production of metastable [22] and negatively charged droplets [23], and first predicted the ^{3}He and ^{4}He droplets internal temperatures (0.15 K and 0.4 K respectively [24]) based on classical evaporation theory. Shortly after, it was demonstrated that it is possible to use spectroscopy to monitor the attachment of an impurity to a rare gas cluster (often referred to as the pickup technique [25–27]), giving rise to the field of spectroscopy of doped helium droplets. It's important to remember that the pickup approach is not limited to materials that are gaseous at room temperature, because a column density of only $\sim 10^{-2}$ Pa cm is necessary. Hence, the technique is well suited for all species that cannot easily sustain a high vapor pressure, such as metal atoms and thermolabile molecules.

In 1992 vibrational spectroscopy on SF_6, performed with line-tunable CO_2 lasers, was used to show that absorption lines are narrow compared to those obtained in conventional matrices [27] and that by pickup of more than one molecule per droplet, molecular complexes can be formed [28]. In a breakthrough experiment carried out in Göttingen, which made use of a continuously-tunable diode laser, rotationally resolved spectra were later obtained [29, 30] demonstrating free rotation (albeit with reduced rotational constants, i.e., increased moments of inertia) of the dopant molecule and allowing the measurement of the droplet's temperature. The latter was found to be 0.37 K, in excellent agreement with the value of

0.4 K computed by Brink and Stringari in 1990 [31]. The superfluid nature of the droplets above a critical size ($\approx$60 atoms) has also been recently elegantly demonstrated through spectroscopy of OCS in ^{4}He, ^{3}He and mixed droplets [32]. As we shall see, there is an intimate connection between superfluidity and the characteristic spectra we observe. In particular, superfluidity is a necessary condition for coherent rotation of the solvated molecule, and superfluid hydrodynamics can be effectively used to quantitatively explain the reduced moments of inertia.

The unique properties of He droplets have been further studied and exploited in several recent experiments, in which the excitation spectrum of the superfluid has been seen [33–35], large metallic clusters have been synthesized [36], and ionization mechanisms have been studied [37]. In particular, it has been recently demonstrated that He droplets have an enormous potential as ultracold matrices for the production of metastable aggregates of atoms (e.g., spin-polarized alkali dimers and trimers [38, 39]) and the self-assembly of metastable molecular superstructures (e.g., linear chains of up to 7 HCN molecules [40], and planar rings of 6 H_2O molecules [41]).

1.2 Current issues

Exploitation of the droplets' unusual cooling and trapping ability is a promising and indeed rapidly growing field. A large part of its success stems from the possibility to apply to doped He droplets most of the methods and concepts of high-resolution spectroscopy. In other words, if the He droplets introduce only small perturbations to the spectrum of the free system (true in most cases, so far, but somewhat depending on the property being measured), the observed spectra can be analyzed with well established techniques, and a large amount of

information on the system (notably, the structure) can be extracted in a rather straightforward way. This is particularly true for rotational and ro-vibrational spectra, the benchmark against which most molecular models (in the gas phase) are tested.

As mastery of the He droplet technique increases, attention has shifted to more complex dopants, such as fullerenes [42,43], molecules of biological interest [44,45] and radicals or ions (see below). As complexity increases, the ability to obtain information on the dopants by "automated" processing of their spectra is progressively impaired. Two factors mainly contribute to "degrading" of ro-vibrational spectra of dopant molecules in He droplets: reduced rotational constants and increased linewidths. Rotational constants decrease, compared to the free molecule values, because of the added inertia of the surrounding medium; notably this effect is more pronounced for larger molecules, which already have small rotational constants, and for which the structural information provided by the spectrum would be more desirable. An increase of linewidth was indeed expected, as a consequence of the reduced lifetime of the molecular states under investigation; however, as the list of sampled molecules grew, an intimate connection between spectral line broadening and the finite size of He droplets became apparent [46]. The initial picture of a He droplet as a perfect thermostat where molecules sit, cold and undisturbed, is now being replaced by that of a confining potential where molecules rattle and tumble, pushing their way through an ideal liquid environment (or, as some view it, through a vacuum with peculiar properties [47]).

In spite of spectral degradation, the great advantage of helium nanodroplet isolation (HENDI) spectroscopy remains the possibility of producing a large flux of cold molecules. In a droplet, even large molecules will cool to $\approx 0.4\,\mathrm{K}$; in contrast, in a supersonic expansion (the technique commonly used to produce

cold free molecules), the same can only be achieved for small molecules at a high dilution level (the latter is needed to avoid condensation of the seeded molecules).

1.3 This work

Helium droplet research in most laboratories is carried out with a "chemical" approach in mind, the ultimate goal being the use of He droplets to stabilize species that would otherwise be too rare, too short-lived, or just impossible to produce. Successful examples include the high-spin alkali metal trimers [39], the HCN [40] and water [41] polymers mentioned above, or even the more exotic alkali–He excimers, which form after laser excitation of an alkali atom residing on the surface of a He droplet [48].

With this in mind, the work done in this thesis has focussed on refining the "diagnostic" capabilities of helium droplet spectroscopy, with obvious ramifications on the dynamics of excited molecules in the superfluid medium. That this is an essential step, should be evident from the following considerations. First, if one wants to know that the droplets have been successfully loaded with the species of interest, and that the experimental parameters are optimized to that purpose, a spectral fingerprint is obviously necessary. Second, if one wants to trigger a chemical reaction by exciting the reactants with radiation, the most suitable transition has to be found. Finally, since a pulse of radiation (or a tailored sequence of pulses) would have to be used, knowledge of the dynamics after excitation is also desirable.

As we said, the presence of the helium does somewhat perturb the spectrum of the species under investigation. A valid strategy is then to learn the effects and mechanisms of the perturbation from "normal" molecules, whose spectrum

in the gas phase is accurately known, and subsequently transfer this knowledge to the more exotic complexes that are created exclusively in He droplets. Ideally, this can be done to such an extent that the absorption spectra of exotic molecules in He droplets can be predicted, prior to observation, from accurate simulations, just as it currently done for most molecules in the gas phase.

In this thesis, the effects of helium droplets on the ro-vibrational spectra of acetylenic molecules (the definition loosely includes HCN) are studied. Specifically, the first overtone of the ≡CH stretch ($2\nu_1$) is investigated. It is shown that the effective rotational constants and line shifts can be quantitatively predicted by calculations that are well within the capabilities of a modern workstation. Further, the dynamics of motion inside the droplet, is studied for one of the molecules of the set (cyanoacetylene) by means of microwave-microwave (purely rotational) and microwave-infrared (≡CH stretch fundamental, ν_1) double-resonance spectroscopy. It is found that line-broadening is predominantly inhomogeneous, and almost certainly originates from the motion of the molecule inside the droplet. It is also shown that exchange between different inhomogeneous classes occurs on the nanosecond time scale, thus making hole-burning impossible with cw sources. Arguably, pulsed sources of radiation operating in the 100 ps range would be optimal to further pursue double-resonance spectroscopy, as well as to trigger chemical reactions, in helium droplets.

This thesis project merges two branches of research that have been independently conducted in our laboratory for more than a decade: helium droplets spectroscopy, and high resolution spectroscopy applied to intramolecular dynamics. Obviously, this project relies on the knowledge accumulated, and the many technological advances made in that lapse of time, by former members of this group. In fact, laser spectroscopy in He droplets was born in this group (David Schutt's the-

sis, 1992) with the first spectra of SF_6. The original schemes of the cluster source and of the dopant pickup cell have been used almost unmodified in the present experimental setup. Also, in Schutt's project, the problem of the perturbation induced by the droplet on the dopant molecule is first attacked. A high level of expertise has subsequently been reached with investigation of the electronic transitions of alkali atoms on the surface of He droplets, both in the frequency (John Higgins, 1998) and time domain (James Reho, 2000). In particular those studies show the versatility of He droplets to produce unusual complexes and study their laser-initiated chemical dynamics. On the other side, a large part of the present thesis is devoted to the investigation of the ≡CH stretch overtone in He droplets. As such, this work is the continuation of work on the same mode, both in isolated molecules (Brooks Pate, 1992) and van der Waals complexes (Erik Kerstel, 1993). Those experiments are indispensable to the present project: not only they contribute to our expertise on intramolecular dynamics, but often they are the sole source of a gas-phase spectrum of the transition being measured in He droplets. Finally, the recording of the spectra of the ≡CH stretch overtone in He droplets with sufficient signal-to-noise ratio would have been simply impossible without the use of a power buildup cavity, which was originally introduced (and perfected) for the study of gas-phase intramolecular vibrational relaxation of overtone stretches (Joan Gambogi, 1995; Andrea Callegari, 1998).

1.4 Outline of the thesis

Chapter 2 contains a detailed description of the experimental apparatus used to perform all of the experiments presented in this thesis, with the exception of one experiment performed in collaboration with the group of Roger E. Miller at the

University of North Carolina, which is the subject of a separate chapter. Furthermore, those modifications of the experimental apparatus which were necessary to perform a specific experiment are presented in the corresponding chapter. In describing the experimental procedures, particular attention is paid to the production of a droplet beam and the optimization of molecule pickup; the concept of beam depletion as a detection method, making use of an optothermal detector (bolometer), is also presented. The problem of small transition strength, exacerbated by line broadening, poses a key challenge, which is met by minimizing mechanical and laser-induced noise on the detector. Also essential is the use of a resonant cavity to increase ($\times$400) the effective laser power interacting with the droplet beam. The latter part of the apparatus is only briefly described, because it pre-existed the current experiment [49] and has not been modified.

Chapter 3 contains the recorded spectra of the $2\nu_1$ transition for the following molecules: hydrogen cyanide (HCN), monodeuteroacetylene (DCCH), cyanoacetylene (NCCCH), propyne (CH_3CCH), trifluoropropyne (CF_3CCH), 3,3-dimethylbutyne [*tert*-butylacetylene $(CH_3)_3CCCH$, hereafter TBA], and trimethylsilylacetylene [$(CH_3)_3SiCCH$, hereafter TMSA]; this more than doubles the number of molecules (the other ones being SF_6, water, ammonia, OCS) for which a rovibrational spectrum was ever measured in liquid He. With one exception, we fit the measured spectra to those of rotors of the appropriate symmetry, and extract the values of several spectroscopic constants (in particular, band shifts and rotational constants). In addition, we have taken saturation measurements for HCN, propyne, and TMSA, from which we deduce the homogeneous linewidth for these molecules. The results presented in this chapter are important because they substantially increase the number of molecules for which HENDI spectra are available, and because we show that the spectra can be analyzed quantitatively by

numerical simulations. In this chapter we also address the question of solvation effects on vibrational energy relaxation, motivated by the extensive knowledge previously acquired in our group for the same set of molecules in the gas phase.

Chapter 4 deals in detail with the contribution of He II to the effective moment of inertia of a molecule rotating inside the droplet, and develops a hydrodynamic model to estimate its value. This is the most significant contribution of this thesis work on two counts. First, while it was already known that the increased moments of inertia of molecules in He droplets must originate from the additional motion of the helium in the vicinity of the molecule, the only models previously proposed were either heuristic [29, 32] or too simplified [46]. The model proposed in this thesis is based on simple equations, firmly supported by basic physical principles. With a manageable computational cost, even for large droplets, it allows one to accurately estimate many important quantities, such as the velocity of the fluid at each point and the amount of kinetic energy and angular momentum carried by the fluid. Second, the model is of general validity, and only requires the previous knowledge of the He–molecule pair potential, which can nowadays be accurately calculated (see Appendix A). For this reason the method is, in principle, applicable to any molecule and has the potential to become a powerful predictive tool. We only applied it to linear molecules because the associated symmetry makes the problem easily tractable, and more suitable for testing. It's barely necessary to mention here that, in the case of gas phase molecules, the combination of rotational spectroscopy and isotopic substitution is a technique of primary importance for structural analysis.

Chapter 5 presents single- and double-resonance (purely rotational) microwave spectroscopy data for NCCCH in He droplets. Because of the role of energy relaxation inside the droplet, in our detection scheme, it was not *a priori* obvious that

these spectra could actually be detected. Indeed, the magnitude of the observed signal sets an upper limit (tens of ns) on the rotational relaxation time. A combination of different experiments was used to bracket this time within the 2–20 ns range. Saturation measurements of the R(4) line clearly demonstrated that, at least for this molecule, the lines are dominated by inhomogeneous broadening. Surprisingly, the double-resonance spectra did not exhibit the narrow (homogeneous) lines that were initially expected. This was explained with rapid (i.e., faster than rotational relaxation) migration within the manifold of states responsible for the inhomogeneous broadening. These measurements have opened the way to the microwave-infrared double resonance experiments reported in Chapter 6, and have shown that purely rotational spectroscopy might become the most valid tool for the investigation of the motion of *light molecules* in He droplets [50].

Chapter 6 presents the results of an experiment performed in collaboration with the group of Roger E. Miller at the University of North Carolina. These MW-IR double-resonance measurements, carried out on NCCCH, nicely complement the MW-MW double resonance data of Chapter 5, in that the use of an infrared laser eliminates the need of sequentially absorbing a large number of low energy MW photons to obtain a measurable signal. Furthermore, the IR laser can be tuned through the entire rotational manifold of the band, thus providing additional information on the rotational relaxation of the molecule. Particularly remarkable is the fact that the population transfer induced by the microwave pump radiation is quickly distributed among all rotational levels, with a pattern that depends on the average size of the droplets. In order to explain the observed patterns, we have to assume that at large droplet sizes a "strong collision" regime holds. That is: the rotational state of the NCCCH molecule is completely randomized in a single "relaxation event". Note that this assumption does not require knowledge

of the actual relaxation mechanism, but by exclusion we can identify the latter as the interaction between the molecule and the surface modes of the droplet (ripplons). Most of the experimental observations presented in this Chapter were unexpected. Indeed, the models we propose are not fully satisfactory at explaining them quantitatively, but they clearly indicate the direction for future treatment.

Bibliography

[1] I. F. Silvera, Rev. Mod. Phys. **52**, 393 (1980), and references therein.

[2] F. London, Phys. Rev. **54**, 947 (1938).

[3] L. Tisza, Nature **141**, 913 (1938).

[4] W. E. Keller, in *Helium-3 and Helium-4, The International Cryogenics Monograph*, edited by K. Mendelssohn and K. D. Timmerhaus (Plenum Press, New York, 1969).

[5] A. N. Gerritsen and J. Koolhaas, Physica **10**, 49 (1943).

[6] J. Levine and T. M. Sanders, Phys. Rev. Lett. **8**, 159 (1962).

[7] A. V. Phelps and S. C. Brown, Phys. Rev. **86**, 102 (1952).

[8] K. R. Atkins, Phys. Rev. **116**, 1339 (1959).

[9] K. W. Schwarz, in *Advances in Chemical Physics*, edited by I. Prigogine and S. A. Rice (John Wiley and Sons, New York, 1975), Vol. 33, pp. 1–49.

[10] B. Tabbert, H. Günther, and G. zu Putlitz, J. Low Temp. Phys. **109**, 653 (1997).

[11] J. P. Toennies and A. F. Vilesov, in *Annual Review of Physical Chemistry*, edited by H. L. Strauss (Annual Reviews, Palo Alto, CA, 1998), Vol. 49, pp. 1–41.

[12] J. W. Keto, F. J. Soley, M. Stockton, and W. A. Fitzsimmons, Phys. Rev. A **10**, 872 (1974).

[13] F. J. Soley and W. A. Fitzsimmons, Phys. Rev. Lett. **32**, 988 (1974).

[14] G. G. Ihas and T. M. Sanders, Jr., Phys. Lett. A **31**, 502 (1970).

[15] W. W. Johnson and W. I. Glaberson, Phys. Rev. Lett. **29**, 214 (1972).

[16] E. B. Gordon, V. V. Khmelenko, A. A. Pelmenev, E. A. Popov, O. F. Pugachev, and A. F. Shestakov, Chem. Phys. **170**, 411 (1993).

[17] E. B. Gordon, A. A. Pelmenev, O. F. Pugachev, and V. V. Khmelenko, JETP Lett. **37**, 283 (1983).

[18] E. W. Becker, R. Klingelhöfer, and P. Lohse, Z. Naturforsch. A **16A**, 1259 (1959).

[19] J. Gspann and G. Krieg, J. Chem. Phys. **61**, 4037 (1974).

[20] J. Gspann and H. Vollmar, Journal de Physique **39**, C6 (1978).

[21] J. Gspann, Z. Phys. B **98**, 405 (1995).

[22] J. Gspann and H. Vollmar, J. Chem. Phys. **73**, 1657 (1980).

[23] J. Gspann, Physica B **169**, 519 (1991).

[24] J. Gspann, in *Physics of electronic and atomic collisions*, edited by S. Datz (North Holland, Amsterdam, 1982), p. 79.

[25] T. E. Gough, M. Mengel, P. A. Rowntree, and G. Scoles, J. Chem. Phys. **83**, 4958 (1985).

[26] A. Scheidemann, J. P. Toennies, and J. A. Northby, Phys. Rev. Lett. **64**, 1899 (1990).

[27] S. Goyal, D. L. Schutt, and G. Scoles, Phys. Rev. Lett. **69**, 933 (1992).

[28] S. Goyal, D. L. Schutt, and G. Scoles, J. Phys. Chem. **97**, 2236 (1993).

[29] M. Hartmann, R. E. Miller, J. P. Toennies, and A. Vilesov, Phys. Rev. Lett. **75**, 1566 (1995).

[30] J. Harms, M. Hartmann, J. P. Toennies, A. F. Vilesov, and B. Sartakov, J. Mol. Spectrosc. **185**, 204 (1997).

[31] D. Brink and S. Stringari, Z. Phys. D **15**, 257 (1990).

[32] S. Grebenev, J. P. Toennies, and A. F. Vilesov, Science **279**, 2083 (1998).

[33] M. Hartmann, Ph.D. thesis, University of Göttingen, Göttingen, Germany, 1997.

[34] M. Hartmann, F. Mielke, J. P. Toennies, A. F. Vilesov, and G. Benedek, Phys. Rev. Lett. **76**, 4560 (1996).

[35] J. Higgins, C. Callegari, J. Reho, F. Stienkemeier, W. E. Ernst, M. Gutowski, and G. Scoles, J. Phys. Chem. A **102**, 4952 (1998).

[36] A. Bartelt, J. D. Close, F. Federmann, N. Quaas, and J. P. Toennies, Phys. Rev. Lett. **77**, 3525 (1996).

[37] T. Ruchti, K. Förde, B. E. Callicoat, H. Ludwigs, and K. C. Janda, J. Chem. Phys. **109**, 10679 (1998).

[38] J. Higgins, C. Callegari, J. Reho, F. Stienkemeier, W. E. Ernst, K. K. Lehmann, M. Gutowski, and G. Scoles, Science **273**, 629 (1996).

[39] J. Higgins, W. E. Ernst, C. Callegari, J. Reho, K. K. Lehmann, M. Gutowski, and G. Scoles, Phys. Rev. Lett. **77**, 4532 (1996).

[40] K. Nauta and R. E. Miller, Science **283**, 1895 (1999).

[41] K. Nauta and R. E. Miller, Science **287**, 293 (2000).

[42] J. D. Close, F. Federmann, K. Hoffmann, and N. Quaas, Chem. Phys. Lett. **276**, 393 (1997).

[43] J. D. Close, F. Federmann, K. Hoffmann, and N. Quaas, J. Low Temp. Phys. **111**, 661 (1998).

[44] F. Huisken, O. Verhahn, A. Y. Ivanov, and S. A. Krasnokutski, J. Chem. Phys. **111**, 2978 (1999).

[45] A. Lindiger, J. P. Toennies, and A. F. Vilesov, J. Chem. Phys. **110**, 1429 (1999).

[46] K. K. Lehmann, Mol. Phys. **97**, 645 (1999).

[47] D. Ceperley, Physics World **11**, 19 (1998).

[48] J. Reho, C. Callegari, J. Higgins, W. E. Ernst, K. K. Lehmann, and G. Scoles, Faraday Discuss. Chem. Soc. **108**, 161 (1997).

[49] J. E. Gambogi, M. Becucci, C. J. O'Brien, K. K. Lehmann, and G. Scoles, Ber. Bunsenges. Phys. Chem. **99**, 548 (1995).

[50] A. Conjusteau, C. Callegari, I. Reinhard, K. K. Lehmann, and G. Scoles, J. Chem. Phys. (2000), in press.

Chapter 2

Experimental

2.1 Production: Droplet source

All the experiments have been carried out using a helium droplet spectrometer, which was built by modifying an existing optothermal detection molecular beam spectrometer, previously used to study IVR in isolated molecules [1]. A schematic of the apparatus is presented in figure 2.1.

A beam of ^{4}He nanodroplets is obtained from the free expansion of research grade (99.9999 %) helium gas through a 5 μm nozzle at a backing pressure of 1500 psi (10.2 MPa). The nozzle is attached to the cold stage of a closed-cycle refrigerator (Cryodyne, Mod. 1020 CP), and is temperature-stabilized (better than $\pm$ 0.05 K) by a PID temperature controller (Lake Shore, Mod. 321). The temperature of the nozzle, $T_{\rm n}$, can be set to any value in the range 35–16 K, which leads to droplets with mean size $\bar{N}$ ranging from 750 to 18000 atoms, respectively [2] (See Figure 2.2). A smaller refrigerator (Cryodyne, Mod. 22) is used to precool the He gas, in order to reduce the thermal load on the main refrigerator, and also to condense (before it reaches the nozzle) any impurity that may be present in the gas line. For fixed source conditions, the droplet size distribution is believed to follow

a log-normal distribution with a spread (standard deviation) of $\approx 0.6\,\bar{N}$ [3]. Assuming that the average density of the droplets, $\bar{\rho_0}$, matches the bulk liquid value ($0.0218\,\text{Å}^{-3}$, at saturated vapor pressure and 0.38 K temperature [4]), the droplets have a radius of $0.22\,N^{1/3}$ nm and thus have a cross section of $0.15\,N^{2/3}\,\text{nm}^2$.

2.2 Dopant pickup

The droplet beam is collimated by a 500 μm skimmer, about 1 cm from the nozzle. After collimation, the droplets are seeded with the molecule of interest by passing them through a small (2.5 cm long) gas pickup cell that contains ~ 0.05 Pa of the appropriate gas [5–7]. Pickup will deflect the small droplets from the beam

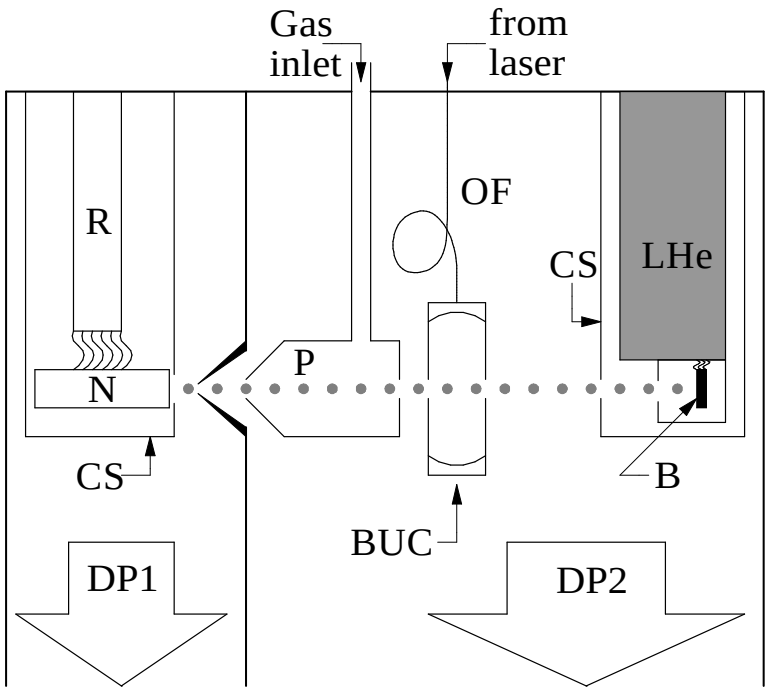

Figure 2.1: Schematic of the experimental apparatus. B: bolometer; BUC: buildup cavity; CS: cold shield; DP1, DP2: diffusion pumps; LHe: liquid helium; N: nozzle; OF: optic fiber; P: pickup cell; R: closed-cycle refrigerator.

axis, but the large droplets will continue with little change in direction (e.g., for pickup of HCN, we estimate an average deflection of $\sim 4/N$ rad). It is worth to remark that, once past the seeding region, the droplets are, effectively, isolated systems. Because of the very low temperature of the nanodroplets, the ro-vibrational spectrum of a typical molecule spans $\sim 1\,\mathrm{cm}^{-1}$; in general then, the spectra of molecular complexes formed in He droplets are shifted enough that they do not overlap with the spectrum of the single molecule. Hence, pickup of more than one molecule per droplet will only decrease the intensity of the single-molecule spectrum, without affecting its shape. For this reason, high purity of the dopant gas is desirable but not essential. Previous work has demonstrated that the number of solutes in each droplet approximately follows a Poisson distribution [8], as expected if each pickup event is statistically independent. Under

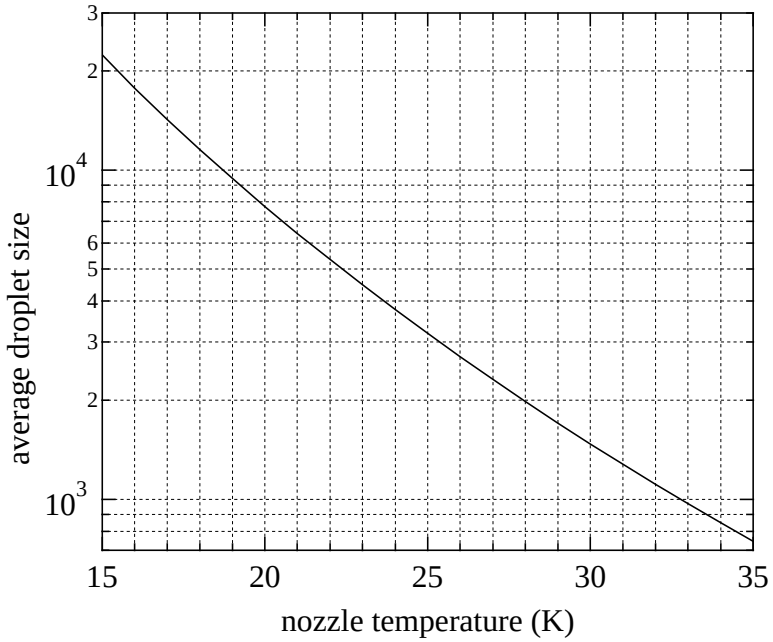

Figure 2.2: Average ^{4}He droplet size, $\bar{N}$, as a function of nozzle temperature, for a 5 μm nozzle and a stagnation pressure of 1500 psi.

this assumption, the single-molecule signal is maximum when the mean number of pickup events is one per droplet, at which value, only a fraction of 1/e (37 %) of the droplets will contain a single solute molecule.

The initial internal energy of the molecules and their translational energy (relative to the droplet), as well as the energy of solvation (the latter is $\sim 300\,\mathrm{K}$ for HCN) are believed to be rapidly dissipated into the droplet and result in evaporation of He atoms (each taking off 5.5–7 K [9]) leading to a microcanonical system cooled to 0.38 K. A rough estimate gives about 200–250 evaporated He atoms due to pickup of one room temperature HCN molecule.

All the compounds used in this experiment were bought at their highest commercially available purity [10], with two exceptions. Hydrogen cyanide (HCN) was obtained from the reaction of potassium cyanide with stearic acid, and cyanoacetylene was synthesized according to the method of Ref. [11]. In both syntheses, the gaseous product of the reaction was collected in a cold trap, and no further purification was performed. The FTIR spectra of both samples were obtained to check that the species of interest was the dominant component.

2.3 Excitation: Laser and buildup cavity

Downstream from the pickup region, the doped droplets orthogonally cross a resonant Fabry-Pérot cavity where they interact with an infrared laser beam. In the wave number region from 6500 to $6570\,\mathrm{cm}^{-1}$ covered in this study, the circulating laser power is enhanced by a factor of about 400 inside the cavity. The laser radiation is provided by a NaOH F-Center laser [12], and is coupled to the buildup cavity via fiber optics. A more detailed description of the cavity setup has been reported previously [13]. The laser is scanned under computer

control, as previously described [1]. For absolute frequency calibration purposes, a reference spectrum is simultaneously recorded in a White-type multipass cell filled with 0.5 Torr acetylene, and is later fit against a standard [14]. A home-built wavemeter is used to get a coarse reading of the laser wavelength in real time. Relative frequency calibration is obtained with a temperature-stabilized scanning confocal étalon (150 MHz free spectral range).

2.4 Detection: Beam depletion and bolometer

Beam depletion detection is accomplished by monitoring the total on-axis flux of helium by means of a liquid-helium-cooled semiconducting bolometer with a detectivity of 7.7×10^5 V/W and a noise equivalent power of $3.5\text{–}4.5 \times 10^{-14}$ W/$\sqrt{\text{Hz}}$, as specified by the manufacturer [15]. The absolute beam flux can be estimated by mechanically chopping the molecular beam: assuming $T_\text{n} = 20$ K and the beam velocity to be $\sqrt{5kT_\text{n}}$ [16], we estimate from the measured signal that $\sim 10^{13}$ He atoms per second are striking the bolometer. A crude estimate based on the gas flux from an ideal supersonic source [16], neglecting beam attenuation effects and assuming unity accommodation coefficient, gives $\sim 10^{15}$ atoms/s impinging on the bolometer.

When the laser is tuned to a vibrational resonance, the molecule/droplet system absorbs radiation, leading to vibrational relaxation inside the droplet, which is followed by the evaporation of ^{4}He atoms (~ 1300/photon at 6500 cm^{-1} if the He atoms evaporate at the temperature of the droplet). These evaporating atoms will carry away little net momentum (the rms value is $\sim 0.05\,\%$ of the droplet momentum, for $N = 5000$), and thus all but the smallest droplets are expected to continue on to reach the detector. In the laboratory frame the evaporating

atoms trace a forward cone of ~ 0.1 rad, and largely miss the detector. The IR spectrum of a solute in He droplets is detected as the depletion of bolometer signal as a function of the laser frequency. To achieve this, the laser is chopped at a frequency of 307 Hz (which corresponds to a minimum of the noise spectral density), and the signal it induces is demodulated with a lock-in amplifier. We observe a significant background signal, due to laser radiation that scatters from the buildup cavity and heats the detector. Since this background is by necessity modulated at the chopping frequency, it is not filtered out by the lock-in. While photons instantly reach the detector, it takes ~ 1 ms for a He droplet to travel from the interaction region to the detector. This corresponds to a phase lag of almost exactly 90°, which can be exploited, by finely adjusting the phase of the lock-in, to eliminate the background signal with only modest loss in the true beam depletion signal. The operating temperature of the detector (~ 1.6 K) is kept below the He superfluid transition (~ 2 K) to eliminate mechanical noise induced by the boiling of helium. Furthermore, a JFET preamplifier [17] has been mounted on the bolometer cold finger to lower the output impedance of the bolometer from $\sim 12\,\mathrm{M}\Omega$ (dynamic) to $500\,\Omega$, thus reducing the microphonic noise induced by the refrigerators.

2.5 Sensitivity

With this apparatus, we obtained a typical signal to noise ratio of $70/\sqrt{\mathrm{Hz}}$ when observing the spectrum of propyne inside helium droplets. For the sake of comparison, roughly the same signal-to-noise ratio can be inferred from visual inspection (assuming comparable acquisition rates) for the fundamental of the ν_3 vibrational band of SF_6, measured in Ref. [18] via mass spectrometric detection. However,

the CH overtone studied in this work has an integrated power absorption cross section ≈ 1300 times smaller than that of the SF_6 ν_3 fundamental [19,20], our lines are ≈ 5 times wider, and the interaction region (i.e., time spent by the molecule in the laser field) is 2000 times shorter than in the apparatus of Ref. [18]. This more than 10^7 fold disadvantage is partly compensated by the fact that the laser power circulating in our cavity is about 250 000 times higher than the laser power used in Ref. [18]. Thus, we can conclude that bolometric detection is ~ 50 times more sensitive than mass spectrometric detection.

Bibliography

[1] E. R. T. Kerstel, K. K. Lehmann, T. F. Mentel, B. H. Pate, and G. Scoles, J. Phys. Chem. **95**, 8282 (1991).

[2] E. L. Knuth, B. Schilling, and J. P. Toennies, in *International Symposium on Rarefied Gas Dynamics (19th: 1994 University of Oxford)*, edited by J. Harvey and G. Lord (Oxford University Press, Oxford, 1995), Vol. 19, pp. 270–276. $\langle \mathrm{N} \rangle$ was calculated according to the scaling law given in this reference; since no explicit dependence of $\langle \mathrm{N} \rangle$ on the scaling parameter Γ is given, the data in Fig. 1 were fit to a line, obtaining: $\ln(\langle \mathrm{N} \rangle) = 2.44 + 2.25 \ln(\Gamma)$.

[3] M. Hartmann, N. Portner, B. Sartakov, J. P. Toennies, and A. F. Vilesov, J. Chem. Phys. **110**, 5109 (1999).

[4] R. J. Donnelly and C. F. Barenghi, J. Phys. Chem. Ref. Data **27**, 1217 (1998).

[5] S. Goyal, D. L. Schutt, and G. Scoles, Phys. Rev. Lett. **69**, 933 (1992).

[6] S. Goyal, D. L. Schutt, and G. Scoles, J. Chem. Phys. **97**, 2236 (1993).

[7] T. E. Gough, M. Mengel, P. A. Rowntree, and G. Scoles, J. Chem. Phys. **83**, 4958 (1985).

[8] M. Lewerenz, B. Schilling, and J. P. Toennies, J. Chem. Phys. **102**, 8191 (1995).

[9] S. A. Chin and E. Krotscheck, Phys. Rev. B **52**, 10405 (1995). The binding energy per atom (E, in K), as a function of droplet size N, is given by: $E = -7.21 + 17.71N^{-1/3} - 5.95N^{-2/3}$.

[10] Propyne was obtained from Lancaster Synthesis, Inc., with a nominal purity of 98%; DCCH from ICON; trifluoropropyne from PCR, Inc.; *tert*-butylacetylene and trimethylsilylacetylene from Aldrich Chemical Company, Inc.

[11] F. A. Miller and D. H. Lemmon, Spectrochim. Acta, Part A **23**, 1415 (1967).

[12] Burleigh FCL-130, Burleigh Instruments Inc.

[13] J. E. Gambogi, M. Becucci, C. J. O'Brien, K. K. Lehmann, and G. Scoles, Ber. Bunsenges. Phys. Chem. **99**, 548 (1995).

[14] G. Guelachvili and K. N. Rao, *Handbook of infrared standards* (Academic Press, Boston, 1993), Vol. II.

[15] Silicon bolometer, composite type, Infrared Laboratories, Tucson, AZ.

[16] D. R. Miller, in *Atomic and Molecular Beam Methods*, edited by G. Scoles (Oxford University Press, New York, 1988), Vol. 1, Chap. 2, pp. 14–53.

[17] LN-6C cold module, Infrared Laboratories, Tucson, AZ.

[18] M. Hartmann, R. E. Miller, J. P. Toennies, and A. Vilesov, Phys. Rev. Lett. **75**, 1566 (1995).

[19] C. Chapados and G. Birnbaum, J. Mol. Spectrosc. **132**, 323 (1988).

[20] A. M. Smith, S. L. Coy, W. Klemperer, and K. K. Lehmann, J. Mol. Spectr. **134**, 134 (1989).

Chapter 3

Overtone spectroscopy of the ≡CH chromophore in He droplets

3.1 Introduction

In Helium Nanodroplet Isolation (HENDI) Spectroscopy [1, 2], a beam of helium nanodroplets, seeded with one or more guest molecules, is interrogated by laser spectroscopy using beam depletion or fluorescence detection. This technique combines many of the advantages of conventional cryogenic matrix isolation spectroscopy (i.e., the stabilization of unstable species) with those of molecular beam spectroscopy (i.e., the absolute isolation of the molecule under study). Using this new method it is now possible to study novel chemical species [3–5], and to elucidate the properties of liquid helium [6] and its interactions with atomic and molecular impurities [7–10].

While the absolute isolation achieved in a molecular beam is desirable because very detailed static and dynamic information can so be obtained via high resolution spectroscopy, molecules in the condensed phase are of course a chemically more interesting system. Disorder, hindered mobility, and strong interactions, all contribute however to degrade the spectral resolution, thus limiting the amount

of information that can be obtained spectroscopically from condensed systems. In this respect, the study of intramolecular dynamics, which is an important theme of modern chemical physics research is no exception. While many important details of the nature of intramolecular dynamical processes in the gas phase are becoming established [11, 12], far less is known about what happens in the condensed phase. In particular there is interest in establishing how the dynamics of the isolated molecule is modified when symmetry, angular momentum, and energy constraints can be lifted by the (perhaps weak) interaction with a solvent. Since superfluid helium is a highly uniform, weakly interacting medium, its potential in this respect is quite clear.

A recent investigation of the ν_3 fundamental vibration of SF_6-doped droplets has shown the possibility of obtaining rotationally resolved spectra, and of measuring the temperature of the system, which turns out to be 0.38 K [13, 14]. In the same experiment, it was observed that the spectral lines could be adequately described by Lorentzian line shapes, confirming the initial assumptions that the solvation effects would be dominated by homogeneous broadening mechanisms. On the other hand, the recent observation of pure rotational transitions in the microwave spectrum of cyanoacetylene embedded in helium droplets [15] and a very recent microwave-infrared double-resonance experiment on the same system [16] have shown unambiguously that the line profiles, at least for that molecule, are dominated by inhomogeneous broadening mechanisms, which are likely to arise from the motion of the impurity inside the droplet [17].

For gas phase molecules, two factors are most important in determining the intramolecular dynamics after vibrational excitation: the density of low-order resonances through which vibrational energy can be dissipated to the "bath" states, and their coupling to the initially prepared state (the "bright" state). The pres-

ence of the liquid helium environment has two consequences: first, it provides a bath with a very high density of states, whose coupling to molecular vibrations is however unknown (one can speculate that the coupling should be weak for high frequency modes, and grow stronger for the low frequency ones). The second consequence is that liquid helium may change the coupling between the internal states of the molecule, particularly in the case of weakly bound complexes. The group of R. E. Miller at the University of North Carolina (hereafter, the UNC group) has recently published the first results in this exciting new frontier, in which they studied the solvent-mediated vibrational relaxation of the HCN dimer molecule [18]. This is the first experiment where two different chromophores within the same liquid-helium-solvated molecule (the "free" and "hydrogen bonded" CH stretches) have been observed. The "internal" CH stretch turns out to relax 40 times faster than in the gas phase, and its vibrational frequency is red shifted, with respect to the gas phase, by $4\,\mathrm{cm}^{-1}$, that is, an order of magnitude larger than the shift of the "external" CH stretch ($0.25\,\mathrm{cm}^{-1}$). The UNC group rationalizes this observation by suggesting two main mechanisms. In the first, the helium might act as a confining potential, reducing the amplitude of the dimer bending motion, making the dimer more linear and effectively increasing the strength of the hydrogen-bond. In the second, the additional polarizability associated with the liquid helium may give extra stability to the dimer, again increasing the strength of the hydrogen bond by shortening it. A further, important feature of those spectra is that the "free" CH spectrum is clearly asymmetric—a signature of inhomogeneous broadening—while the "internal" CH stretch is well described by a Lorentzian (40 times broader than in the gas phase), which leads to believe that the width of the latter line is lifetime limited.

In this Chapter, we report work done over the past two years [19], in which

we have greatly expanded the number of molecules whose rotationally resolved HENDI spectra have been observed, also studying the effects of the liquid He solvent on intramolecular vibrational relaxation (IVR). In addition to HCN, we have selected a set of substituted acetylene compounds and we have measured the spectrum of their acetylenic CH stretch in the first overtone. This mode is very convenient because it is extremely well localized and its characteristics (force constant, anharmonicity,...) are almost independent of the substituent. In recent times, our laboratory has thoroughly investigated the gas phase dynamics of these and other related molecules; this allows us to base the present study on a firm understanding of the dynamics in absence of the interactions with helium. Given the broad span, in size and complexity, covered by our set of molecules, their first overtone gas phase spectra range from fully resolved (with no IVR) for small molecules, through intermediate (still eigenstate-resolved, but with significant IVR) to statistical (with irreversible IVR) at the large molecule limit [20–28].

The Wilson notation will be used to label vibrational normal modes. Standard symbols will be used for the molecular constants (see, e.g., Ref. [29]); a bar over a symbol will indicate the average of the ground state and vibrationally excited state values.

3.2 Results

3.2.1 HCN

Hydrogen cyanide is the simplest molecule containing the ≡C-H stretching mode chromophore that is common to all the molecules considered in this study. It has a very sparse set of vibrational energy levels in the region of the first overtone,

$2\nu_1$, and thus does not display any IVR in the isolated molecule. For the same reason, solvation in liquid He is not expected to greatly change this picture. Since the maximum energy for elementary excitations ($\sim 20\,\mathrm{K}$ [30]) is much smaller than the vibrational level separation in HCN (the closest known vibrational levels below $2\nu_1$ are [0,3^3,2], [0,3^1,2], and [0,0,3], at distances of 223, 252, and $291\,\mathrm{cm}^{-1}$, respectively [31]), vibrational energy dissipation into the He bath is a high-order process, and as such, strongly suppressed in comparison to the heavier molecules

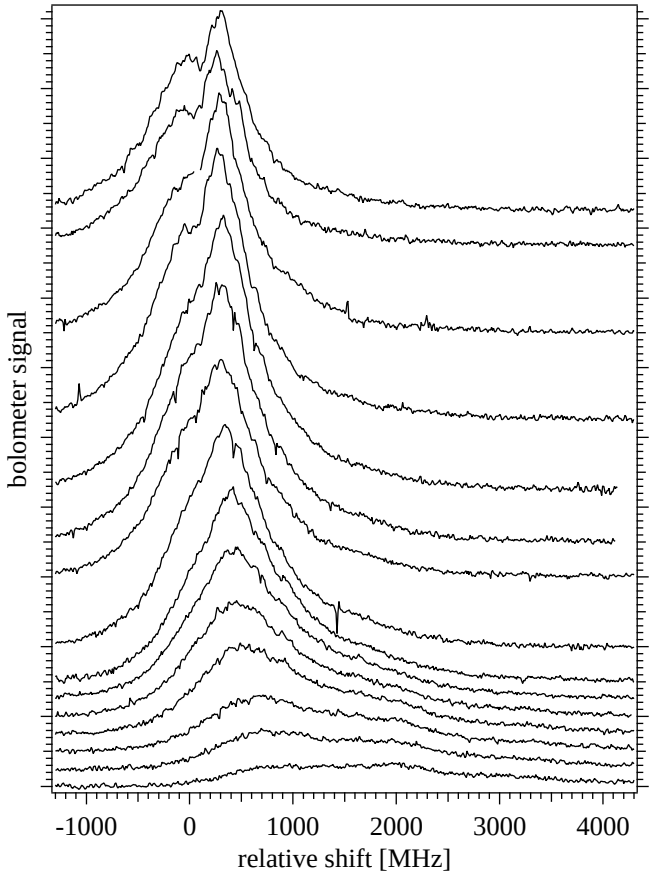

Figure 3.1: R(0) line of HCN at different droplet sizes. The spectra shown have been recorded at nozzle temperatures from 19 K (top trace) to 33 K (bottom trace) at 1 K intervals. The shift is measured from the asymptotic limit: $6521.434\,\mathrm{cm}^{-1}$ (see Fig. 3.3)

discussed later. For this reason we decided *a priori* that HCN would be a good yardstick to measure vibrational relaxation in ^{4}He for our series of molecules.

We scanned the HCN spectrum in the region of the gas phase $2\nu_1$ transition. Only one transition was observed, with a width much less than the expected separation of rotational lines. Figure 3.1 shows this transition as a function of nozzle temperature, which, as discussed above, determines the mean size of the droplets. The integrated intensity of the spectrum as a function of mean droplet size is shown in Figure 3.2. The observed dependence can be only qualitatively justified, since many factors contribute to it:

- as the pressure in the pickup cell is kept constant, the probability of one pickup per droplet decreases rapidly, away from the optimal droplet size.
- small droplets have a smaller chance of surviving the pickup event.
- the average droplet size, $\bar{N}$, grows approximately as $1/T_{\rm n}^4$, while the total He flux only grows as $1/\sqrt{T_{\rm n}}$, hence the number of available He droplets decreases with increasing size.
- the droplet beam kinetic energy, which is ultimately the quantity detected by the bolometer, is linear with $T_{\rm n}$, hence detection efficiency decreases with increasing size.

We have assigned this transition to the R(0) line of the $2\nu_1$ vibrational band. Because of the low temperature of He nanodroplets (0.38 K) it is expected that only the $J = 0$ rotational level will have significant population, unless the effective rotational constant in the droplet is considerably smaller than in the gas phase. The UNC group has observed the ν_1 fundamental of HCN using an apparatus of similar design, which uses a 3 μm F-center laser to excite the droplets [32]. An

important additional feature of their machine is the ability to apply a large static electric field in the region where the molecules interact with the laser. The field can be used to induce transition intensity in the zero-field-forbidden Q(0) line, thus allowing the rotational constant of HCN (in the ν_1 state) to be measured as $1.175\,\mathrm{cm}^{-1}$ (35.225 GHz) [32]. From this rotational constant, neglecting the small change with vibrational excitation, the estimated population of the $J = 1$ level at 0.38 K is 0.04 %, consistent with our failure to detect any ro-vibrational transitions from any but the ground rotational state.

The R(0) transition in Fig. 3.1 is seen to narrow and shift to lower wave number as the average droplet size, $\bar{N}$, is increased. Similar behavior has also been reported for the ν_3 transition of SF_6 [33]. Both experiments [34] and theory [9,35] indicate that rotational constants should not change with droplet size, at least for fully solvated molecules. Thus we can exclude a variation of the rotational constant as the cause of the observed shift.

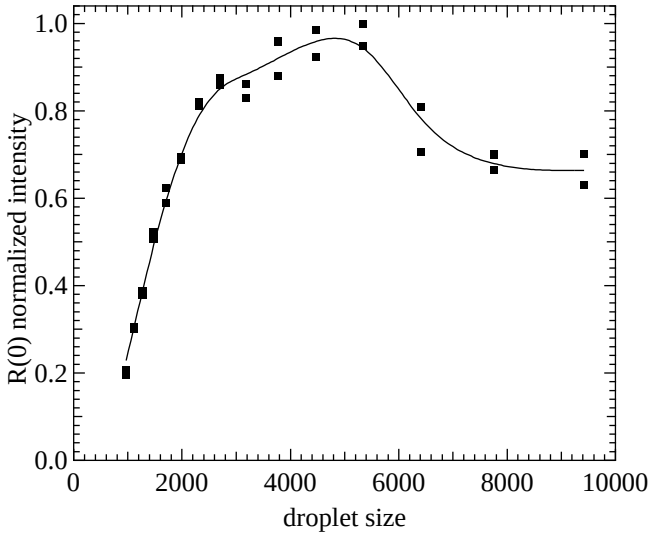

Figure 3.2: Normalized integrated intensity of the R(0) line of HCN as a function of average droplet size, $\bar{N}$.

If ν is the position of the R(0) line, as measured by its center of mass, a simple model based on the energetics of solvation (see Sec. 3.3.1) predicts $\nu(\bar{N}) - \nu(\infty) \propto \bar{N}^{-1}$. Figure 3.3 shows a set of experimental values of $\nu(\bar{N})$, and the best fit to the formula $\nu(\bar{N}) = \nu(\infty) + a/(\bar{N} - \bar{N}_0)$; the quantity $\bar{N}_0$ has been added to the original model of Sec. 3.3.1 as an extra parameter to compensate for our imperfect knowledge of the droplet size as a function of $T_{\rm n}$. The best fit parameters are: $\nu(\infty) = 6521.434 \pm 0.001\,{\rm cm}^{-1}$, $a = 42 \pm 2\,{\rm cm}^{-1}$, $\bar{N}_0 = 350 \pm 30$. $\bar{N}_0$ is just a "first order correction" to the estimated value of $\bar{N}$, but it can also be interpreted as the number of He atoms evaporated from a droplet upon pickup of an HCN molecule. It is interesting to observe that our estimate of the latter quantity (Chapter 2) is very close to the best fit value of $\bar{N}_0$.

Because the transition frequency varies with droplet size, we can anticipate that the spread of droplets sizes produced at any given source condition would lead to an inhomogeneous broadening in the spectrum. Using the log-normal

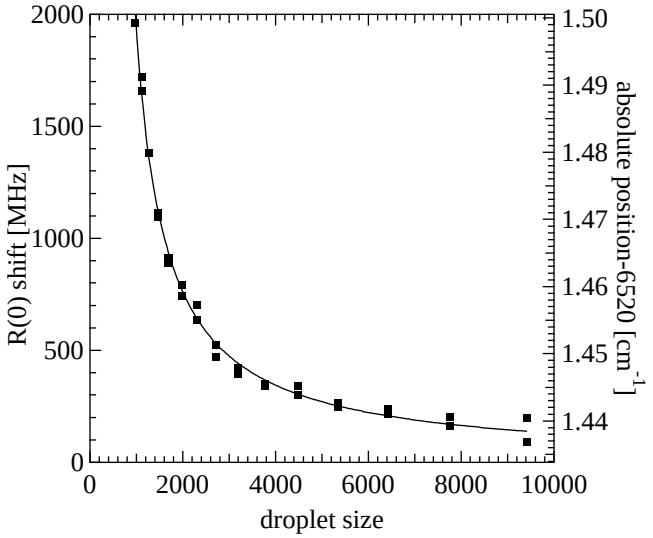

Figure 3.3: Shift of the center of gravity of the HCN R(0) line as a function of average droplet size.

droplet size distribution inferred from previous work [33,36], we can predict what the line shape would be if there were no other sources of line broadening. In Figure 3.4, the observed and predicted line shapes, at $T_{\rm n} = 23\,{\rm K}$ ($\bar{N} = 4500$) are compared. One can see that the droplet-size-induced linewidth is only a fraction of the total linewidth, hence other sources of broadening must be present. Also, the linewidth induced by the droplet-size distribution grows larger at smaller droplet sizes, but so does the total width; as a consequence, the ratio between the two remains approximately constant.

Figure 3.5 shows the R(0) line behavior as a function of the laser power incident on the molecular beam (P). If the line was homogeneously broadened, the available power would be insufficient to saturate the transition, and the signal would be expected to increase linearly with P. Instead a sub-linear power dependence is

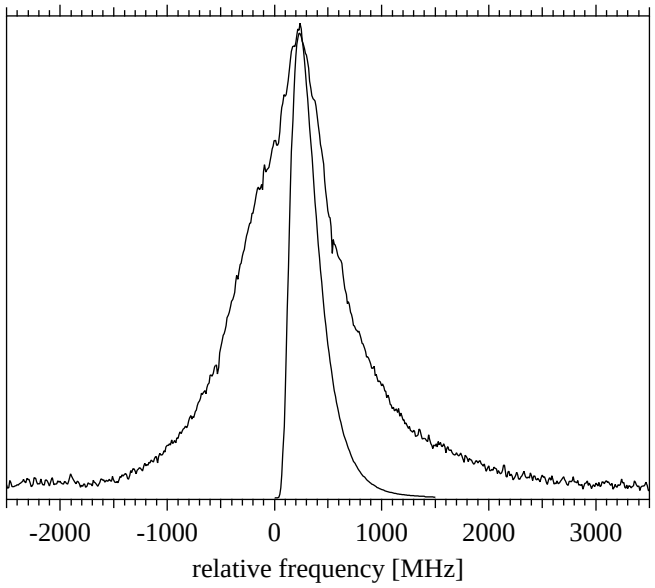

Figure 3.4: Predicted line shape of the HCN R(0) transition, at $\bar{N} = 4500$, assuming the finite droplet-size distribution as the sole source of broadening. Also shown is the observed line shape at the same droplet size.

observed, clearly demonstrating the presence of saturation and of inhomogeneous broadening. Quantitative information can be extracted from the integrated intensity of the R(0) line (I_{R_0}) as a function of P (Figure 3.6, bottom curve). For this purpose we used a simple model for the saturation of an inhomogeneous line (see Section 3.5), which predicts the following functional form:

$$I_{R_0}(P) \propto \frac{P}{\sqrt{1 + P/P_{sat}}} \tag{3.1}$$

The best fit to this functional form gives a saturation power $P_{sat} = 2 \pm 0.7\,\mathrm{W}$, from which (see Section 3.5) a homogeneous linewidth of $17 \pm 6\,\mathrm{MHz}$ can be estimated. The intracavity power inside the buildup cavity was estimated from the power incident onto the cavity, assuming a gain factor of 400. Obvious sources of error which have not been included in this estimate (approximate knowledge of the

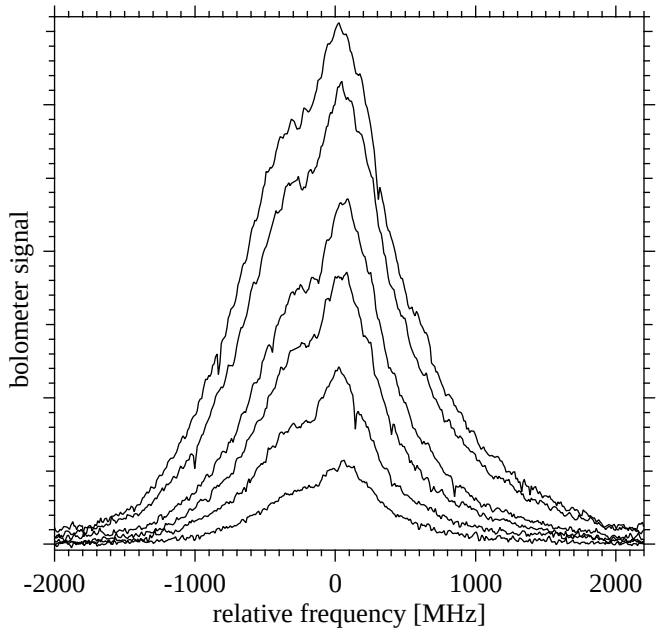

Figure 3.5: Saturation behavior of the HCN R(0) line. The spectra shown have been recorded at $T_n = 23\,\mathrm{K}$. The intracavity laser power is, from bottom to top, 1.5, 3.6, 6.1, 12, 17, 27 W, corresponding to the data points in Fig. 3.6.

gain factor, and of the coupling to the cavity) will result in a correspondingly inaccurate estimate of the saturation power and of the homogeneous linewidth. What is important to observe is that the estimated homogeneous linewidth is narrower than the observed linewidth by more than an order of magnitude.

A moderate increase of the line width, as measured by its second central moment (Figure 3.6, top curve), is observed at high P. If this width increase was due to power broadening of the inhomogeneous line shape, it should become observable, given our estimate of the homogeneous linewidth, at much higher P. One alternative explanation is that the saturation power is not the same for the whole line, but rather increases at the wings. As a consequence, the intensity of the line would grow faster at the wings than at the center.

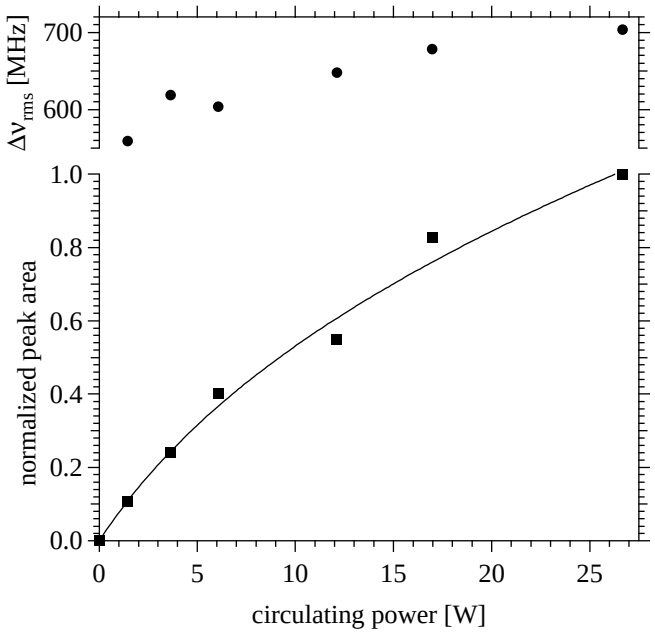

Figure 3.6: Saturation behavior of the HCN R(0) line as a function of intracavity power, P, (see Fig. 3.5). Squares: normalized integrated intensity, and fit to the "inhomogeneous" model of Section 3.5. Circles: square root of the second central moment of the peak.

3.2.2 DCCH

We also attempted to observe the $\nu_1 + \nu_3$ band of HCCH, which in the local mode picture corresponds to two quanta of vibration in one CH bond; despite repeated attempts, no such spectrum could be detected. In order to establish that this was not due to some artifact related to the chemical instability of the molecule, we also investigated DCCH, which has a ≡CH stretching overtone in the same spectral region with an estimated band strength approximately one half that of the $\nu_1 + \nu_3$ band of HCCH. Figure 3.7 shows the spectrum obtained. As in the case of HCN, we observe only a single line, which we interpret to be the R(0) line of the $2\nu_1$ vibrational band. Also using HENDI spectroscopy, the UNC group successfully observed, in the 3 μm region, the R(0) line both for HCCH (ν_3, asymmetric CH stretch), and DCCH (ν_1, CH stretch) [37,38]; the former turns out to be ~ 4 times broader than the latter. Our current hypothesis is that the presence of the $2\nu_1$ state just 54 cm^{-1} below the $\nu_1 + \nu_3$ state, greatly facilitates energy exchange with

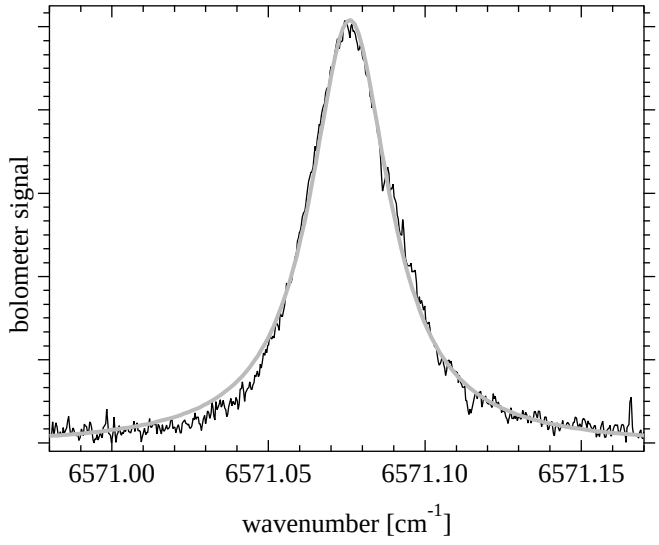

Figure 3.7: Overtone spectrum of DCCH, recorded at $T_\mathrm{n} = 25\,\mathrm{K}$. The thick line is the best fit to a Lorentzian curve.

the droplet, thereby decreasing the lifetime of the transition, and making it too broad to be detected.

It is interesting to observe that HCN and DCCH are quite similar molecules, in size and structure, yet their spectra in He droplets are remarkably different: the R(0) line of HCN is visibly asymmetric and is split into two components. The same line in DCCH can be nicely fit with a Lorentzian shape (centered at $6571.076\,\mathrm{cm}^{-1}$ and with a FWHM of 920 MHz). We believe the difference is due to the polar versus non-polar nature of the two molecules, as suggested by experimental [32] and theoretical [17] investigation of HCN in He droplets.

3.2.3 NCCCH

NCCCH is a linear molecule whose gas phase spectrum in the region of the second overtone ($3\nu_1$) was previously studied in this laboratory [28]. The density of vibrational states ($\approx 31/\mathrm{cm}^{-1}$) placed this spectrum in the intermediate regime of IVR; in the first overtone the density of states is low enough that no IVR is expected. It was therefore possible that in the liquid He environment, where strict intramolecular energy conservation is no longer required, solvent-mediated vibrational energy transfer could lead, already in the first overtone, to an accelerated relaxation of the optically excited state, thus causing additional line broadening.

Figure 3.8 shows the $2\nu_1$ spectrum observed at $T_\mathrm{n} = 26\,\mathrm{K}$, for which $\bar{N} = 2700$ is estimated. As in the case of the ν_3 band of OCS [8], the spectrum clearly displays the rotational structure of a linear molecule, but with considerably reduced rotational constants. Except for overall broader lines, the spectrum has remarkable similarities with that measured for the fundamental (ν_1) transition [16], in particular the pronounced asymmetry of the R(0) and P(1) lines. For this reason,

Table 3.1: Molecular constants from the fit of the NCCCH spectrum displayed in Fig. 3.8. Units are MHz, unless otherwise indicated.

	ν_0 (cm^{-1})	$\bar{B}$	ΔB	$\bar{D}_J$	T (K)
Free	6551.980(2)[a]	4549[b]	-14.14(5)[a]	5.4×10^{-4} [b]	⋯
In ^{4}He	6551.804(1)	1552(2)	-44(1)	4.7(1)	0.391(2)

[a]From Ref. [39]. [b]Ground state value, truncated (from Ref. [40]).

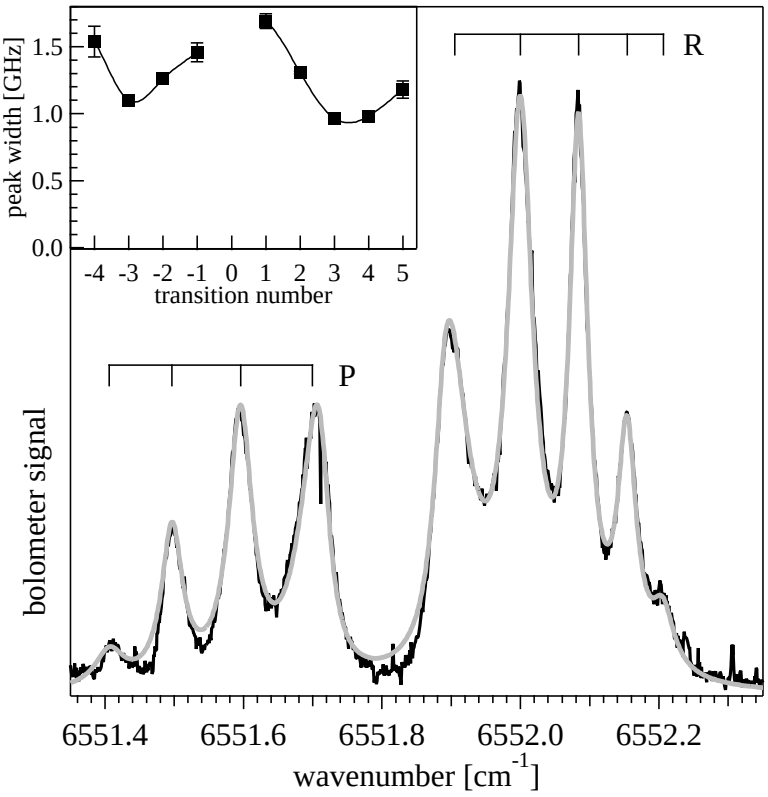

Figure 3.8: NCCCH overtone spectrum, recorded at $T_{\rm n} = 26\,{\rm K}$. The thick line is a fit to a linear rotor, with the parameters of Table 3.1. The inset shows the FWHM linewidths, which are also free parameters of the fit; a spline fit is superimposed as a guide to the eye.

just as in Ref. [16], we fit these two lines with the convolution of a Lorentzian and a half exponential, and use a simple Lorentzian to fit all other features.

The entire spectrum is fit as a whole, with the intensity (integrated area) and position (center of gravity) of each line dictated by a linear rotor Hamiltonian. The free parameters of the fit are the Lorentzian linewidths, the decay constant of the exponential (for the R(0) and P(1) lines only), the rotational temperature, and the parameters of the Hamiltonian up to third order. Table 3.1 gives the spectroscopic constants determined by the least squares fit, along with the statistical uncertainties ($1\,\sigma$) of the parameters. For all the fits performed in this work, long term fluctuations of dopant pressure are not accounted for, when estimating the accuracy of the measured signal. As a result, the uncertainties on the fitting parameters, particularly the droplet temperature, are most likely underestimated. The full width at half maximum of each line as a function of the transition number, m, is plotted in the inset of Fig. 3.8. The estimated temperature (0.39 K) is in agreement with prior observations. One interesting feature of the spectrum is that the linewidth of the rotational lines decreases with increasing rotational quanta, is minimum at $|m| = 3$, and then increases again. The same has been observed for the ν_1 band [16].

Figure 3.9 shows the spectrum of NCCCH recorded for different values of the average droplet size. As in the case of HCN, a moderate broadening at small droplet sizes can be observed.

3.2.4 CH_3CCH

Propyne is the first molecule we studied for which evidence of (limited) IVR was observed in the gas phase spectrum of the first overtone, $2\nu_1$. In that spectrum,

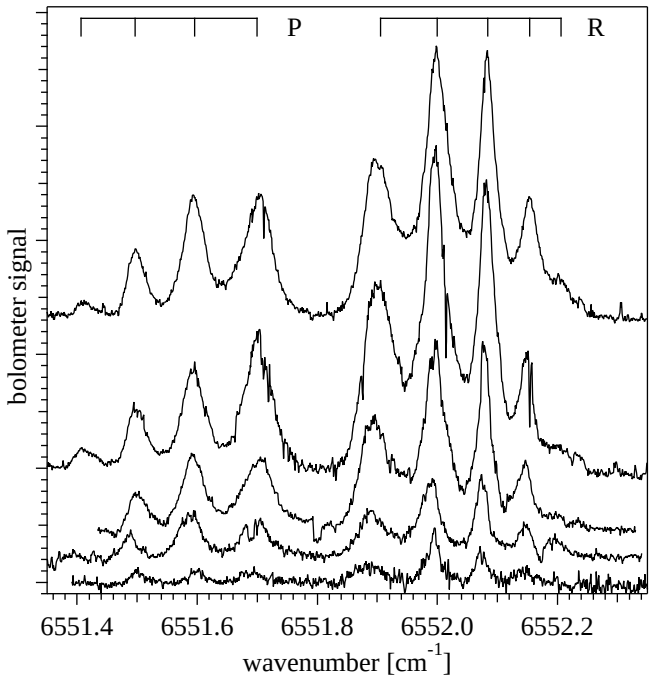

Figure 3.9: NCCCH overtone spectrum, recorded at $T_{\mathrm{n}} = 26\,\mathrm{K}$, 23 K, 21.5 K, 19 K, 17 K (top to bottom).

the $K = 0$ sub-band showed no evidence of IVR, but sub-bands with higher K did [26]. The IVR dynamics of this molecule has been extensively studied, over a wide range of overtone and combination states [23–26]. Because for the gas phase $2\nu_1$ transition, the density of states is high enough that the onset of IVR is observed, one could in principle expect solvent-induced effects to be visible in this case.

Figure 3.10 shows the measured spectrum, acquired at $T_{\mathrm{n}} = 24.5\,\mathrm{K}$. The spectrum clearly displays a Q branch in addition to the P, and R branches. While the A rotational constant of propyne is sufficiently large that one would expect no thermal population in the $K \neq 0$ levels (and thus no Q branch), quantum symmetry effects have to be taken into account. The C_{3v} symmetry of the molecule, in connection with the symmetry of the nuclear wave function, insures that two

symmetry modifications (A and E) of the rotational wave function are present, associated to $K = 0, 3, 6, \ldots$, and $K = 1, 2, 4, 5, \ldots$, respectively. For an isolated molecule, only very weak spin–rotation coupling of different rotational levels can induce relaxation between the two modifications, and this can be expected to take far longer than the few hundred microseconds elapsing between the pickup and optical interrogation in our experiments. For example, a timescale of several hours has been measured for nuclear spin relaxation of methane in an argon matrix [41]. Hence at 0.38 K both the $K = 0$ and $K = 1$ states, and only these two, will be populated. Similar "conservation of nuclear spin species" has been observed in the spectrum of SF_6 in He droplets [13].

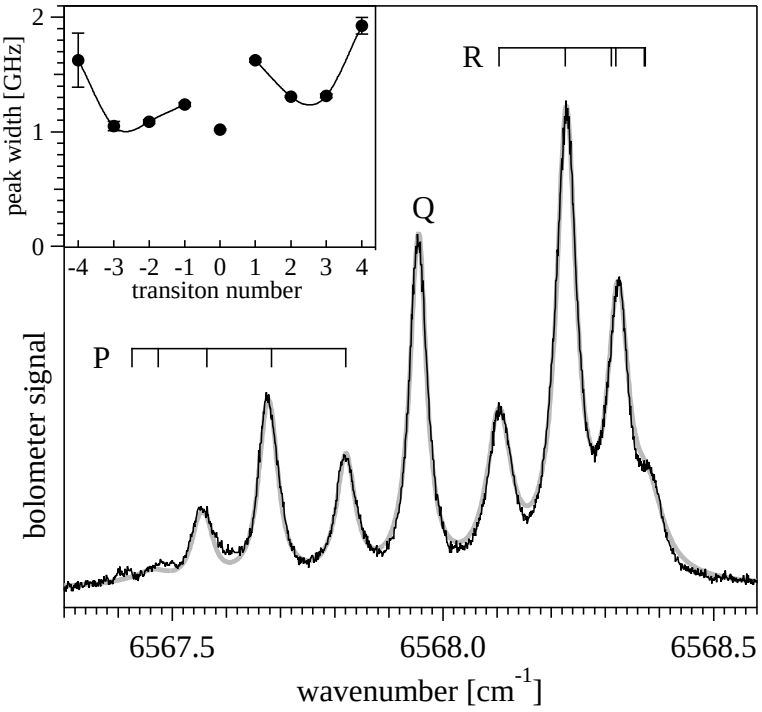

Figure 3.10: Propyne overtone spectrum, recorded at $T_n = 24.5$ K. The thick line is a fit to a symmetric top, with the parameters of Table 3.2. The inset shows the FWHM linewidths, which are also free parameters of the fit.

Due to the rather large rotational constants and slightly narrower lines, this molecule gives the best resolved rotational spectrum. The rotational lines are in this case quite symmetric, and are best fitted by Lorentzian shapes. As we did for NCCCH, we fit the entire spectrum as a whole, this time using a symmetric-top Hamiltonian. Although there is no *a priori* reason to assume that the same symmetry should be used as that of the gas phase molecule, this has, so far, proven to be correct for almost all the molecules studied (for an exception, see Ref. [42]). This is another consequence of the weakness of the perturbation induced by the liquid He environment.

In order to perform the fit, it is necessary to assume a partition of populations between the A and E modifications. In the limit of long nuclear spin relaxation time, the room temperature equilibrium partition should apply. By including the proper degeneracy over nuclear spin and rotational states, one obtains equal populations for the two modifications. Table 3.2 shows the spectroscopic parameters determined from the fit. Note that, even though the K structure in the higher transitions is not resolved, the position of the Q branch (to which only $K = 1$ contributes) relative to the R(0) and P(1) lines (to which only $K = 0$ contributes) dictates the value of $\Delta(A - B)$. The Q branch shows an unresolved set of lines which, in the fit, we constrain to have the same width, independent of J. Given the small value of ΔB and the low number of populated rotational levels, the whole Q branch is only ≈ 150 MHz broader than each of the lines contributing to it. Likewise, $\Delta(A - B) \neq 0$ leads to a splitting, too small to be observed, between the $K = 0$ and $K = 1$ lines in the R and P branch. The global fit is shown in Figure 3.10 as a thick solid line. A droplet temperature of 0.394 K is estimated from it. Note that with these fit parameters the R branch has a bandhead, and as a consequence the R(3) and R(4) lines overlap and cannot be

Table 3.2: Molecular constants from the fit of the propyne spectrum displayed in Fig. 3.10. Units are MHz, unless otherwise indicated.

	ν_0 (cm^{-1})	$\bar{B}$	ΔB	$\bar{D}_J$	$\bar{D}_{JK}$	$\Delta(A-B)$	T (K)
Free	6568.1716(2)[a]	8546[b]	-45.59(8)[a]	0.0029[b]	0.16[b]	569(9)[a]	···
In ^{4}He	6567.965(1)	2151(2)	-78(1)	14.6(1)	-59(4)	-104(6)	0.394(2)

[a]From Ref. [26]. [b]Ground state values, truncated, from Ref. [43].

resolved [also, the R(5) line overlaps with the R(2)]. For this reason the R(3), R(4), R(5) lines have been constrained to share the same linewidth parameter in the fit. The FWHM linewidths are plotted versus the transition number in the inset of Figure 3.10. Note the behavior, somewhat similar to that of NCCCH, and the peculiar narrowness of the Q branch.

Since it is narrower, intense, and only slightly overlapping with the neighboring lines, the Q branch was chosen to test the saturation behavior of propyne. In contrast to the case of HCN, a linear dependence of the IR signal as a function of laser power was found up to an intracavity power of 27 W, indicating negligible saturation over the available range of laser intensity. By comparison with the HCN R(0) line, assuming for simplicity the same transition strength, the homogeneous linewidth of propyne must be at least 30 times broader than that of HCN.

3.2.5 CF_3CCH

Trifluoropropyne is the first molecule in the present study for which extensive IVR was previously observed in the gas phase $2\nu_1$ spectrum [22]. The lowest J transitions were found to consist of very dense "clumps" of lines, and the measured density of states in the R(0) transition was found to be consistent with the total density of vibrational energy levels of A_1 symmetry. Finally, the spacing statistics of the states was of the type expected for a spectrum with chaotic dynamics.

Figure 3.11 shows the spectrum measured in He droplets. Because $A \sim B$, the Q branch is much more intense (relative to the P and R branches) than in the case of propyne. Because of the much smaller rotational constants and increased linewidth, the P and R branches are only partially resolved. Nevertheless, a global fit of the whole spectrum is still possible, as long as the populations of rotational

Table 3.3: Molecular constants from the fit of the trifluoropropyne spectrum displayed in Fig. 3.11. Units are MHz, unless otherwise indicated.

	ν_0 (cm^{-1})	$\bar{B}$	ΔB	$\bar{D}_J$	$\bar{D}_{JK}$	$\bar{A}-\bar{B}$	$\Delta(A-B)$	T (K)
Free	6557.872(5)[a]	2878[b]	-7.75(10)[c]	2.7×10^{-4} [b]	6.3×10^{-3} [b]	2841[b]	8.0(1)[c]	···
In ^{4}He	6557.496(1)	1065(2)	-26(1)	2.38(5)	-7(2)	1945(45)	17(3)	0.393(3)

[a]Extrapolated from Ref. [22]. [b]Ground state values, truncated, from Ref [44]. [c]Twice the ν_1 value, from Ref. [22].

levels are reliably constrained by the molecular parameters. As in the case of propyne, the spectrum has been simulated as that of a symmetric top, using Lorentzian line shapes. Since both H and F atoms have nuclear spin 1/2, the same considerations made for propyne also hold for trifluoropropyne. In this case too, equal populations in the A and E modification have been assumed; unlike the case of propyne, now the value of the rotational constant A is low enough that levels with $K > 1$ are thermally populated. The relative intensity of the Q branch then allows an estimate of the A rotational constant to be made, despite the fact that the position of the transitions does not depend upon this spectroscopic constant.

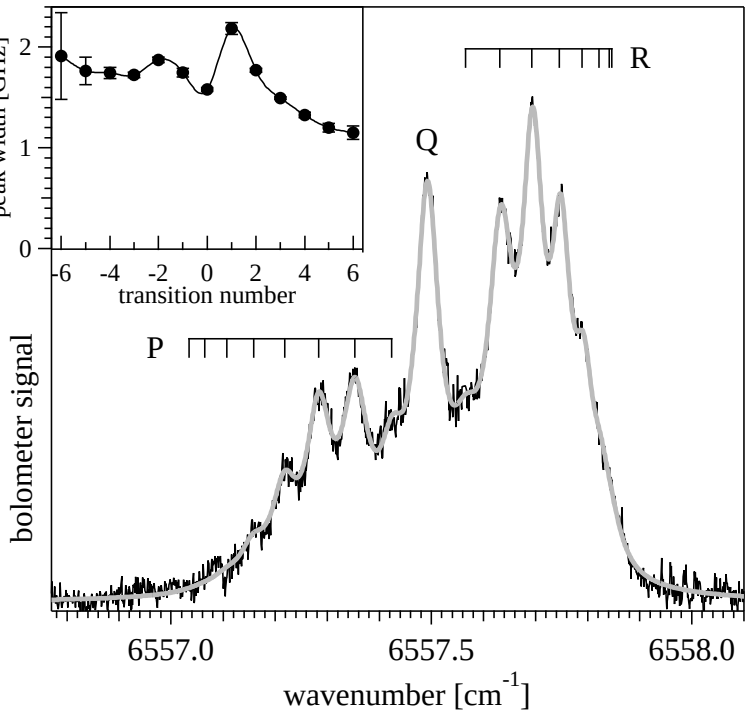

Figure 3.11: Trifluororopyne overtone spectrum, recorded at $T_{\mathrm{n}} = 23\,\mathrm{K}$. The thick line is a fit to a symmetric top, with the parameters of Table 3.3. The inset shows the FWHM linewidths.

The spectroscopic parameters of the fit are given in Table 3.3, and the fit is plotted in Fig. 3.11. The widths of individual lines are plotted versus the transition number, m, in the inset of the figure. In order to obtain an accurate partition of populations, all the levels with J up to 11 and K up to 8 have been included, but unresolved high-J transitions ($|m| \geq 5$) within the same branch are constrained to share the same linewidth parameter. As in the case of propyne, the Q branch is narrower than its immediate neighbors.

Interestingly, the value of the A rotational constant is about 50 % of the gas phase value. So far it was observed that heavy molecules with high non-sphericity undergo a much larger reduction of rotational constants (typically 1/3 of the gas phase value), while light, quasi-spherical molecules undergo little or no change at all. This intermediate case is discussed in Sec. 3.3.3.

3.2.6 $(CH_3)_3SiCCH$ and $(CH_3)_3CCCH$

$(CH_3)_3SiCCH$ (TMSA) and $(CH_3)_3CCCH$ (TBA) have been shown to display "large molecule limit" (i.e., statistical) IVR in the gas phase spectra of both ν_1 and $2\nu_1$. For both molecules, the lines of the $2\nu_1$ band were found to have a Lorentzian shape with homogeneous line widths of 50 and 1400 MHz respectively [21] (with some additional inhomogeneous broadening due to the K structure). It is commonly believed that the total density of states, as opposed to the density of low-order resonances, is the relevant quantitiy in determining IVR rates. The much narrower linewidth for TMSA, despite a 50-fold larger density of states [20], and despite the fact that the two molecules are otherwise extremely similar, convincingly demonstrated the limitation of this assumption.

The $2\nu_1$ spectrum of TMSA is shown in Figure 3.12, along with the best fit

simulation as a symmetric top. Another, less intense spectrum, clearly identifiable as that of a symmetric top (most likely a dimer of TMSA), appears to the red of it. Since the two spectra partly overlap, we chose to fit them simultaneously, but we will describe their fit separately, starting with that of TMSA. As before, nuclear spin symmetry has to be taken into account. Due to the presence of the three equivalent methyl groups, the symmetry group is no longer C_{3v}, but the much more complicated G_{162}. The nuclear spin weights for this class of molecules have been calculated by Lehmann and Pate [45], and will be used here.

Even for this extremely heavy, highly anisotropic molecule, the spectrum

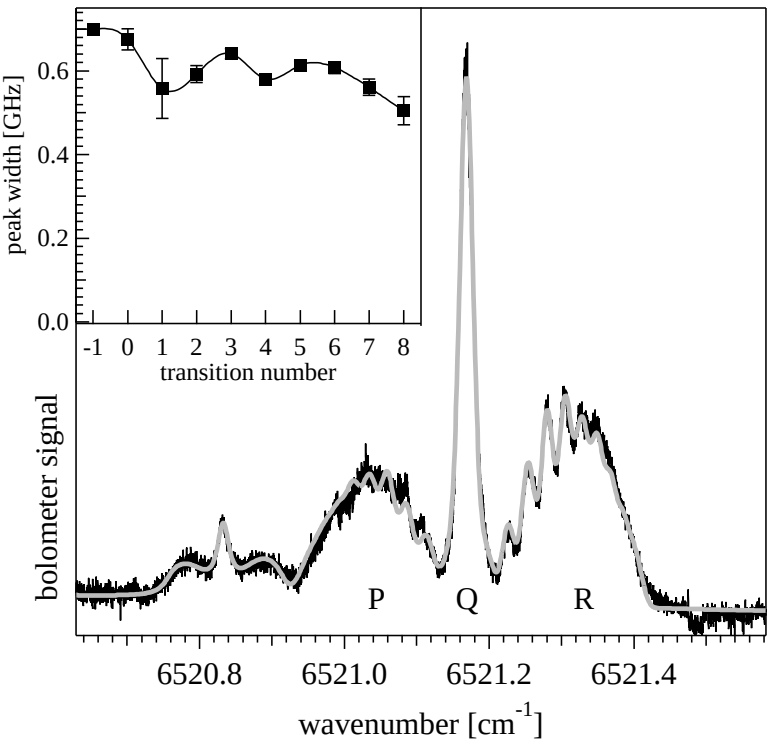

Figure 3.12: Trimethylsilylacetylene overtone spectrum, recorded at $T_{\mathrm{n}} = 23\,\mathrm{K}$. The thick line is a fit to a symmetric top, with the parameters of Table 3.4. The inset shows the FWHM linewidths. The weak spectrum to the red is assigned to a dimer of TMSA (see text and Table 3.5).

clearly shows the remnants of a resolved rotational structure. It was in fact possible to use the widths of the Q and R branch lines as free parameters in the fit. Due to lack of resolution in the P branch, the corresponding line widths had to be constrained to a fixed value. The latter has been arbitrarily set at 700 MHz (FWHM), which best reproduces the barely resolved structure of the P branch. In order to properly evaluate the partition function, all states with J up to 13 and K up to 11 have been included. In order to limit the number of free parameters in the fit, all the high-J transitions of the R branch ($m \geq 8$) share the same linewidth parameter. Quite to our surprise, Lorentzian line shapes gave us a poor fit. Therefore we choose a Voigt profile (Gaussian width 496 ± 15 MHz, Lorentzian width 300 ± 16 MHz) for the Q branch, and Gaussian line shapes for the P and R branches. From this observation we deduce that for this molecule line broadening is predominantly inhomogeneous. As in the case of propyne, the linewidths are approximately constant with J, with the difference that in that case the broadening mechanism was predominantly homogeneous.

Table 3.4 gives the constants determined from the fit. The rotational temperature (0.47 K) is slightly higher than usually observed. Even conceding that we may be somewhat underestimating the uncertainty on the rotational temperature, our data are not consistent with the usual value of 0.38 K.

It is also remarkable that the lines are substantially narrower than even those of HCN and DCCH. Power-dependent measurements of the Q branch of this spectrum, analogous to those shown in Figs. 3.5 and 3.6 clearly demonstrated that we could saturate this transition. The saturation power is estimated to be $\sim 10 \pm 5$ W.

The less intense spectrum to the red of the TMSA spectrum clearly belongs to a highly symmetric, heavy rotor, which is likely a van der Waals complex

Table 3.4: Molecular constants from the fit of the trimethylsilylacetylene spectrum displayed in Fig. 3.12. Units are MHz, unless otherwise indicated.

	ν_0 (cm^{-1})	$\bar{B}$	ΔB	$\bar{D}_J$	$\bar{D}_{JK}$	$\bar{A}-\bar{B}$	$\Delta(A-B)$	T (K)
Free	6520.305[a]	1962[b]	-6.8[a]	2.5×10^{-4} [b]	⋯	1204[c]	$\approx -\Delta B$ [a]	⋯
In ^{4}He	6521.170(1)	431(1)	1.0(2)	0.469(7)	1.1(1)	392(12)	-4.4(6)	0.475(3)

[a]From Ref. [21]. [b]Ground state values, from Ref. [46]. [c]Calculated from A of $(CH_3)_3SiH$ [47].

Table 3.5: Molecular constants from the fit of the assumed $(TMSA)_2$ spectrum displayed in Fig. 3.12. Units are MHz, unless otherwise indicated.

			FWHM	
ν_0 (cm^{-1})	$\bar{B}$	$\bar{A}-\bar{B}$	P,R branches	Q branch
6520.833(1)	85(2)	35(5)	720(10)	615(50)

containing TMSA. In order to fit it, we assume that the complex has the same symmetry and rotational temperature as TMSA itself. While these assumptions are not totally justified, they are reasonable for the amount of information that we want to extract from this spectrum. The parameters of the fit are reported in Table 3.5.

From the measured $\bar{B}$ constant we can roughly estimate the size of this complex: if we assume the same mass as TMSA, its gyration radius is 2.25 larger than that of TMSA, while if we assume a mass twice as large, the gyration radius

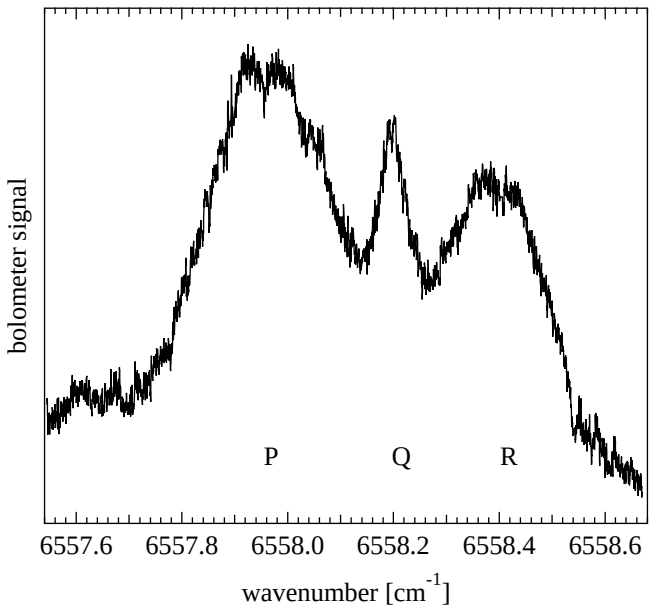

Figure 3.13: *Tert*-butylacetylene overtone spectrum, recorded at $T_n = 22\,K$.

is 1.6 times larger than that of TMSA. If this spectrum was due to a complex between an impurity present in the experimental chamber and TMSA, the most likely candidates would be N_2, O_2 or water, which are very light partners and therefore not consistent with the above estimates. For this reason we tentatively assign the spectrum to a dimer of TMSA.

The $2\nu_1$ spectrum of TBA is shown in Figure 3.13. In this case, no fit is possible, due to lack of rotational resolution and to a rather intense background (evidenced by the sloping baseline and by the unphysical fact that the intensity of the P branch appears to be greater than that of the R branch). The band center, and an estimate of the linewidth can still be extracted; we obtain: $\nu_0 = 6558.196(3)\,\mathrm{cm}^{-1}$; Q-branch width = 2800 MHz (FWHM). We note that unlike TMSA which has the narrowest lines, TBA has the largest line width of all the molecules considered in this study.

3.3 Discussion

3.3.1 Solvation shifts

Table 3.6 lists the solvent-induced shifts of the vibrational band origins. For both HCN and DCCH, we only observe one transition; the vibrational origins can only be calculated if we have estimates of the rotational constant of the molecules in liquid He droplets. The rotational constant of HCN in the ν_1 level (35.225 GHz) has been recently determined by the UNC group, as already mentioned. More recently, we have observed the millimeter wave $J = 0 \rightarrow 1$ transition of HCN in He droplets at 72.14 GHz [34]. From these data, we can produce a first-order formula for the rotational constant as a function of the vibrational quanta, v, in the

Table 3.6: Summary of the spectral features of the ≡CH chromophore

Molecule	ν_0 (cm^{-1}) Free	ν_0 (cm^{-1}) In ^{4}He	Shift (cm^{-1})	FWHM (MHz)
HCN	6519.610[a]	6519.140	-0.470	930 (500[b])
DCCH	6569.410[c]	6569.35[d]	-0.06[d]	920
NCCCH	6551.980	6551.804	-0.176	970
CH_3CCH	6568.172	6567.965	-0.207	1020
CF_3CCH	6557.865	6557.496	-0.369	1580
TBA	6557.025	6558.196	1.171	2800 (1400[e])
TMSA	6520.305	6521.170	0.865	675 (625[e])

[a]Ref. [31]. [b]Estimated width of the narrower of two components. [c]Ref. [48]. [d]Only R(0) observed. See text for the estimate of this value. [e]Gas phase value FWHM subtracted.

ν_1 mode: $B/\mathrm{GHz} = 36.07 - 0.845\,v$, which gives $B_{v=2} = 34.38\,\mathrm{GHz}$. For DCCH, we can also estimate the value of B (more crudely) from the spectrum of the ν_3 fundamental of HCCH, measured in ^{4}He droplets by the UNC group. Because of the symmetry of HCCH, both $J'' = 0$ and $J'' = 1$ remain populated, and so the position of the $J' = 0, 1, 2$ levels in the excited state has been determined. From the $J' = 0, 1$ spacing, the effective rotational constant in the ^{4}He droplet can be estimated (30.08 GHz). From this quantity, the increase in moment of inertia ΔI (relative to the bare molecule) can be estimated. By assuming the same ΔI for DCCH, we can then estimate the rotational constant of DCCH in ^{4}He droplets. As a result of these approximations, the solvent shift for DCCH is estimated with less accuracy than for the other molecules.

For most of the molecules, we see a small shift to a lower wave number. This is

consistent with the shifts observed for other stretching modes of molecules in He droplets. In contrast, the two molecules with tert-butyl groups have positive shifts, which previously had only been observed for bending modes. The solvent-induced shift of vibrational transitions are known to include contributions of opposite sign. The presence of a solvent hinders the vibrational motion, via short-range repulsive forces, and causes a blue shift of the transition. On the other side, vibrational excitation normally increases the long-range, attractive interactions (induction and dispersion) between the molecule and the solvent, and causes a red shift of the transition.

More specifically, the blue shift is caused by the following effect: As the CH stretch is excited, the bond length increases, much faster than the solvent can respond, and the H atom pushes against the repulsive wall of the H–He potential. This increases the effective force constant of the mode, relative to the free molecule, and thus raises the vibrational frequency. This effect is the largest for low frequency bending vibrations, both because they have small force constants and because they involve large displacements against the solvent. One would like to assume that the "blue shift" for the acetylenic CH stretch be approximately constant across the series of molecules studied. Indeed, this mode is very localized, and as such, not greatly affected by the series of very different substituents we span: It is then plausible that the motion of the H atom "into" the He, caused by vibrational excitation, stays the same regardless of the substituent. However the assumption of constant blue shift is only reasonable if also the density of He in the direction of the CH motion is approximately the same for all the substituents; in reality it is known that the van der Waals interaction between the molecule and the helium is strong enough to induce the formation, around the solute, of a highly inhomogeneous solvent shell, whose structure and density change drastically from

molecule to molecule (Chapter 4). Therefore we neither have a quantitative model for the blue shift, nor can assume that it is approximately constant for the series of molecules studied here.

The red shift is easier to model because it depends on long-range interactions, whose functional form is known. Also, information can be extracted from the droplet-size dependence of the shift, for which short-range effects cancel out. Normally, the interaction between the molecule and the solvent atoms is treated as pairwise additive, and only the leading term of the long-range molecule-atom interaction (of the form $-C_6/r^6$) is retained [49]. Further, it is assumed that the molecule is confined near the center of the droplet, which has been predicted to be the case, based on the energetics of solvation [17]. It is then easy to demonstrate that the absolute red shift $\Delta\nu_r$ is given by:

$$\Delta\nu_{\mathrm{r}} = -\Delta C_6 \int \frac{\rho(\mathbf{r})}{r^6} d\mathbf{r} \tag{3.2}$$

where $\rho(\mathbf{r})$ is the density of the droplet and ΔC_6 the change in C_6 upon vibrational excitation. With the asymptotic value of $\Delta\nu_{\mathrm{r}}$ taken as 0, the dependence on droplet size is given by the "excluded volume" model [50]:

$$\Delta\nu_{\mathrm{r}}(N) = \left(\frac{4}{3}\pi\rho_0\right)^2 \frac{\Delta C_6}{N} \tag{3.3}$$

which is minimum (redmost) for $N \to \infty$; this formula is the equivalent of the one introduced in Sec. 3.2.1. We have made the tacit assumption that the first solvation layers around the molecule do not change with droplet size, so that the deviation from the asymptotic value is due solely to the "missing long range interaction" as the amount of He interacting with the molecule is decreased; note that this allows us to replace $\rho(\mathbf{r})$ with its average value for the pure droplet, ρ_0.

We will now analyze the 3 mechanisms that contribute to ΔC_6. Note that usually the permanent dipole moment μ and polarizability α of a molecule increase

upon vibrational excitation, hence all the contributions to ΔC_6 listed below are usually positive. We will also give the numerical results for HCN, and demonstrate that the observed shift must result from partial cancellation of larger red and blue shifts. We take the He–HCN interaction parameters mostly from Atkins and Hutson [51], experimental dipole moments from Smith *et al.* [52], and polarizability derivatives from Dion *et al.* [53]; we calculate $\rho(\mathbf{r})$ for a HCN·He_{1000} droplet by use of a Density Functional method [9]. The three separate contributions are:

1. The dynamic dipole-induced dipole effect discussed by LeRoy [49] gives $\Delta C_6 = \Delta v\, \alpha_{\mathrm{He}}\, 2\mu_{01}^2$, where Δv is the change in vibrational quantum number, α_{He} the static polarizability of He, and μ_{01} the transition dipole moment for the *fundamental* (ν_1) transition. For HCN we obtain an absolute red shift $\Delta\nu_{\mathrm{r}} = 0.14\,\mathrm{cm}^{-1}$, and a droplet-size dependence $\Delta\nu_{\mathrm{r}}(N) = (0.25/N)\,\mathrm{cm}^{-1}$.

2. The change of permanent dipole moment upon vibrational excitation gives $\Delta C_6 = \alpha_{\mathrm{He}}(\mu_{v=2}^2 - \mu_{v=0}^2)$. For HCN we obtain $\Delta\nu_{\mathrm{r}} = 1.67\,\mathrm{cm}^{-1}$, $\Delta\nu_{\mathrm{r}}(N) = (3.04/N)\,\mathrm{cm}^{-1}$.

3. The change in polarizability upon vibrational excitation gives $\Delta C_6 \approx C_6 \Delta\alpha/\alpha$. For HCN, keeping into account the angular dependence of ΔC_6, we obtain $\nu_{\mathrm{r}} = 4.98\,\mathrm{cm}^{-1}$, $\Delta\nu_{\mathrm{r}}(N) = (10.4/N)\,\mathrm{cm}^{-1}$

In total, we have an absolute red shift of $\approx 6.8\,\mathrm{cm}^{-1}$, which is more than ten times larger than the experimental value ($\approx 0.5\,\mathrm{cm}^{-1}$). Since our estimate cannot be off by an order of magnitude, we have to conclude that red and blue shifts are, at least for HCN, of comparable magnitude and nearly cancel out. The droplet-size dependence of the shift sums out to $\approx (14/N)\,\mathrm{cm}^{-1}$, which is a factor of 3 smaller than our experimental value (Sec. 3.2.1). The discrepancy may come from an

incorrect estimate of either the droplet size (which is based on scaling laws) or the value of ΔC_6. In conclusion, one can see that the various contributions to the red shift would be straightforward to calculate, from quantities that can in principle be obtained via accurate *ab initio* calculations. Such calculations are necessary if the cause of the surprising blue shift observed for TMSA and TBA is to be determined; at present too many factors (polarizability, dipole moment, molecular volume, and He density in the nearest solvation shells) are known with insufficient precision.

3.3.2 Spectral broadening and solvent-mediated vibrational relaxation

We chose the molecules studied in this experiment with the goal of studying the effect of the He superfluidity on the intramolecular vibrational relaxation. A few reasonable assumptions can be made: (1) That the observed mode has a strongly local character, virtually independent of the substituent. (2) That direct interaction between the CH stretch and the He does not significantly accelerate the relaxation. (3) That a molecule with well separated modes, such as HCN, would exhibit the narrowest lines, whose width would be an accurate measure of solvent-induced effects. Condition (1) is certainly true for the acetylenic CH stretch, whose spectral parameters (harmonic frequency, anharmonicity) in the gas phase are largely independent of the molecule it belongs to. The intramolecular relaxation rate of the mode, which is the quantity we want to study, does of course depend on the molecule. Condition (2) is supposed to hold because of the large mismatch between the high frequency of the CH stretch and the low frequency of the He modes. Further, the superfluid properties of the droplet preserve rotational

coherence, which suggests that dephasing effects should be minimal for vibrations too. Condition (3) is based on the assumption that for a molecule with well separated modes, which does not exhibit intramolecular relaxation in the gas phase, no further intramolecular relaxation would be induced by the helium, for the same reasons given at point 2.

With the R(0) line of HCN as a yardstick, one would interpret any extra width in the larger molecules as evidence of intramolecular vibrational relaxation. The latter would occur because the presence of the helium increases either the coupling to, or the density of, molecular states into which vibrational energy is relaxed. This analysis, however, is complicated by the fact that the R(0) line of HCN is clearly broadened by inhomogeneous mechanisms, whose effects need to be factored out. Inhomogeneous broadening was originally not expected, because of the superfluid state of the solvent, but several facts demonstrate that it is indeed present, if not dominant: (1) We can saturate the HCN R(0) transition. If the line were homogeneously broadened, the saturation power would be at least 30 times larger than what we measured in Section 3.2.1. The model presented in Section 3.5 lets us estimate an homogeneous width of 17 MHz, compared with a total linewidth of almost 1 GHz. (2) In the large droplet limit, the line is clearly asymmetric and split into at least two transitions. In the fundamental transition, measured by the UNC group [32], the line is narrower by more than a factor of 2 and the two components of the transition are more clearly separated. (3) Inhomogeneous broadening of comparable magnitude has been observed for the purely rotational transitions of NCCCH in He droplets [15].

Lehmann has devised a quantitative model in which the confined motion of HCN inside a finite-size He droplet combines with the thermal spread of translational velocities to produce inhomogeneous broadening of rotational lines [17].

The hydrodynamic part of this model appears to correctly predict the R(0) line shape, and shows that the two peaks arise from the splitting of the triply degenerate $J = 1$ state, as experimentally verified [32], but the line width is a factor of 6.5 narrower than the experimental measurement in the fundamental [32]. Given our estimate of the homogeneous linewidth of the R(0) line in the overtone, most of the linewidth difference between the ν_1 and the $2\nu_1$ transition must be due to increased inhomogeneous broadening. We note that the model of Ref. [17] does not deal with vibrationally excited molecules, but contains quantities (such as the C_6 HCN–He interaction coefficients) which do change upon vibrational excitation. These changes would probably increase the amount of inhomogeneous broadening without modifying its functional form, thus giving a better agreement between theory and experiment.

We will proceed with the hypothesis that inhomogeneous broadening is roughly the same for all the molecules considered here. Also, we assume that the relaxation rate of those molecules which in the gas phase exhibit either no IVR or fast IVR, is not measurably affected by solvation in He. The first case (no IVR) has been justified above; the second (fast IVR) is a restatement of the idea that direct interaction between the CH stretch and the He does not affect the relaxation rate. The IVR rate of molecules in an intermediate condition will instead be affected by solvation in He. For example, in the gas phase, the $2\nu_1$ transition of propyne is barely below the threshold for IVR: solvation in He will increase the density of states (including the low-order resonances, which control the rate of the relaxation) and, as a consequence, the width of the spectral features will increase.

Note that we are implicitly assuming that the *couplings* between the states are *not* greatly affected by the helium, particularly in the case of the (high energy) states participating in low-order resonances. Indeed, if the couplings did increase

significantly upon solvation, we would expect homogeneous lines that are one or more orders of magnitude larger than what we observe here. For sake of comparison, the strongly coupled OH stretch of propynol, has, *already in the fundamental* an IVR lifetime in the gas phase of ≈ 62 ps, i.e., an order of magnitude faster than that of the acetylenic CH stretch in the same molecule [54].

We have taken saturation measurements for one molecule in each class, which allows us to estimate the corresponding homogeneous linewidth: for HCN we get 17 MHz which is close both to our experimental resolution and the to limit one obtains from the *rotational* lifetime of NCCCH in He [15]. For TMSA we obtain 85 MHz, consistent with the 50 MHz measured for the gas phase molecule. Finally, for propyne we get a lower limit of ~ 500 MHz. Even if these data are scarce and of limited accuracy, they are consistent with our initial hypothesis that solvation in He will accelerate the relaxation only for molecules in the intermediate IVR regime.

Table 3.6 shows the observed widths of the transitions. For HCN we list two widths, the observed FWHM of the line and the width of the "narrower" feature, assuming that the line is in fact the sum of two transitions. For NCCCH, we list the narrowest of the observed widths. By extrapolation from the molecules whose homogeneous linewidths we know, it can be seen that in all cases it is reasonable to assume more or less a constant inhomogeneous contribution in the 500–1000 MHz range. Given our present inability to account quantitatively for the inhomogeneous linewidth (even in the simplest case of HCN) any statement about the changes in solvent-induced vibrational relaxation for this series of molecules should be taken with extreme caution. Still, the data are consistent with very modest solvent-induced vibrational relaxation and/or changes in the intramolecular IVR rates, somewhat amplified for molecules on the threshold for

IVR dynamics. Ultimately, we expect that the concepts used to treat IVR in the gas phase will prove to be transferable to vibrational dynamics inside liquid He, without strong modifications.

3.3.3 Rotational constants

In this section we will not follow the practice, standard in ro-vibrational spectroscopy, of directly reporting the values of the molecular constants extracted from the measured spectra. Instead, in Table 3.7, we list the measured moments of inertia. We choose this approach because moments of inertia are additive quantities, hence it is physically meaningful to speak of the contribution of the solvent to the moment of inertia. Centrifugal distortion constants, where available, were reported in previous sections and will be qualitatively discussed here.

Some definitions: I is the moment of inertia of the bare molecule, ΔI its change upon vibrational excitation; I_{eff} and ΔI_{eff} are the corresponding quantities for the molecule solvated in He; $I_{\text{s}} = I_{\text{eff}} - I$ is the moment of inertia associated with the solvent, and $\Delta I_{\text{s}} = \Delta(I_{\text{eff}} - I) = \Delta I_{\text{eff}} - \Delta I$ its change upon vibrational excitation. Unless otherwise indicated, the value of I (and similarly I_{eff}) is the average of the ground and vibrationally excited states values, and has been obtained via the formula: $I \cdot \bar{B} = 505379.05\,\text{MHz} \cdot \text{u}\text{Å}^2$.

It can be readily seen that the solvation in ^{4}He makes the moment of inertia larger than in the gas phase, and that the effect is more pronounced as the molecules get larger and more anisotropic. The same behavior has been observed in the vibrational spectra of other molecules studied in He droplets, and has been discussed in the literature [8, 9, 13, 35, 42]. In simplified terms, the helium in the first solvation shell(s) is behaving (depending on the point of view) either as a

Table 3.7: Moments of inertia and their variation upon vibrational excitation, and/or solvation in He droplets. I is the moment of inertia of the bare molecule, ΔI its change upon vibrational excitation; I_{eff} and ΔI_{eff} are the corresponding quantities for the molecule solvated in He; $I_{\text{s}} = I_{\text{eff}} - I$ is the moment of inertia associated with the solvent, and $\Delta I_{\text{s}} = \Delta(I_{\text{eff}} - I) = \Delta I_{\text{eff}} - \Delta I$ its change upon vibrational excitation. Unless otherwise indicated, the value of I (and similarly I_{eff}) is the average of the ground and vibrationally excited states values, and has been obtained via the formula: $I \cdot \bar{B} = 505379.05\,\text{MHz} \cdot \text{u\AA}^2$. Entries have been arbitrarily truncated. Units are $\text{u\AA}^2$.

Molecule	I	ΔI	I_{eff}	ΔI_{eff}	I_{s}	ΔI_{s}
HCN	11.49	0.166	14.35	0.688	2.86	0.522
DCCH	17.11	0.227	19.56[a]	···	2.45[b]	···
NCCCH	111.10	0.345	325.63	9.232	214.54	8.886
CH_3CCH	59.14	0.315	234.95	8.520	175.81	8.204
CF_3CCH[c]	175.60	0.481	474.53	11.585	298.93	11.104
CF_3CCH[d]	88.37	···	167.90	···	79.53	···
TBA	188.35	0.404	···	···	···	···
TMSA	257.56	0.445	1172.57	-2.721	915.01	-3.166

[a]Calculated as $I + I_{\text{s}}$. [b]Assumed to be the same as for HCCH [37]. [c]Rotation around B axis. [d]Rotation around A axis.

liquid hindering the motion of the solute molecule, or as a solid rotating with it. In both cases it causes an increase of the moment of inertia. It has been established that the very lightest rotors have only a small increase (+ 0–25 %) in moment of inertia upon solvation in ^{4}He, both because they tend to have weakly anisotropic interactions, and because their rotation is very fast (i.e., because the helium cannot adiabatically follow the rotational motion [35]). For heavier (i.e., slower) and more anisotropic molecules, the helium density is believed to adiabatically follow the rotation of the solute molecules, and the increase is substantial (+ 200–300 %). We have recently solved the hydrodynamic equations for superfluid ^{4}He surrounding a rotating solute molecule, from which we obtained a hydrodynamic contribution to the moments of inertia [9]. The agreement with experiment is excellent for all the heavy molecules that could be analyzed (likely within the accuracy limits of density functional theory in estimating the true He density profiles). HCN and DCCH are intermediate between fully decoupled and fully coupled molecule-superfluid motion and for them the hydrodynamic model predicts values of I_s larger than those measured experimentally [9].

Rotation of trifluoropropyne *around its symmetry axis* is an interesting case of mixed behavior, because of the high value of the gas phase A constant (which makes trifluoropropyne a slow rotor), combined with a low anisotropy. The balance of these two facts is reflected in the increase of the corresponding moment of inertia (+ 90 %), which is intermediate between the two classes into which all other molecules fall.

With the exception of TMSA, the value of ΔI_s is, when available, always positive, and larger than the corresponding gas-phase quantity, ΔI. Vibrational excitation causes a slight distortion of the solute molecule (which increases the volume of liquid displaced) and a slight increase of the He–solute interaction (which

results in a higher density of the first solvation layer). Both of these effects cause ΔI_s to increase, the second effect being in all likelihood larger than the first. The small negative ΔI_s observed for TMSA is difficult to rationalize. Notice however, that TMSA, and TBA (for which ΔI_s could not be measured), are the only molecules exhibiting blue shifts upon solvation in He; a blue shift and a negative ΔI_s are both consistent with a decreased molecule–He interaction in the vibrationally excited state. Also notice that this decrease in interaction only needs to occur locally, in a region where the density of the solvation shell is high, such as (likely) the "bay" between the methyl groups and the CC triple bond. As in the case of many other quantities measured in this work, very accurate (but feasible) calculations would be needed to confirm this picture. Finally, the particularly large value of ΔI_s for HCN has to be interpreted as an amplification effect due to the fact that coupling between the He and fast rotor improves as the rotor slows down [9, 34].

The last molecular constant to consider is the centrifugal distortion constant D_J whose value in He is a few MHz for all our molecules. Such a dramatic increase (a factor of $\sim 10^4$) relative to the gas phase value was already observed for OCS and SF_6. In a recent paper on the OCS spectrum, Grebenev *et al.* attempted to estimate this constant, considering the weak binding of He to the OCS molecule, and obtained a result ~ 50 times smaller than the observed value [55]. Notice that even the *sign* of the D_J value is surprising. As discussed above, it is expected that as a molecule rotates faster, the He will have greater difficulty to "follow" the rotational motion; as a result the hydrodynamic inertia will decrease, which expressed in terms of a rotational Hamiltonian corresponds to a negative D_J value! Further, it should be noted that faster rotational motion reduces the solvation energy, as the helium effectively interacts with a "rotationally averaged molecule".

Based upon these considerations, it appears inevitable that the large positive D_J values obtained from the fit will only describe the low rotational quantum number levels of the spectrum; we can anticipate that at some J value, the energy level spacing will begin to increase faster than what predicted by a rigid rotor formula. In particular, this must happen before we get to a J value such that $BJ(J+1)-D_J J^2(J+1)^2 < 0$, otherwise levels with higher J would be energetically favored! Unfortunately, it appears that the low temperature of liquid He droplets results in negligible rotational population for levels where this "uncoupling" of molecular rotation and hydrodynamic motion will occur.

For the low rotational state regime explored by existing experiments, density functional theory will likely provide a new way to estimate the D_J constant: At present, the density profile of the helium solvating a molecule has been found by minimizing the static energy, i.e., by neglecting the energy of hydrodynamic motion [9]. If this correction is added perturbatively to the density functional, we will get a moment of inertia that is slightly dependent on J, i.e., an estimate for D_J. Such calculations are planned for the near future.

3.4 Summary

Rotationally resolved spectra of the acetylenic CH stretch in the first overtone have been measured for the following molecules embedded in a superfluid He droplet: HCN, DCCH, NCCCH, CH_3CCH, CF_3CCH, $(CH_3)_3CCCH$ and $(CH_3)_3SiCCH$. Several spectroscopic parameters have been extracted from the spectra, including the band shift upon solvation, the effective rotational constants, and the homogeneous and inhomogeneous line widths. The latter two quantities have been discussed in the attempt to determine the influence of the superfluid He envi-

ronment on intramolecular vibrational relaxation (IVR). Although more data are needed to draw a definite conclusion, our results seem to indicate that a strong, inhomogeneous broadening is always present, and is in fact approximately constant across our series of molecules. If the homogeneous line width is taken as a measure of the IVR rate, our data seem to indicate that the latter undergoes, upon solvation, modest increases which are larger the larger is the molecule. Finally, we have tried to quantitatively account for most of the observables we measured, and we have shown that in most cases accurate models are available to this purpose. These models are in general computationally demanding (more so for those quantities which result from small variations, or near cancellation, of larger quantities), but well within the current capabilities of molecular modeling; it is our hope that the results presented here stimulate further activity in this direction.

3.5 Saturation model

We describe here the model used to predict the saturation behavior of an inhomogeneously broadened line given our experimental geometry. The model was used to fit the saturation data of the R(0) line of HCN (Sec. 3.2.1) and TMSA (Sec. 3.2.6). Since we want to know the absolute magnitude of the saturation power, we need estimates of the laser power circulating inside the buildup cavity, and of the strength of the transition been observed.

The first estimate is made by measuring the laser power immediately before the interface with the vacuum chamber; this value is then rescaled by our typical coupling losses ($\times 0.65$) and gain inside the cavity ($\times 400$).

For the second estimate we assume:

1. That the vibrational transition intensity of HCN in the droplet is the same

as that measured in the gas phase ($S = 1.4 \times 10^{-19}$ cm) [56].

2. That doped droplets can absorb at most one IR photon during the transit time through the spot of the laser beam ($T_1 = 0.7$ μs).

3. That the inhomogeneous broadening in the spectrum is static on that time scale of transit through the laser spot so that the same subset of molecules is pumped the entire time.

Numerical simulation of inhomogeneous saturation behavior under these assumptions leads to the following relationship between homogeneous width ($\Delta\nu$) and saturation power (P_s):

$$\Delta\nu = \frac{1.7 S P_\mathrm{s}}{\sqrt{2} h\nu \pi^{1.5} v \omega_0}\, c \tag{3.4}$$

where c is the speed of light, $h\nu$ is the energy of the transition, S is the integrated line strength, v the droplet velocity, and ω_0 is the waist (radius) of the laser beam inside the buildup cavity. The saturation power is obtained from a fit of the line intensity $I(P)$ versus circulating power P, according to the equation:

$$I(P) = \frac{aP}{\sqrt{1 + P/P_\mathrm{s}}} \tag{3.5}$$

where a and P_s are the fit parameters. The parameters for the HCN R(0) line are: $h\nu = 6521\,\mathrm{cm}^{-1}$, $P_\mathrm{s} = 2\,\mathrm{W}$ (from fit), $v = 500\,\mathrm{m/s}$ (beam velocity at 23 K), and $\omega_0 = 172\,\mu\mathrm{m}$ [57]. The weakest assumption in this model is likely that the inhomogeneous shifts are static. Our microwave double resonance measurements in NCCCH have indicated that the T_1 time for microwave absorption is $\approx 10\,\mathrm{ns}$ [15]. In our model, if we reduce T_1, we will have to decrease the homogeneous width by the same factor, so the above estimate is likely to be only an upper bound.

Bibliography

[1] S. Goyal, D. L. Schutt, and G. Scoles, Phys. Rev. Lett. **69**, 933 (1992).

[2] F. Stienkemeier, J. Higgins, W. E. Ernst, and G. Scoles, Phys. Rev. Lett. **74**, 3592 (1995).

[3] J. Higgins, C. Callegari, J. Reho, F. Stienkemeier, W. E. Ernst, K. K. Lehmann, M. Gutowski, and G. Scoles, Science **273**, 629 (1996).

[4] K. Nauta and R. E. Miller, Science **283**, 1895 (1999).

[5] K. Nauta and R. E. Miller, Science **287**, 293 (2000).

[6] M. Hartmann, F. Mielke, J. P. Toennies, A. F. Vilesov, and G. Benedek, Phys. Rev. Lett. **76**, 4560 (1996).

[7] J. Reho, C. Callegari, J. Higgins, W. E. Ernst, K. K. Lehmann, and G. Scoles, Faraday Discuss. Chem. Soc. **108**, 161 (1997).

[8] S. Grebenev, J. P. Toennies, and A. F. Vilesov, Science **279**, 2083 (1998).

[9] C. Callegari, A. Conjusteau, I. Reinhard, K. Lehmann, G. Scoles, and F. Dalfovo, Phys. Rev. Lett. **83**, 5058 (1999).

[10] F. Stienkemeier, F. Meier, A. Hagele, H. O. Lutz, E. Schreiber, C. P. Schulz, and I. V. Hertel, Phys. Rev. Lett. **82**, 2320 (1999).

[11] M. Quack and W. Kutzelnigg, Ber. Bunsenges. Phys. Chem. **99**, 231 (1995).

[12] M. Gruebele and R. Bigwood, Int. Rev. Phys. Chem. **17**, 91 (1998).

[13] M. Hartmann, R. E. Miller, J. P. Toennies, and A. Vilesov, Phys. Rev. Lett. **75**, 1566 (1995).

[14] J. Harms, M. Hartmann, J. P. Toennies, A. F. Vilesov, and B. Sartakov, J. Mol. Spectrosc. **185**, 204 (1997).

[15] I. Reinhard, C. Callegari, A. Conjusteau, K. K. Lehmann, and G. Scoles, Phys. Rev. Lett. **82**, 5036 (1999).

[16] C. Callegari, I. Reinhard, K. K. Lehmann, G. Scoles, K. Nauta, and R. E. Miller, J. Chem. Phys., submitted.

[17] K. K. Lehmann, Mol. Phys. **97**, 645 (1999).

[18] K. Nauta and R. E. Miller, J. Chem. Phys. **111**, 3426 (1999).

[19] C. Callegari, I. Reinhard, A. Conjusteau, K. K. Lehmann, and G. Scoles, 53$^{\text{rd}}$ Ohio State University International Symposium on Molecular Spectroscopy, 1998, A. Conjusteau, C. Callegari, I. Reinhard, K. K. Lehmann, and G. Scoles, *ibid*, I. Reinhard, C. Callegari, K. K. Lehmann, and G. Scoles, *ibid*.

[20] K. K. Lehmann, B. H. Pate, and G. Scoles, in *Mode selective chemistry*, Jerusalem Symposium on Quantum Chemistry and Biochemistry, Jerusalem, Israel, edited by J. Jortner, R. D. Levine, and B. Pullman (Kluwer Academic Publishers, Dordrecht; Boston, 1991), Vol. 24, pp. 17–23.

[21] E. R. T. Kerstel, K. K. Lehmann, T. F. Mentel, B. H. Pate, and G. Scoles, J. Phys. Chem. **95**, 8282 (1991).

[22] B. H. Pate, K. K. Lehmann, and G. Scoles, J. Chem. Phys. **95**, 3891 (1991).

[23] J. E. Gambogi, J. H. Timmermans, K. K. Lehmann, and G. Scoles, J. Chem. Phys. **99**, 9314 (1993).

[24] J. E. Gambogi, E. R. T. Kerstel, K. K. Lehmann, and G. Scoles, J. Chem. Phys. **100**, 2612 (1994).

[25] E. R. T. Kerstel, K. K. Lehmann, B. H. Pate, and G. Scoles, J. Chem. Phys. **100**, 2588 (1994).

[26] A. McIlroy, D. Nesbitt, E. R. T. Kerstel, B. H. Pate, K. K. Lehmann, and G. Scoles, J. Chem. Phys. **100**, 2596 (1994).

[27] J. E. Gambogi, M. Becucci, C. J. O'Brien, K. K. Lehmann, and G. Scoles, Ber. Bunsenges. Phys. Chem. **99**, 548 (1995).

[28] J. E. Gambogi, E. R. T. Kerstel, X. M. Yang, K. K. Lehmann, and G. Scoles, J. Mol. Spectrosc. **175**, 198 (1996).

[29] G. Herzberg, *Molecular spectra and molecular structure* (Krieger Publishing Company, Malabar, Florida, 1991), Vol. 2: Infrared and Raman Spectra of Polyatomic Molecules.

[30] E. Manousakis and V. R. Pandharipande, Phys. Rev. B **33**, 150 (1986).

[31] A. Maki, W. Quapp, S. Klee, G. C. Mellau, and S. Albert, J. Mol. Spectrosc. **180**, 323 (1996).

[32] K. Nauta and R. E. Miller, Phys. Rev. Lett. **82**, 4480 (1999).

[33] M. Hartmann, N. Portner, B. Sartakov, J. P. Toennies, and A. F. Vilesov, J. Chem. Phys. **110**, 5109 (1999).

[34] A. Conjusteau, C. Callegari, I. Reinhard, K. K. Lehmann, and G. Scoles, J. Chem. Phys., in press.

[35] E. Lee, D. Farrelly, and K. B. Whaley, Phys. Rev. Lett. **83**, 3812 (1999).

[36] M. Lewerenz, B. Schilling, and J. P. Toennies, Chem. Phys. Lett. **206**, 381 (1993).

[37] K. Nauta and R. E. Miller, Acetylene solvated in superfluid helium nanodroplets: Spectroscopic evidence for near resonant coupling between molecular rotation and rotons, preprint, 2000.

[38] R. E. Miller, private communication.

[39] P. D. Mallinson and A. Fayt, Mol. Phys. **32**, 473 (1976).

[40] K. Yamada, A. Moravec, and G. Winnewisser, Z. Naturforsch. A **50**, 1179 (1995).

[41] F. M. Frayer and G. E. Ewing, J. Chem. Phys. **48**, 781 (1968).

[42] K. Nauta, D. T. Moore, and R. E. Miller, Faraday Discuss. Chem. Soc. **113**, 261 (1999).

[43] V. M. Horneman, G. Graner, H. Fakour, and G. Tarrago, J. Mol. Spectrosc. **137**, 1 (1989).

[44] H. Harder, C. Gerke, H. Mäder, J. Cosléou, R. Bocquet, J. Demaison, D. Papoušek, and K. Sarka, J. Mol. Spectrosc. **167**, 24 (1994).

[45] K. K. Lehmann and B. Pate, J. Mol. Spectrosc. **144**, 443 (1990).

[46] A. J. Alexander, S. Firth, H. W. Kroto, and D. R. M. Walton, J. Chem. Soc. Faraday Trans. **88**, 531 (1992).

[47] L. Pierce and D. H. Petersen, J. Chem. Phys. **33**, 907 (1960).

[48] J. Liévin, M. A. Temsamani, P. Gaspard, and M. Herman, Chem. Phys. **190**, 419 (1995).

[49] D. Eichenauer and R. J. LeRoy, J. Chem. Phys. **88**, 2898 (1988).

[50] J. Jortner and N. Ben-Horin, J. Chem. Phys. **98**, 9346 (1993).

[51] K. M. Atkins and J. M. Hutson, J. Chem. Phys. **105**, 440 (1996).

[52] A. M. Smith, W. Klemperer, and K. K. Lehmann, J. Chem. Phys. **94**, 5040 (1991).

[53] C. M. Dion, A. Keller, O. Atabek, and A. D. Bandrauk, Phys. Rev. A **59**, 1382 (1999).

[54] E. Hudspeth, D. A. McWhorter, and B. H. Pate, J. Chem. Phys. **109**, 4316 (1998).

[55] S. Grebenev, M. Hartmann, M. Havenith, B. Sartakov, J. P. Toennies, and A. F. Vilesov, J. Chem. Phys. **112**, 4485 (2000).

[56] A. M. Smith, S. L. Coy, W. Klemperer, and K. K. Lehmann, J. Mol. Spectrosc. **134**, 134 (1989).

[57] C. O'Brien, Senior thesis, Princeton University, 1994.

Chapter 4

A Superfluid Hydrodynamic Model for the Enhanced Moments of Inertia of Molecules in Liquid ^{4}He *

4.1 Introduction

The spectroscopy of atoms and molecules dissolved in He nanodroplets provides both a new way to study microscopic dynamics of this unique quantum fluid [1], and a very cold matrix (0.4 K [2]) to create and study novel species [3–5]. Recent experiments have demonstrated that even heavy and anisotropic molecules display rotationally resolved vibrational spectra with a structure reflecting the gas phase symmetry of the molecule. However, the rotational constants required to reproduce the spectra are often substantially reduced from those of the isolated molecule. For example, the ν_3 vibrational band of SF_6 dissolved in He nanodroplets (first observed by Goyal *et al.* [6] and later rotationally resolved and

*This chapter has been published in Phys. Rev. Lett., **83**, 5058 (1999); (E) **84**, 1848 (2000) by C. Callegari, A. Conjusteau, I. Reinhard, K. K. Lehmann, G. Scoles, and F. Dalfovo.

analyzed by Hartmann *et al.* [2,7]) indicates that the effective moment of inertia, I_{eff}, in liquid ^{4}He is 2.8 times that of the isolated molecule. The same qualitative behavior has been found for a wide range of other molecules [1, 8–11]. In an elegant recent experiment, it has been demonstrated that the rotational structure of OCS broadens and collapses in pure ^{3}He droplets, and is recovered when ≈ 60 ^{4}He atoms are co-dissolved in the ^{3}He [1]. The association of the weakly damped, unhindered rotation with the Bose symmetry of ^{4}He suggests that this phenomenon is a manifestation of superfluidity, and the experiment has been called the microscopic Andronikashvili experiment [1].

A theory able to reproduce the observed increase, ΔI, in molecular moments of inertia would be of interest for at least two reasons. First, the enhanced inertia provides a window into the dynamics of the liquid. Second, the ability to predict the rotational constants would further improve the utility of He nanodroplet isolation spectroscopy for the characterization of novel chemical species.

The first model proposed to explain the observed ΔI assumed that a certain number of He atoms, trapped in the interaction potential of the solute, rotate rigidly with the latter [2]. In the case of SF_6, 8 He atoms trapped in the octahedral global potential minima would create a rigidly rotating "supermolecule" that would have approximately the observed I_{eff}. In the case of OCS, putting a six He atom "donut" in the potential well around the molecule also reproduces the observed I_{eff} [12]. Recent Diffusion Monte Carlo (DMC) calculations [13] have predicted that the effective rotational constant of SF_6–He_N monotonically decreases from that of the isolated molecule to the large cluster limit, reached at $N = 8$, and remains essentially constant for $N = 8$–20. The supermolecule model has been recently extended to consider the rigid rotation of a "normal fluid fraction" of the He density which is claimed to be significant only in the first solvation layer [1,12],

based on Path Integral Monte Carlo calculations of Kwon *et al.* [14] which show a molecule-induced reduction of the superfluid fraction. These calculations have been recently used to propose a definition of a spatially dependent normal fluid fraction which reproduces the observed $I_{\rm eff}$ of solvated SF_6 [15]. An alternative point of view has been recently proposed by Babichenko and Kagan [16].

The limitations of the supermolecule model are made clear by the ΔI observed for HCN in He droplets [8] which is only $\approx 5\,\%$ of the ΔI observed upon formation of a gas phase He·HCN van der Waals complex [17]. Furthermore, it has been previously recognized that in principle there is also a superfluid hydrodynamic contribution, $I_{\rm h}$, to ΔI [1,18,19]. Previous estimates, based upon a classic treatment of the rotation of an ellipsoid in a fluid of uniform density, found that $I_{\rm h}$ is only a small fraction of the observed ΔI, at least for heavy rotors such as OCS [12, 19]. In this report, we show that if the spatial variation of the He solvation density around the solute molecule is taken into account, the calculated $I_{\rm h}$ is instead rather large and agrees well with experimental data. We compare our calculations with the experimental results available in the literature (OCS [1], HCN [8]) and with results recently obtained in our laboratory for $HCCCH_3$ and HCCCN, and in the laboratory of R. E. Miller for $(HCN)_2$ [9] and HCCH [10].

We first calculate the ground state He density, ρ, around a static solute molecule. The molecule is then considered to undergo classical rotation, slowly enough that the helium ground state density adiabatically follows the molecular rotation. The kinetic energy associated with the He flow (assumed viscousless and irrotational) is used to calculate $I_{\rm h}$.

4.2 Density Functional calculations

The main input of our hydrodynamic model is the ground state density of He around the solute. DMC calculations can provide this density with a minimum of assumptions beyond the interaction potentials [20], but are computationally expensive. The Density Functional method, which is a good compromise between accuracy and computational cost, consists in numerically minimizing the total energy of the many-body system in the form of a semiempirical functional of the He density: $E = \int d\mathbf{r}\, \mathcal{H}[\rho(\mathbf{r})]$. The energy density $\mathcal{H}$ contains an effective non-local interaction with a few parameters fixed to reproduce known properties of bulk liquid He. The functional used here is the one termed Orsay-Paris [21], which was shown to accurately reproduce the static properties of pure and doped He clusters [22]. The need to treat axially symmetric molecules implies moving from one to two-dimensional equations. The new routines have been extensively tested against previously calculated spherically symmetric systems. The minimization of energy is carried out by mapping the density distribution on a grid of points and propagating it in imaginary time, starting from a trial distribution.

The density functional also contains the interaction between the He and the impurity molecule. The interaction, assumed pairwise, is treated as a static external potential, since the molecules considered here are expected to have negligible zero point motion. Existing potentials for He–HCN [23], He–HCCH [24], and He–OCS [25] have been used without modifications. The He–$(HCN)_2$ potential was generated as the superposition of the potential due to two HCN molecules whose centers of mass are separated by 4.44 Å(the equilibrium distance for the gas phase dimer [26]). The repulsive part of the He–HCCCN potential has been taken from [27]; the attractive part from the He–HCN and He–HCCH poten-

tials, using the concepts of distributed interaction and transferability [28]. The He–HCCH [24] and He–CH_4 [29] interactions were used to generate the potential between He and $HCCCH_3$, treating the latter molecule as cylindrically symmetric. Full detail on all potentials used are available from the authors, and will be published separately [30].

4.3 Hydrodynamic equations

Once the helium density profiles are calculated, the molecules are assumed to rotate perpendicularly to their symmetry axis with angular velocity ω. We assume that the He density adiabatically follows this rotation, which allows us to calculate the laboratory-frame time-dependent density at each point in the liquid. This assumption is only valid if at each point the velocity of the fluid, $v(\mathbf{r})$, is less than a critical velocity, v_c. If v_c is taken to be the velocity of sound, this is true for all our molecules, at the temperature of the droplet: 0.4 K. A further justification to our assumption is also the fact that no critical value of angular momentum is experimentally observed for a wide class of molecules (i.e., for a wide range of fluid velocities).

The second assumption that we make is that the He behaves entirely as a superfluid undergoing irrotational flow. The assumption that the motion is irrotational implies that $\mathbf{v}(\mathbf{r})$ can be written as the gradient of a scalar potential: $\mathbf{v} = -\boldsymbol{\nabla}\phi$ (the dependence of $\rho, \mathbf{v}, \phi$ on $\mathbf{r}$ will be implicit from now on), where ϕ is known as the velocity potential. These assumptions lead to the following hydrodynamic equation for the velocity potential [31]:

$$\boldsymbol{\nabla} \cdot (\rho \boldsymbol{\nabla}\phi) = \frac{\partial \rho}{\partial t} = -(\boldsymbol{\nabla}\rho) \cdot (\boldsymbol{\omega} \times \mathbf{r}\,). \tag{4.1}$$

The first equality is just the continuity equation, while the second reflects the statement that the density is time-independent in the rotating frame. We select our axis system with z along the symmetry axis of the molecule, and assume that rotation takes place round the x axis with angular velocity $\boldsymbol{\omega} = \omega\,\hat{\mathbf{x}}$. In order to better exploit the symmetry of the problem, we have used elliptical coordinates ξ, θ, φ, where $x = f\,\sqrt{\xi^2-1}\sin(\theta)\cos(\varphi)$, $y = f\,\sqrt{\xi^2-1}\sin(\theta)\,\sin(\varphi)$, and $z = f\,\xi\,\cos(\theta)$. The surfaces of constant ξ are ellipses of rotation with foci at $z = \pm f$. Two such surfaces limit the region where Eq. (4.1) is solved. The inner boundary excludes the volume occupied by the impurity, and is chosen as the largest ellipse contained in the region where $\rho < 0.005\,\rho_0$ ($\rho_0 = 0.0218\,\text{Å}^{-3}$ is the bulk liquid density). Von Neumann boundary conditions $\hat{n}\cdot\boldsymbol{\nabla}\phi = -\hat{n}\cdot(\boldsymbol{\omega}\times\mathbf{r})$ insure that the normal component of velocity matches the normal component of motion of the boundary [31]. Note that we define the surface normal as pointing *out* of the region occupied by the liquid. For the outer boundary, any ellipse large enough that the motion of the outside fluid is negligible can be chosen (with Dirichlet boundary conditions $\phi = 0$). These boundary conditions result in a unique solution to the hydrodynamic equations. Other solutions exist if we do not require the fluid to be irrotational, but it is known that these are higher in energy [32], and will include any solutions that have some portion (a "normal component" or a He "snowball") of the He density that rigidly rotates with the molecule.

Given the solution, ϕ, to the hydrodynamic equation, we can calculate the kinetic energy, $K_{\rm h}$, in the motion of the fluid by the following:

$$K_{\rm h} = \frac{1}{2}\,I_{\rm h}\,\omega^2 = \frac{1}{2}\,m_{\rm He}\int \rho\,(\boldsymbol{\nabla}\phi)\cdot(\boldsymbol{\nabla}\phi)\,dV \tag{4.2}$$

$$K_{\rm h} = \frac{1}{2}\,m_{\rm He}\left[-\int \phi\,\left(\frac{\partial\rho}{\partial t}\right)dV + \int \rho\,\phi\,(\boldsymbol{\nabla}\phi)\cdot d\mathbf{S}\right]. \tag{4.3}$$

Eq. (4.2) follows directly from the definition of kinetic energy; Eq. (4.3) is derived from Eq. (4.2) using standard vector identities and assuming that ϕ is a solution of Eq. (4.1). $I_{\rm h}$ is the hydrodynamic contribution to the moment of inertia for rotation about the x axis, and $m_{\rm He}$ is the atomic mass of helium. Both $(\partial\rho/\partial t)$ and ϕ, are proportional to ω, thus the above definition of $I_{\rm h}$ is independent of ω. The total kinetic energy of rotation will include the contribution from the molecule, $K_{\rm m} = \frac{1}{2}\, I_{\rm m}\, \omega^2$, where $I_{\rm m}$ is the moment of inertia of the free molecule. We can also calculate the net angular momentum created by the motion of the He fluid: $\mathbf{J}_{\rm h} = m_{\rm He} \int \rho\, \mathbf{r} \times (-\boldsymbol{\nabla}\phi)\, dV$. By use of standard vector identities and Eq. (4.1), this definition can be shown to lead to $\mathbf{J}_{\rm h} = I_{\rm h}\, \boldsymbol{\omega}$. Thus the total angular momentum of the system is just the sum of the angular momenta of the molecule and the superfluid helium. The local shape of the velocity field $\mathbf{v}(\mathbf{r})$ can be rather complex due to the presence of strong inhomogeneities in the density distribution.

4.4 Hydrodynamic moments of inertia

We calculate $I_{\rm h}$ by solving the hydrodynamic equation, Eq. (4.1) for ϕ, assuming unit angular velocity rotation around the x axis. It is computationally convenient to solve a slightly transformed version of Eq. (4.1), where the smoother function $\ln\rho(\mathbf{r})$ appears instead of $\rho(\mathbf{r})$:

$$\nabla^2\phi + (\boldsymbol{\nabla} \ln\rho) \cdot (\boldsymbol{\nabla}\phi + \hat{\mathbf{x}} \times \mathbf{r}) = 0. \tag{4.4}$$

Eq. (4.4) is solved, subject to the boundary conditions, by converting it to a set of finite difference equations on a grid of points in our elliptical coordinate system and using the *Gauss-Seidel* relaxation method [33]. Both Eq. (4.2) and Eq. (4.3)

are then evaluated by simple numerical quadrature, and are found to give the same value of $I_{\rm h}$ within a few percent. We also carefully tested the convergence of $I_{\rm h}$ with grid size.

As an example of density distribution and velocity field, Fig. 4.1 shows our results for the OCS molecule in a cluster of 300 He atoms. On the left we give the contour plot of the He density near the molecule. One clearly sees the complex structure which results from the tendency to have He atoms near local minima of the impurity-He potential. The highest peak, at $(y, z) = (-3.6, -1.2)$, corresponds to a ring of atoms perpendicular to the axis of the molecule. The integral of the density within this structure gives 6.5 atoms, and indeed 7–8 is the number of He atoms one expects to fit into such a ring by close-packing. On the right side of the same figure we plot the current density, $\rho\,\mathbf{v}$. We find that most of the kinetic energy density, $\frac{1}{2}\rho\,\mathbf{v}^2$, comes from the first solvation layer, the outer part of the cluster giving a negligible effect.

4.5 Discussion and conclusions

In Table 4.1 our results are compared with existing experimental values for several molecules in He nanodroplets. There is an overall good agreement between the predicted and observed enhancements of the effective moment of inertia. From a quantitative viewpoint, one notices that the predicted moments of inertia tend to *overestimate* the experimental values. In the case of the lightest rotors (HCN and HCCH) the large discrepancy suggests the breakdown of the assumption of adiabatic following as recently predicted [13]. In that paper the importance of He exchange is pointed out; it is also shown that the interplay of the rotational constant with the potential anisotropy determines the extent to which the anisotropic

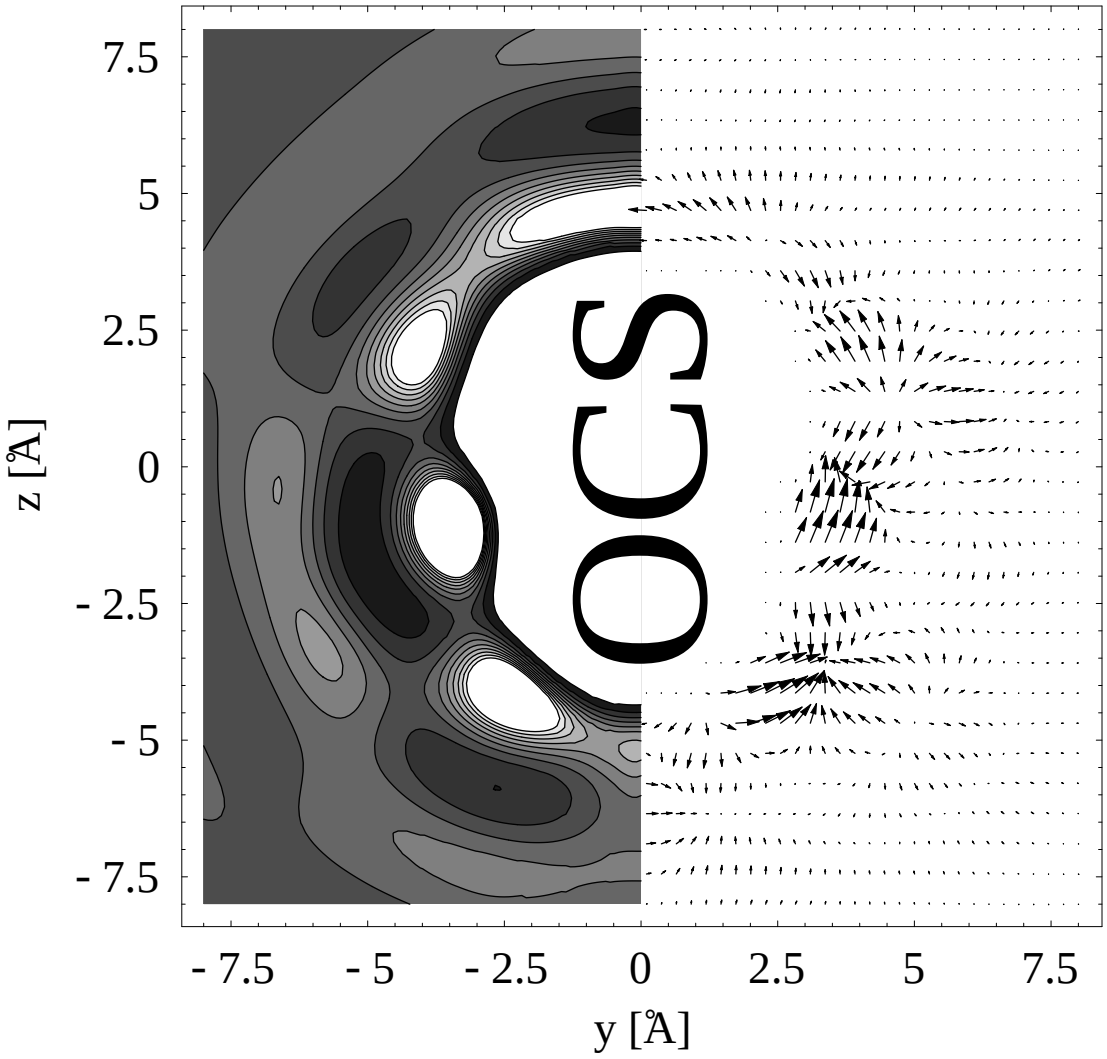

Figure 4.1: He density, ρ, (left) and He current density, $\rho\,\mathbf{v}$, (right) distributions for a cluster of 300 He atoms, with OCS in its center rotating counterclockwise. For the sake of showing details, the highest He density peaks have been clipped (white areas), and the dynamic range of the current has been compressed.

He solvation density can adiabatically follow the rotation of the molecule. When the rotational constant of SF_6 is arbitrarily increased in the calculation by a factor of 10, the He density in the molecule-fixed frame becomes much more isotropic and the solvation-induced ΔI decreases by a factor of 20 [13]. We have recently obtained experimental evidence that ΔI is larger for DCN than for HCN, which we believe to be direct experimental evidence for this effect [34]. It is interesting to note that for these light (i.e., fast spinning) rotors the maximum of $\mathbf{v}(\mathbf{r})$ approaches the bulk ^{4}He sound velocity. The overestimate of the moments of inertia for the other molecules likely reflects the uncertainties in the calculated $\rho(\mathbf{r})$. We should remark here that while, by construction, the Orsay-Paris functional prevents $\bar{\rho}$ (the density averaged over an atomic volume) from becoming much larger than ρ_0, the functional was not constructed to deal with density gradients as high as those found in the first solvation layer. We observed that small changes in the

Table 4.1: Moments of inertia for the molecules studied in this work. Units are u Å^2. The quantities I_{m} and I_{eff} are the observed moments of inertia when the molecule is free and dissolved in the cluster, respectively. Their difference, ΔI, in the fourth column is compared with the hydrodynamic moment of inertia, I_{h}, of the present calculation.

	I_{m}	I_{eff} (exp.)	ΔI	I_{h} (calc.)	ref.
HCN	11.39	14.04	2.65	5.7	[8]
DCN	14.0	16.9	2.9	5.6	[34]
HCCH	14.26	16.08	1.82	9.4	[10]
$HCCCH_3$	59.14	224.0	164.8	190	[11]
OCS	83.10	230.0	146.9	197	[1]
HCCCN	111.1	330.7	219.6	226	[11]
$(HCN)_2$	289.5	872.5	583	619	[9]

form of the He density within the deep potential well of those molecules produce significant variations of the predicted moments of inertia, limiting the accuracy of the final results to 20%–30%. This uncertainty does not affect the main result emerging from Table 4.1 that the hydrodynamic contribution to the moment of inertia of these systems, instead of being negligible, is rather large and can explain the observed rotational constants.

One could object that the density values found at the minima of the He-molecule interaction potential (e.g., $\approx 11\,\rho_0$ for OCS) are too high to be treated as those of a liquid, and should be interpreted as localized He atoms rigidly rotating with the molecule; it has been proposed that the He density distribution around the OCS–He_6 supermolecule is only weakly anisotropic and thus can rotate without generating a significant hydrodynamic contribution [12]. We have calculated the above density distribution, and found that it is still strongly anisotropic, leading to a hydrodynamic moment of inertia of over $400\,\mathrm{u\,\AA^2}$. When combined with the moment of inertia of the OCS-He_6 supermolecule, this gives a total effective moment of inertia of over $650\,\mathrm{u\,\AA^2}$, dramatically larger than the experimental value ($230\,\mathrm{u\,\AA^2}$).

In summary, the spatial dependence of the He density, which is caused by the molecule–He interaction, results in a hydrodynamic contribution to the moment of inertia more than an order of magnitude larger (in the case of the heavier rotors) than that predicted for the rotation of a reasonably sized ellipsoid in He of uniform bulk liquid density. Furthermore, the present calculations suggest that the effective moments of inertia of molecules in He nanodroplets (and likely also bulk He) can be quantitatively predicted by assuming irrotational flow of a spatially inhomogeneous superfluid.

Bibliography

[1] S. Grebenev, J. P. Toennies, and A. F. Vilesov, Science **279**, 2083 (1998).

[2] M. Hartmann, R. E. Miller, J. P. Toennies, and A. Vilesov, Phys. Rev. Lett. **75**, 1566 (1995).

[3] J. Higgins, C. Callegari, J. Reho, F. Stienkemeier, W. E. Ernst, K. K. Lehmann, M. Gutowski, and G. Scoles, Science **273**, 629 (1996).

[4] K. K. Lehmann and G. Scoles, Science **279**, 2065 (1998).

[5] K. Nauta and R. E. Miller, Science **283**, 1895 (1999).

[6] S. Goyal, D. L. Schutt, and G. Scoles, Phys. Rev. Lett. **69**, 933 (1992).

[7] R. Fröchtenicht, J. P. Tonnies, and A. F. Vilesov, Chem. Phys. Lett. **229**, 1 (1994).

[8] K. Nauta and R. E. Miller, Phys. Rev. Lett. **82**, 4480 (1999).

[9] K. Nauta and R. E. Miller, J. Chem. Phys. **111**, 3426 (1999).

[10] K. Nauta and R. E. Miller, Acetylene solvated in superfluid helium nanodroplets: Spectroscopic evidence for near resonant coupling between molecular rotation and rotons, preprint, 2000.

[11] C. Callegari, A. Conjusteau, I. Reinhard, K. K. Lehmann, and G. Scoles, First overtone helium nanodroplet isolation spectroscopy of molecules bearing the acetylenic CH chromophore, in preparation, 2000.

[12] S. Grebenev, M. Hartmann, M. Havenith, B. Sartakov, J. P. Toennies, and A. F. Vilesov, J. Chem. Phys. **112**, 4485 (2000).

[13] E. Lee, D. Farrelly, and K. Whaley, Phys. Rev. Lett. **83**, 3812 (1999).

[14] Y. Kwon, D. M. Ceperley, and K. B. Whaley, J. Chem. Phys. **104**, 2341

(1996).

[15] Y. Kwon and K. B. Whaley, Phys. Rev. Lett. **83**, 4108 (1999).

[16] V. S. Babichenko and Y. Kagan, Phys. Rev. Lett. **83**, 3458 (1999).

[17] S. Drucker, F.-M. Tao, and W. Klemperer, J. Phys. Chem. **99**, 2646 (1995).

[18] K. B. Whaley, in *Advances in Molecular Vibrations and Collision Dynamics*, edited by J. M. Bowman and Z. Bacic (JAI Press, Inc., Greenwich, CT, 1998), Vol. III, p. 397.

[19] K. K. Lehmann, Mol. Phys. **97**, 645 (1999).

[20] R. N. Barnett and K. B. Whaley, J. Chem. Phys. **99**, 9730 (1990).

[21] J. Dupont-Roc, M. Himbert, N. Pavloff, and J. Treiner, J. Low Temp. Phys. **81**, 31 (1990).

[22] F. Dalfovo, Z. Phys. D **29**, 61 (1994).

[23] K. M. Atkins and J. M. Hutson, J. Chem. Phys. **105**, 440 (1996).

[24] R. Moszynsky, P. E. S. Wormer, and A. van der Avoird, J. Chem. Phys. **102**, 8385 (1995).

[25] K. Higgins and W. Klemperer, J. Chem. Phys. **110**, 1383 (1999).

[26] K. W. Jucks and R. E. Miller, J. Chem. Phys. **88**, 6059 (1988).

[27] E. M. Cabaleiro-Lago and M. A. Ríos, J. Chem. Phys. **109**, 8398 (1998).

[28] R. J. Bemish, R. E. Miller, X. Yang, and G. Scoles, J. Chem. Phys. **105**, 10171 (1996).

[29] U. Buck, K. H. Kohl, A. Kohlhase, M. Faubel, and V. Staemmler, Mol. Phys. **55**, 1255 (1985).

[30] C. Callegari, A. Conjusteau, I. Reinhard, K. K. Lehmann, and G. Scoles, in preparation, 2000.

[31] L. M. Milne-Thomson, *Theoretical Hydrodynamics*, fifth ed. (Dover Publications, Inc., Mineola, NY, 1996).

[32] Kelvin's minimum energy theorem. The proof in [31] is easily extended to the nonuniform density case.

[33] W. H. Press, S. A. Teulkosky, W. T. Vetterling, and B. P. Flannery, in *Numerical Recipes in Fortran 77: The art of scientific computing*, 2nd ed., edited by W. H. Press (Cambridge University Press, Cambridge, 1992), Chap. 19.

[34] A. Conjusteau, C. Callegari, I. Reinhard, K. K. Lehmann, and G. Scoles, J. Chem. Phys. (2000), in press.

Chapter 5

Single and Double Resonance Microwave Spectroscopy in Superfluid ^{4}He Clusters *

5.1 Introduction

The spectroscopy of molecules embedded in large ^{4}He clusters has recently received considerable experimental and theoretical attention [1, 2]. Nanometer scale helium clusters (nanodroplets), containing from several hundreds to more than 10^4 He atoms, provide a unique environment for high resolution matrix spectroscopy where the advantages of both conventional matrix spectroscopy and molecular beam spectroscopy are combined [3]. Since these clusters will pick up molecules or atoms that they encounter on their path without being appreciably deflected [4], they allow for a high degree of synthetic flexibility, and in particular for the formation and stabilization of weakly bound and unstable species [5–9]. Evaporative cooling has been found to maintain ^{4}He nanodroplets at a temperature of 0.4 K [10, 11], well below the predicted superfluid transition temperature which

*This chapter has been published in Phys. Rev. Lett., **82**, 5036 (1999) by I. Reinhard, C. Callegari, A. Conjusteau, K. K. Lehmann, and G. Scoles.

ranges from 2.14 K in bulk liquid helium to 1.5 K for clusters of only 10^2 He atoms [12]. As the perturbations imposed on the guest molecules by the helium host are minimal, the shift and width of spectroscopic lines in ^{4}He clusters are considerably less than for traditional matrix environments [1]. Furthermore, rotationally resolved spectra have been observed for a large variety of molecules [11,13–18] which show the structure predicted by the gas phase symmetry of the molecules with, however, reduced rotational constants. By showing that ro-vibrational spectra in ^{3}He clusters collapse into a single line, the weakly damped molecular free rotation present in liquid ^{4}He has recently been demonstrated to be a direct consequence of the boson nature of ^{4}He and is considered a microscopic manifestation of superfluidity [16].

An important unresolved question posed by the IR spectra relates to the physical process responsible for the line broadening observed in ro-vibrational transitions, which ranges from 150 MHz in the case of the R(0) line in the ν_3 fundamental in OCS [17] to 5.7 cm^{-1} for the case of the P(1) line in the ν_3 asymmetric stretch in H_2O [18]. For the carefully studied case of the ν_3 fundamental of SF_6 [11], the lines were found to have a Lorentzian shape of width $\approx$300 MHz independent of the rotational transition, which led to the suggestion that the linewidth reflected vibrational relaxation and/or dephasing [17].

Since He clusters remain fluid down to zero temperature and because of the very large zero point motion of the ^{4}He atoms, it appears natural to assume that the spectra of molecules seeded in this medium should not display inhomogeneous effects other than contributions from the cluster size distribution via size-dependent frequency shifts which, however, have been shown to be small [19]. In solids, variations of local binding sites lead to a distribution of vibrational frequencies, which results in inhomogeneous broadening that dominates the linewidths

at low temperature. In contrast, in liquids, local solvation fluctuations lead to dynamic dephasing. Treating the clusters as a classical liquid, one may expect the time scale of the solvation fluctuation (due to the large zero point kinetic energy of the He atoms) to be much faster than the dephasing times observed in most ro-vibrational spectra and hence the effect of fluctuating solvation would likely be strongly motionally averaged [20], leading to homogeneous, Lorentzian line shapes. The spectra of SF_6 [11] and CH_3CCH [13], which are well described with a free rotor Hamiltonian and Lorentzian line shapes, seem to confirm the assumption that the major source of line broadening is of homogeneous nature.

However, at temperatures as low as 0.4 K in a superfluid medium solvation fluctuations are probably more appropriately described in terms of the interaction with the thermally populated fundamental modes of the cluster. For typical cluster sizes (well below N=10^5) only surface excitations (ripplons) have to be considered [10]. The coupling of the molecular vibration to these modes has been estimated and found to be too weak to explain the observed linewidths [21].

The observation of rotational structure in vibrational transitions suggests that pure rotational spectroscopy, by excitation with microwave (MW) radiation, should provide a useful probe of the rotational dynamics of the dopant molecules in the superfluid helium environment. It should be noted, that it was not clear *a priori* whether such spectra could be observed at all. Due to the short absorption path and low densities characteristic of molecular beams, direct MW absorption measurements are not viable. Whereas transitions in the UV and visible spectral range can be efficiently detected by laser induced fluorescence [7, 8, 22, 23], beam depletion spectroscopy is employed to detect transitions in the near and mid IR [5, 11]. In this method, photon absorption and subsequent relaxation of the molecular excitation energy leads to He atom evaporation from the cluster and a decrease

in the flux of He atoms in the droplet beam is observed. While absorption of a single IR photon leads to the evaporation of hundreds or more He atoms from a droplet, at least 10 microwave photons per droplet will need to be absorbed to provide sufficient energy to evaporate a single He atom ($\sim$5 cm^{-1} [24]). In order to produce a signal of sufficient size to be detected, many He atoms per cluster must be evaporated. This requires the rotational relaxation to occur on a time scale significantly shorter than 10 μs. Although a lower limit of the rotational relaxation time of the order of hundreds of ps is established by the linewidth of typically 1 GHz observed in the IR spectra [13], the upper limit could be as high as tens of μs, in which case no signal would be observed. The upper limit is imposed only by the fact that for all observed IR spectra the rotational populations are fully thermalized at the temperature of the He droplets by the time the clusters reach the laser interaction region.

Here we report measurements of the microwave spectrum of NCCCH in He nanoclusters detected by the method of beam depletion spectroscopy. NCCCH was used because of its large dipole moment (3.7 D) and its linear structure (rotational constant B =1.5 GHz in the helium nanodroplets [13, 14]), which leads to strong and well resolved rotational transitions.

5.2 Experimental setup

The molecular beam setup will be described in detail elsewhere [13]. Here we will give only a short summary highlighting the aspects unique to the present study. Clusters are formed in a supersonic free-jet helium expansion from a cold 5 μm diameter nozzle which, in the measurements presented here, is operated at 26 K and a stagnation pressure of 100 atm yielding an average cluster size of $\approx 3\times10^3$

atoms/cluster (estimated from Ref. [25]). After collimation by a conical skimmer, the clusters pass through a pickup cell containing typically 3×10^{-4} torr of the gas of interest and collect (on average) one foreign molecule each. Subsequently the clusters pass through a 10 cm long P-band microwave guide (nominal 12–18 GHz) which is aligned parallel to the cluster beam. The MW amplitude is modulated at 310 Hz. The molecular beam enters and exits the waveguide through two 3 mm holes in E-bends located at each end of the device. If multiple resonant photon absorption and subsequent relaxation of the molecule–helium cluster system occurs, the beam depletion signal is recorded by a liquid-helium-cooled silicon bolometer using a lock-in technique. The microwave radiation is produced by a sweep generator (HP 8350B) with a 0.01–26.5 GHz plug-in (HP 8359A) and is amplified by a traveling wave tube amplifier (Logi Metrics A310/IJ) to a power level between 0.05 W and 3.4 W (corresponding to a field strength of 0.78 to 6.5 kV/m in the center of the P-band waveguide). The power transmitted through the waveguide is attenuated by 30 dB and measured by a crystal detector (HP8473B), the output of which is used to level the power of the sweep generator during frequency scans.

5.3 Results

Spectra of the J=3→4 and the J=4→5 transitions in the ground vibrational state of NCCCH obtained for various MW field strengths between 0.78 and 6.5 kV/m are shown in Fig. 1. The line centers agree well with the line positions predicted from the molecular constants obtained from the ro-vibrational IR spectrum of NCCCH in the helium clusters [13]. The linewidths (FWHM) are observed to increase from ∼0.6 to ∼1 GHz for the J=3→4 transition and from ∼0.8 to ∼1.2 GHz for the J=4→5 transition when the microwave field is increased from 0.78 to

6.5 kV/m. At low MW fields these linewidths are comparable to the width of the corresponding ro-vibrational transitions in the spectra of the fundamental CH stretching mode [14], indicating that vibrational relaxation and dephasing which frequently are the dominant line broadening mechanisms in the spectra of impurities in classical liquids [20] are not the main source of broadening for a molecule such as NCCCH in a superfluid helium cluster. Similar linewidths have been observed by us for the corresponding microwave transitions in CH_3CN and CH_3CCH.

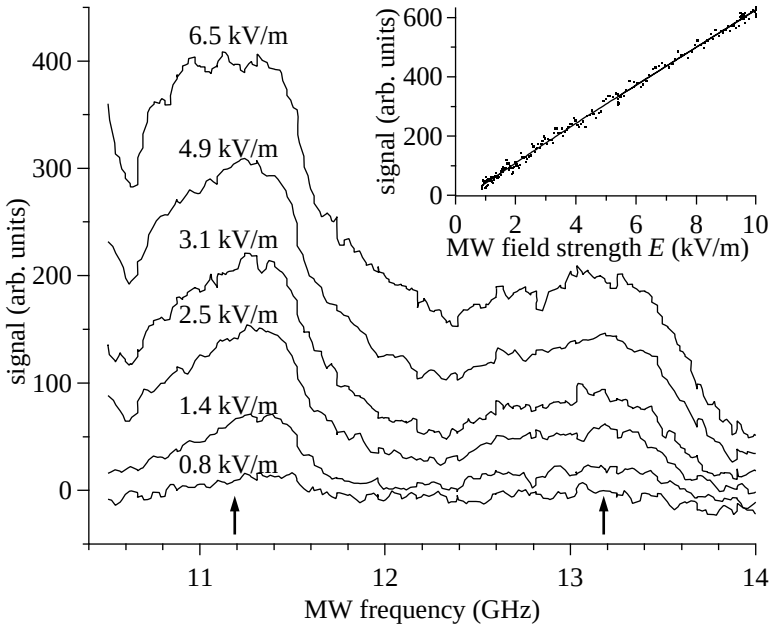

Figure 5.1: Microwave spectra of the J=3→4 and J=4→5 transition in NCCCH in ^{4}He droplets measured at various MW field strengths. The arrows indicate the line positions predicted from the molecular constants obtained from the ro-vibrational spectrum of NCCCH in He clusters. *Inset*: Signal amplitude of the J=4→5 transition at 13.1 GHz as a function of microwave field strength. The linearity of this plot demonstrates the inhomogeneous nature of the dominant line broadening mechanism.

The dependence of the signal amplitude S on the microwave field strength E has been measured for NCCCH with the MW frequency fixed at the top of either the J=3→4 or the J=4→5 transition and is well described by $S \sim E^2/(1+E^2/E_{\rm sat}^2)^{1/2}$ with the saturation field $E_{\rm sat}$ =1.1(2) kV/m (see Inset Fig. 1). This saturation behavior, resulting in a linear dependence of the absorption as function of the MW field intensity for $E \gg E_{\rm sat}$, demonstrates that, in contrast to the previous expectations, the linewidth is dominated by inhomogeneous broadening [26]. With the saturation parameter $(E/E_{\rm sat})^2$, the homogeneous unsaturated linewidth is calculated to be at least a factor of 6 narrower than the inhomogeneous linewidth observed at a MW field intensity of 6.5 kV/m. This sets the lower limit of the rotational relaxation time to about 2 ns.

An upper limit for the rotational relaxation time has been set by a MW amplitude modulation experiment: With the MW frequency fixed on top of the 3→4 transition at a MW field of 7.8 kV/m, the signal height is monitored while the MW field is 100 % square wave modulated at a frequency f. By modelling the 3→4 transition as a driven two-level system, the absorbed microwave power is calculated to increase by a factor of 2 when f changes from $f \ll 1/T_1$ to $f \gg 1/T_1$, where $1/T_1$ is the population relaxation rate for the transition. This is basically independent of the dephasing rate $(1/T_2)$, as long as the microwave power is sufficiently large to allow for saturation. From the fact that no increase in signal is observed for modulation frequencies up to 10 MHz we estimate an upper limit for the rotational relaxation time of about 20 ns. This limit is in agreement with the independent but less stringent estimate inferred from the comparison of the strengths of the MW spectra and the IR spectra [13], which implies that the rotational relaxation takes place at a rate not slower than in tens of ns.

In order to determine the homogeneous linewidth of the rotational transition, microwave-microwave double resonance experiments have been carried out. A second microwave source (HP8690B, plug-in HP8694B: 8–12.4 GHz) is employed to generate microwave radiation at a fixed frequency. While the first microwave field (the probe) is frequency scanned across the 3→4 and the 4→5 transition, the second microwave field pumps the J=3→4 transition at about 11.1 GHz.

As the probe frequency approaches the pump frequency a strong decrease in

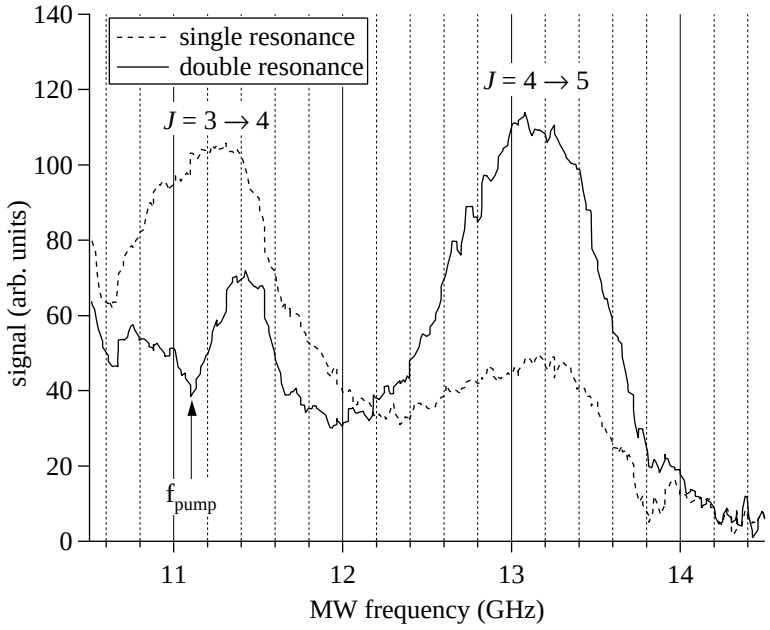

Figure 5.2: MW-MW double resonance spectrum of NCCCH in ^{4}He clusters compared to a single resonance spectrum. The depletion in the J=3→4 and the enhancement in the J=4→5 transition occur over a significant part of the linewidths indicating rapid relaxation among the substates of the inhomogeneous broadening of the individual rotational levels with a rate much faster than the rotational population inversion rate. The J=3→4 transition is pumped with a fixed frequency at 11.1 GHz and a field of 3.75 kV/m while the probing field is 5.3 kV/m.

signal is observed due to the depletion of the J=3 state by the pump, whereas the 4→5 transition signal is increased according to the enhanced population of the J=4 state (Fig. 2). Remarkably, the hole burnt into the 3→4 transition has a width of ≈ 50–70 % of the single resonance linewidth, implying that the rotational population inversion relaxation time is larger than 4 ns. The increase in the 4→5 signal even occurs over the total width of the signal, indicating that there is a fast relaxation within the inhomogeneous distribution of each individual J level. This observation is important as it implies that a substantial part of the inhomogeneous line broadening is due to a dynamic effect rather than to a static effect such as the cluster size distribution.

5.4 Discussion and conclusions

The phenomenon of "dynamic" inhomogeneous broadening can be understood assuming that there are additional degree(s) of freedom associated with a splitting of the rotational state into several substates and that the molecule may transit among these substates. Such transitions, which may well change the kinetic and potential energy of the molecule, but produce only a small change in its rotational energy, will be denoted as "elastic". If the elastic relaxation rate is much less than the spectral line width, the line shape reflects the distribution of resonance frequencies of the molecules in these additional quantum states. Each substate has a homogeneous width much narrower than the width of the inhomogeneous line. A double resonance experiment would be expected to show a correspondingly narrow hole in the pumped transition and a peak on top of the transition starting from the population enhanced rotor level. However, if the relaxation rate for the rotor quantum number is slower still than the relaxation between the substates,

then the population disequilibrium produced by the MW pumping will be spread over many or all the substates. This produces, in our case, a broad depletion in the lower rotor level and an enhancement over the complete width of the higher rotor level.

The relative areas of the depletion and enhancement signals compared to the single resonance MW signal can be used to extract the relative rates of the two relaxation processes. By kinetic modelling of the transition rates between the J=3 and J=4 rotational levels and among the substates of each individual rotational state we estimate that the elastic relaxation within one rotational state is about one order of magnitude faster than the inelastic population inversion relaxation.

In order to determine possible mechanisms underlying the observed inhomogeneous broadening one of the authors has analyzed the dynamics of a neutral impurity in a nanometer scale ^{4}He cluster [21] showing that for an anisotropic impurity significant sources of line broadening arise from the coupling of the molecular rotation with the center of mass motion of the dopant. These couplings arise both from an anisotropic effective potential for the dopant when shifted from the exact center of the clusters, and from an orientationally dependent hydrodynamic contribution to the effective inertial mass of the dopant. It should be noted, however, that it is not clear how the molecular energy is transferred to the cluster since the energy released or absorbed by the molecular rotationally inelastic or elastic transition in general is not likely to match the quantized energy of the lowest cluster excitations.

The measurements presented here are the first observation of a purely rotational spectrum of any molecule in a liquid He environment, and have provided a unique window on the sources of line broadening and in particular onto the rotational dynamics of the dopant in the superfluid helium environment. It has

been unambiguously demonstrated that the rotational lines are dominated by inhomogeneous broadening which is attributed to the coupling of the center of mass motion of the molecule within the finite size cluster to the molecular rotation. The second major observation is that the molecule transits among the quantum states of the inhomogeneous distribution on a time scale much faster than the rotational relaxation. These MW-MW double resonance measurements have been followed by a separate study using microwave-infrared double resonance which provides new information on the relaxation dynamics of the dopant in the cluster and its dependence on the finite cluster size [27].

Bibliography

[1] K. B. Whaley, in *Advances in Molecular Vibrations and Collision Dynamics*, edited by J. M. Bowman and Z. Bacic (JAI Press, Inc., Greenwich, CT, 1998), Vol. III, p. 397.

[2] J. P. Toennies and A. F. Vilesov, in *Annual Review of Physical Chemistry*, edited by H. L. Strauss (Annual Reviews, Palo Alto, CA, 1998), Vol. 49, pp. 1–41.

[3] K. K. Lehmann and G. Scoles, Science **279**, 2065 (1998).

[4] T. E. Gough, M. Mengel, P. A. Rowntree, and G. Scoles, J. Chem. Phys. **83**, 4958 (1985).

[5] S. Goyal, D. L. Schutt, and G. Scoles, J. Phys. Chem. **97**, 2236 (1993).

[6] M. Hartmann, R. E. Miller, J. P. Toennies, and A. F. Vilesov, Science **272**, 1631 (1996).

[7] J. Higgins, W. E. Ernst, C. Callegari, J. Reho, K. K. Lehmann, M. Gutowski, and G. Scoles, Phys. Rev. Lett. **77**, 4532 (1996).

[8] J. Higgins, C. Callegari, J. Reho, F. Stienkemeier, W. E. Ernst, M. Gutowski, and G. Scoles, J. Phys. Chem. A **102**, 4952 (1998).

[9] K. Nauta and R. E. Miller, Science **283**, 1895 (1999).

[10] D. Brink and S. Stringari, Z. Phys. D **15**, 257 (1990).

[11] M. Hartmann, R. E. Miller, J. P. Toennies, and A. Vilesov, Phys. Rev. Lett. **75**, 1566 (1995).

[12] M. V. R. Krishna and K. B. Whaley, in *On Clusters and Clustering*, edited by P. J. Reynolds (North Holland, Amsterdam, 1993), p. 257.

[13] C. Callegari, A. Conjusteau, I. Reinhard, K. K. Lehmann, and G. Scoles, First

overtone helium nanodroplet isolation spectroscopy of molecules bearing the acetylenic CH chromophore, in preparation, 2000.

[14] K. Nauta, D. T. Moore, and R. E. Miller, Faraday Discuss. Chem. Soc. **113**, 261 (1999).

[15] C. Callegari, A. Conjusteau, I. Reinhard, K. Lehmann, G. Scoles, K. Nauta, and R. E. Miller, to be published.

[16] S. Grebenev, J. P. Toennies, and A. F. Vilesov, Science **279**, 2083 (1998).

[17] M. Hartmann, Ph.D. thesis, University of Göttingen, Göttingen, Germany, 1997.

[18] R. Fröchtenicht, M. Kaloudis, M. Koch, and F. Huisken, J. Chem. Phys. **105**, 6128 (1996).

[19] From the analysis of the IR spectra as a function of mean cluster size, it can be concluded that for large clusters (N≈3000), the cluster size distribution should produce a broadening of <200 MHz in the IR spectrum, which is just a small fraction of the observed linewidth of ≈ 1 GHz, though it can be expected to "wash out" any high resolution features in the spectrum.

[20] D. W. Oxtoby, Annu. Rev. Phys. Chem. **32**, 77 (1981).

[21] K. K. Lehmann, Mol. Phys. **97**, 645 (1999).

[22] M. Hartmann, F. Mielke, J. P. Toennies, A. F. Vilesov, and G. Benedek, Phys. Rev. Lett. **76**, 4560 (1996).

[23] M. Hartmann, A. Lindinger, J. P. Toennies, and A. F. Vilesov, Chem. Phys. **239**, 139 (1998).

[24] S. Stringari and J. Treiner, J. Chem. Phys. **87**, 5021 (1987).

[25] E. L. Knuth, B. Schilling, and J. P. Toennies, in *Proceedings of the 19th International Symposium on Rarefied Gas Dynamics* (Oxford University Press, Oxford, 1995), Vol. 19, pp. 270–276.

[26] W. Demtröder, in *Laser Spectroscopy*, 2nd ed. (Springer-Verlag, Berlin, Heidelberg, New York, 1996), Chap. 7.2.

[27] C. Callegari, I. Reinhard, K. K. Lehmann, G. Scoles, K. Nauta, and R. E. Miller, J. Chem. Phys., submitted.

Chapter 6

Finite Size Effects and Rotational Relaxation in Superfluid Helium Nanodroplets: Microwave-Infrared Double-Resonance Spectroscopy of Cyanoacetylene *

6.1 Introduction

Liquid He nanodroplets have attracted considerable attention in recent years, both as a matrix to produce and study novel chemical species [1–5], and as a quantum system with unique properties [6–13]. Owing to its high resolution, sensitivity, and selectivity, laser spectroscopy has become the tool of choice in this kind of experiment. The first spectroscopic studies in He droplets were carried out using a line-tunable CO_2 laser to vibrationally excite a solvated SF_6 molecule [14]. This

*This chapter has been submitted for publication in J. Chem. Phys. by C. Callegari, I. Reinhard, K. K. Lehmann, G. Scoles, K. Nauta, and R. E. Miller.

study showed that the associated absorption bands were sharp and that molecular complexes could be formed within the droplets by the pickup of more than one molecule. The application of tunable diode lasers to this system revealed that the associated spectrum could be rotationally resolved [15], demonstrating that the SF_6 molecule undergoes coherent rotational motion with a dephasing time longer than the rotational period. However, the rotational constant of the solvated molecule is approximately a factor of three smaller than in the gas phase, indicating that the helium contributes to the effective moment of inertia of the system. This study also reported the SF_6 rotational temperature (0.37 K), thus providing the first experimental determination of the droplet temperature, which was found to be in excellent agreement with theoretical predictions [16, 17]. Infrared (IR) spectroscopy of OCS in ^{4}He, ^{3}He, and mixed droplets [9] has recently provided an elegant demonstration of the superfluid nature of ^{4}He droplets above a critical size ($\approx$60 atoms) and shown that the high resolution that is obtained in ^{4}He is a consequence of its superfluidity (although a different interpretation of this phenomenon has recently been given in the literature [13]).

Spectroscopic investigation of doped He droplets is presently becoming quite diversified. Recent work has focused on: (1) the electronic transitions of atoms, molecules and clusters [12,18–20], (2) the use of the droplets as an ultracold matrix for the formation of nonequilibrium species [2, 4], (3) the quantum properties of the droplets themselves [7], (4) the change in moment of inertia undergone by molecules upon solvation, and its microscopic origin [9, 21], and (5) the study of the spectral line shapes [22–25]. In the present study we report on the application of double-resonance spectroscopy to the study of microwave and infrared line shapes for NCCCH (cyanoacetylene) seeded in He nanodroplets of variable size.

The ro-vibrational spectral lines of molecules in He droplets are quite narrow (typically $10^{-2}\,\mathrm{cm}^{-1}$), yet they are 10–100 times broader than the instrumental resolution. Quantitative information on the solvent environment can be extracted from the analysis of the line shapes, provided the source of broadening is understood. Traditionally, spectroscopists divide line shapes into two major, smoothly merging, classes: homogeneous and inhomogeneous. In the first, all of the molecules are in the same environment and the line shape is often Lorentzian, the width reflecting the coherence lifetime of the states under investigation. In the second, the molecules are distributed over a set of states, each giving rise to a slightly different transition frequency. The resulting line profile constitutes an arbitrarily-shaped envelope corresponding to a distribution over much narrower, unresolvable homogeneous lines [26]. The latter class is further divided into two categories, namely static, where each molecule resides in a given state for a time much longer than the time scale of the experiment (e.g., different trapping sites in a solid matrix), and dynamic, sometimes referred to as spectral diffusion, quasistatic broadening or heterogeneous broadening [27]. In the limit of static inhomogeneous lines, a double-resonance scheme is highly effective at "tagging" molecules in specific substates and one expects to "burn a hole" in the inhomogeneous distribution. When homogeneous broadening dominates, as well as in the limit of fast dynamic inhomogeneous broadening, all the molecules can be considered as residing in the same state. In this case "substate tagging" is not possible, and the line profiles are the same in the single- and double-resonance experiments [26]. Intermediate cases are "an immensely complicated question" [27] and have to be treated individually.

In comparison with a solid matrix, superfluid liquid helium is an extremely homogeneous medium; hence—at least in the bulk limit—it has been widely as-

sumed that one would not observe static inhomogeneous broadening. This has naturally lead to the assumption that the observed linewidths are homogeneously broadened (by rotational and vibrational relaxation and/or dephasing) [28]. Such an assumption may be also partly justified by the success in fitting some of these spectra using Lorentzian line shapes [15]. Although inhomogeneous broadening sources must also exist, in the present context these have yet to be analyzed quantitatively. A detailed theoretical discussion of spectral broadening in He droplets can be found in Ref. [24], where several sources of inhomogeneous broadening, related to the finite size of the droplets, are discussed.

Recently, purely rotational transitions of cyanoacetylene in ^{4}He droplets have been detected via microwave (MW) single- and double-resonance spectroscopies [29]. These studies provided evidence of fast (2–20 ns) rotational relaxation, while at the same time the saturation behavior of the observed transitions clearly indicated that the MW line profiles were dominated by inhomogeneous broadening mechanisms. On the other hand, the MW-MW double-resonance spectral holes and peaks had widths comparable to those of the single-resonance lines, a situation usually associated with homogeneous broadening. To rationalize these results it was proposed that the inhomogeneous broadening was dynamic, i.e., that there was a faster, rotationally "elastic", relaxation process occurring within the manifold of states that give rise to the inhomogeneous broadening. Such states, which might for example include the "particle-in-a-box" levels mentioned below, will be referred to as "hidden", because they are not directly probed by the kind of spectroscopy experiments discussed here. In view of the results obtained in the present experiment and of a more refined model for dynamic broadening, some of the previous (yet unpublished) data have been revisited and will be presented in Sec. 6.4.

A recent model for dopant–host interactions in a finite-size He droplet [24] shows that the energy gained by solvation of the dopant generates a trapping potential which confines the dopant in the nanodroplet. Quantization of the motion of the molecule within the droplet, in such a potential, gives levels that are spaced by $\approx 0.015\,\mathrm{cm}^{-1}$ (for SF_6), implying that at 0.4 K hundreds of states will be populated. These levels, which closely resemble those of a 3-D harmonic oscillator, are referred to as "particle-in-a-box" levels to emphasize their origin from the confined translational motion of the impurity. The different solvation energies associated with each "particle-in-a-box" state result in a slight frequency spread for the rotational transitions of the guest molecule, thus providing a mechanism for inhomogeneous broadening. For nonspherical molecules, there is an additional contribution to the frequency spread, which is of comparable magnitude, namely that originating from the orientation- and velocity-dependent hydrodynamic interactions of the molecule with the helium. In particular, for linear polar molecules, theory predicts [24] that the degeneracy over the magnetic quantum number (M) is partially lifted, giving rise to line splittings. Concurrently, Nauta and Miller have observed line splittings for HCN in ^{4}He droplets [22], and were able, by addition of an external Stark field, to correlate the different features of the R(0) line to different values of $|\Delta M|$. These authors interpreted their findings in terms of the model of Ref. [24] and also showed that a relatively modest field ($\approx 5\,\mathrm{kV/cm}$, i.e., $\approx kT/\mu_{\mathrm{HCN}}$ at 0.4 K) can induce line splittings of comparable magnitude to those occurring in the field-free case.

The models proposed in Ref. [24] are to date the only ones that provide a methodology to predict the observed line shapes. However, quantitative agreement with experiments is still lacking, suggesting that important interactions are still missing from the models. Additional experimental data are needed to aid the

development of a quantitative theory. Indeed, experimental schemes that simplify the interpretation of the data are clearly needed. With this in mind, we present here a series of microwave-infrared double-resonance (MW-IR DR) experiments in which the IR probe laser can continuously scan the entire vibrational band, thus probing the entire manifold of rotational states, including those not directly coupled by the MW pump. In principle, absorption of only one IR photon per molecule is necessary to produce a detectable signal (as opposed to the multiple absorption-relaxation cycles in the MW-MW DR experiment [29]), resulting in greater signal-to-noise ratios and a simplified picture of the interaction of the molecule with the probing radiation. Finally, frequency-dependent, MW-induced noise on the bolometer detector, which has been observed to affect the microwave experiments, can be minimized in MW-IR DR experiments by keeping the MW frequency fixed and scanning the probe laser.

By use of bolometer-detected infrared molecular beam spectroscopy, we have measured the single-resonance IR spectra of the ν_1 band of cyanoacetylene embedded in helium droplets. Furthermore, in a double-resonance experiment, a MW field has been overlapped to the IR laser, to "tag" the NCCCH molecules in specific rotational and "hidden" states. A comparison between the spectra obtained in the two experiments provides information on the relative importance of homogeneous and inhomogeneous line broadening for this system; possible candidate mechanisms for broadening are also discussed. Analysis of the observed spectral features as a function of the average droplet size shows that the latter plays an important role in determining the dynamics of rotational relaxation. A qualitative model connecting the rotational relaxation to the bath of surface oscillations of the droplet (ripplons) is proposed to explain this observation.

Concurrent with the present work, an independent MW-IR DR experiment has

been performed on the OCS ν_3 fundamental transition by Grebenev *et al.* [30]. The two studies reach similar conclusions, though many of the details differ, likely reflecting the different dynamics experienced by the respective molecules in the He droplet.

6.2 Experimental

The present experiments were carried out at the University of North Carolina, using a helium nanodroplet spectrometer whose schematic is presented in Fig. 6.1. A detailed description of the apparatus was given previously [31], so only a brief overview is given here, focusing on the modifications that were necessary to perform the MW-IR DR experiments. A beam of helium droplets was formed by expanding ^{4}He (99.9999% pure) from a stagnation pressure of 50 atm, through a 5 μm diameter nozzle cooled to $\approx$ 20 K. A skimmer was used to sample the center of the expansion into a second vacuum chamber, where it passed through a 10 cm long pickup cell, in which a low pressure ($\approx 3 \times 10^{-6}$ Torr, uncorrected for ionization efficiency) of cyanoacetylene was maintained. This pressure was adjusted to maximize the number of singly-doped droplets, by monitoring the laser-induced signals associated with a single molecule solvated in a helium droplet. IR spectra were recorded by exciting the CH stretching vibration (ν_1 band) of cyanoacetylene at $\approx 3327\,\mathrm{cm}^{-1}$ with an F-center laser (Burleigh FCL-20). When an IR photon is absorbed and the resulting vibrational energy relaxes into the helium droplet, the ensuing evaporation of helium ($\approx$ 600 helium atoms per photon) can be detected by a bolometer as a decrease in the droplet beam energy. Control over the average helium droplet size $\langle N \rangle$ was achieved by varying the nozzle temperature T_n and using the calibration given in the literature [32].

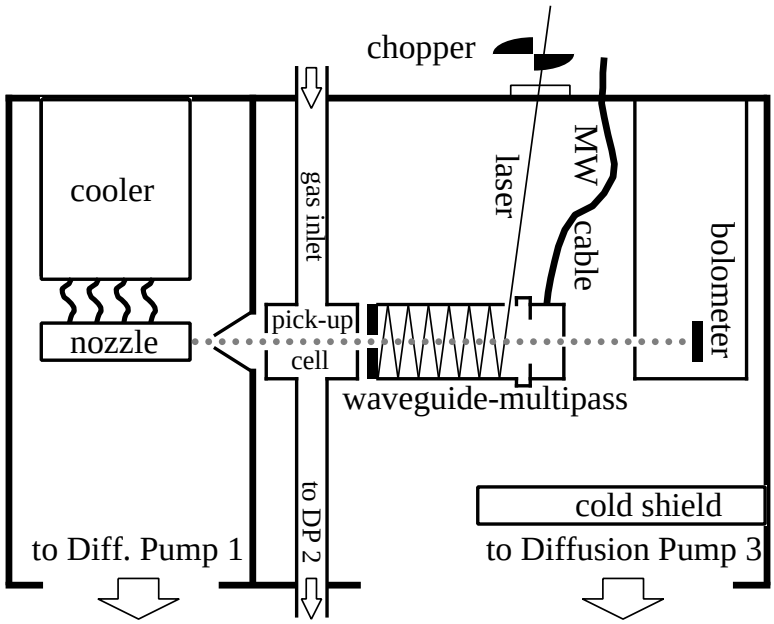

Figure 6.1: Schematic of the experimental apparatus

Given that the laser power ($\approx 30\,\mathrm{mW}$) is insufficient to saturate the cyanoacetylene transitions, we used multiple crossings between the laser and droplet beam to improve the excitation efficiency. Since the entire laser interaction region needs to be irradiated by a contained MW flux, we placed two gold coated glass slides inside an X-band waveguide (facing one another along the short sides) to act as a laser multipass cell. A small hole was drilled in the waveguide to admit the laser, as shown in Fig. 6.1. The MW radiation (typically 100 mW in the frequency range 7–13 GHz, corresponding to a field strength of $0.8\,\mathrm{kV/m}$ in the center of the waveguide) was generated with a sweeper (HP 8350 B)/amplifier (Logi Metrics A310/IJ) combination and coupled into the waveguide via a coaxial cable and a modified SMA-to-waveguide adapter. The other end of the waveguide was terminated with a 1/4" thick plate of absorbing material (Eccosorb MF 124) to minimize both the scattering of microwaves into the experimental chamber and their reflection back

into the waveguide. Small holes in the two ends of the waveguide allowed the helium droplet beam to pass through the excitation region.

To record the single-resonance IR spectra the laser was amplitude-modulated and scanned through the ν_1 band. The relative frequencies were calibrated using three confocal étalons; a wavemeter provided an absolute reference. MW-IR DR spectra were measured by fixing the microwave frequency at 9.08 GHz, corresponding to the $J = 2 \rightarrow 3$ transition of ground state cyanoacetylene. The microwaves were amplitude modulated while the cw laser was scanned without modulation. In both cases, the bolometer signals were processed using a phase sensitive detector (lock-in). As for whether the MW source should be modulated and the IR scanned or viceversa, we found that the mere presence of a MW field (leaking out of the waveguide) inside the bolometer chamber, induced a signal on the bolometer whose magnitude was strongly frequency dependent. If the MW source is kept at a fixed frequency this disturbance only appears as a constant baseline offset on the measured spectrum, whereas, if the MW source is scanned, this disturbance induces additional features that have to be eliminated by subtraction of a blank scan. For this reason the first scheme was chosen; the resulting spectrum is the DR spectrum riding on top of the constant, pure microwave, background at the frequency of the MW pump.

6.3 Single-resonance results: IR

Fig. 6.2 shows the single-resonance ν_1 IR spectrum of cyanoacetylene, solvated in helium nanodroplets of different sizes. One immediately notices that for small droplet sizes (roughly, below 3000 atoms) the spectral lines are irregularly shaped, and exhibit distinct structures (additional sharp peaks or splittings). Qualita-

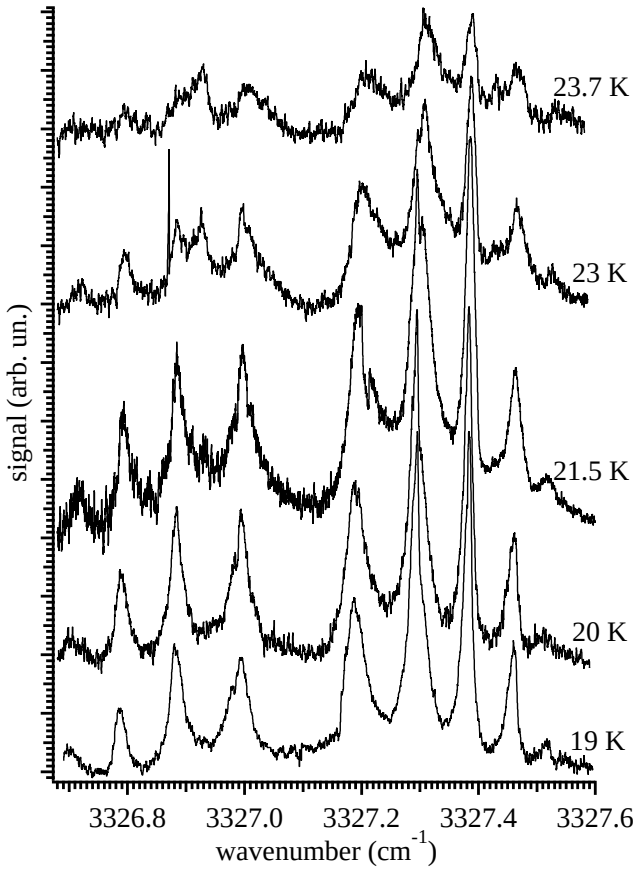

Figure 6.2: Single-resonance spectra of the ν_1 band of NCCCH embedded in ^{4}He clusters for different nozzle temperatures (estimated cluster sizes are, top to bottom: 1650, 1900, 2650, 3650, 4600).

tively, similar structures have been predicted in [24], and later in this paper we will appeal to these similarities to corroborate some of our conclusions. However, a quantitative analysis would require a detailed treatment of a reasonably parameterized NCCCH–droplet Hamiltonian, which is at present not available.

For larger droplet sizes, spectral lines become smoother and better resolved. It is then possible to model their shape with simple empirical functions, facilitating the fitting procedure used to determine the spectroscopic constants. The spectrum obtained at a nozzle temperature of 20 K ($\langle N \rangle \approx 3500$) was chosen for a complete

fit. The intensity (integrated area) and position (center of gravity) of each line are determined by the values of the spectroscopic constants and by the temperature, which, along with the linewidths, are the free parameters of the fit. We found that Lorentzian profiles are well suited to reproduce the shape of all the rotational lines, except for R(0) and P(1) which are visibly asymmetric. To reproduce the shape of the latter two lines, we have tested several simple analytical functions, and found that the most satisfactory is the convolution between a Lorentzian and a half exponential [$\exp(-x/x_0)$ for $x > 0$, and 0 otherwise], which only adds 1 extra parameter, x_0. Although our choice is purely empirical, we note that such a line shape is expected if (in addition to Lorentzian broadening) a line shift mechanism were present such that: (1) the shift is proportional to the thermal energy of the NCCCH molecule, and (2) the density of states is energy-independent. Similar functional forms for the line shape have been obtained in Ref. [24] by use of models in which a dopant molecule with greater thermal energy approaches more closely the surface of the droplet, undergoing therefore a greater line shift.

Table 6.1: Molecular parameters determined for the helium solvated NCCCH (see Fig. 6.3), compared with the corresponding gas phase values [37]. Units are MHz unless otherwise indicated. 1σ statistical uncertainties are given in parenthesis, based upon rms noise in the baseline. Since the rotational lines partially overlap, the intensity of each peak (hence the parameters of the fit) might depend on the functional form chosen to model individual peaks, and slightly more conservative uncertainties should be used.

	T (K)	ν_0 (cm^{-1})	$\overline{B}$	ΔB	$\overline{D}_J$
Free	$\cdots$	3327.37085	4545.422	-7.275	5.430×10^{-4}
Droplet	0.348(2)	3327.092(1)	1573.7(7)	-19.4(6)	5.00(5)

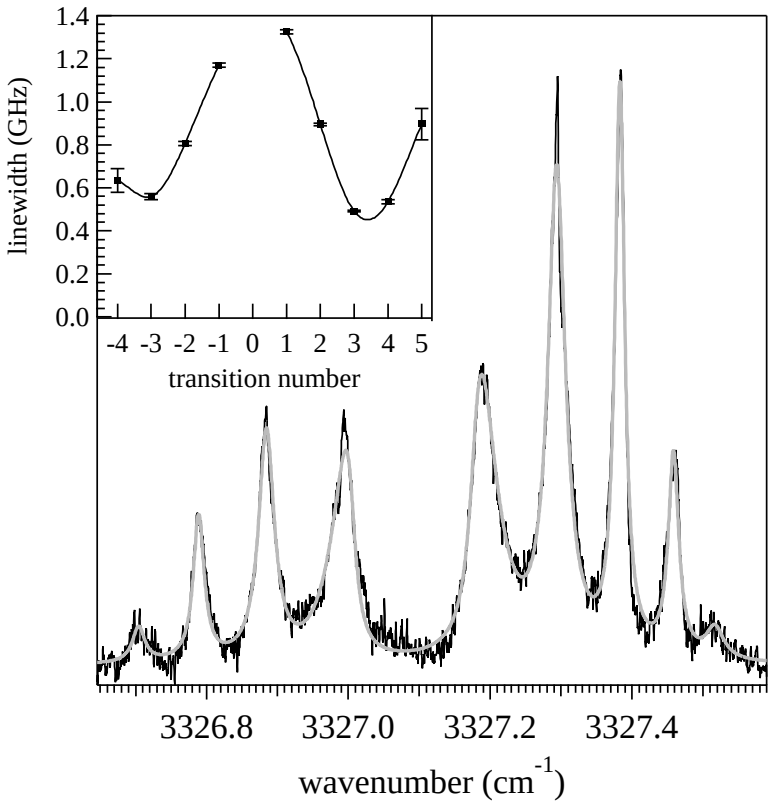

Figure 6.3: Comparison of the experimental spectrum taken at $T_{\mathrm{n}} = 20\,\mathrm{K}$ (see Fig. 6.2) with the best fit to a linear molecule Hamiltonian. Lorentzian line shapes are used for all but the P(1) and R(0) lines (see text). In the inset the linewidths (FWHM) are plotted against the transition number, m, with the line as a guide to the eye. The other fit parameters are reported in Table 6.1.

Typically, the ro-vibrational spectra of molecules in He droplets [9, 15, 31] indicate that the symmetry of the associated rotational Hamiltonian is the same as for the gas phase molecule (for an exception, see Ref. [31]), and indeed our spectra do not show a Q branch, as expected for a linear rotor in a Σ vibronic state. We therefore fit the spectrum to a linear-molecule Hamiltonian, obtaining the parameters given in Table 6.1 (the simulated spectrum is the solid line through the data in Fig. 6.3). Analysis of the results confirms the trends previously observed

for SF_6 and OCS [9, 15], namely: (1) due to the additional inertia of the liquid helium, the rotational constant is a fraction (34.6%) of that of the gas phase molecule; (2) the wave number shift of the band origin relative to the gas phase is small (-0.279 cm^{-1}, the sign indicates a net increase in solvation energy for the excited vibrational state); (3) the distortion constant D_J is increased by several orders of magnitude [15, 21, 33]; (4) the rotational temperature of the molecule is almost identical to previously reported values [9, 15]; the slight difference is most likely a reflection of the fact that rotational lines are partially overlapping, so that their relative intensities somewhat depend on the choice of the function modeling the line shape (see caption to Table 6.1).

The fit also provides us with the linewidths (FWHM), which are plotted against the transition number, m, in the inset of Fig. 6.3. One can appreciate the almost perfect symmetry between the P ($m < 0$) and R ($m > 0$) branches, and the strong dependence on m. It is also interesting that the linewidth decreases with $|m|$ (i.e., with increasing J), reaches a minimum at $|m| = 3$ and then starts increasing again (unlike the case of OCS [33], where the linewidth increases monotonically with $|m|$). While we can't identify the sources of broadening with certainty, our observations for the single-resonance spectra (in particular the asymmetric shape of the R(0) and P(1) lines, and the appearance of sharp features on top of broader peaks observed for small size droplets) indicate that broadening must be predominantly inhomogeneous.

Also, in view of the similarity of the line shapes and widths observed in the single-resonance MW and IR spectra, we believe that the same broadening mechanisms dominate in both cases. Hence, we assume that vibrational dephasing and/or relaxation processes, two common causes of homogeneous broadening, do not dominate the overall linewidth, at least for this particular molecule. If the

narrowest observed linewidth (≈ 500 MHz FWHM) is used to determine a lower limit to vibrational lifetimes, the latter must be much greater than 0.6 ns.

6.4 Revisitation of the MW and MW-MW DR results

In the original microwave work [29], it was proposed that the nature of the inhomogeneous broadening is dynamic, in that, as a result of the random motion of the NCCCH molecule inside the droplet (termed "elastic" relaxation), the frequency associated with a given rotational transition fluctuates at a rate which is faster than that of rotational relaxation. The saturation behavior of the single-resonance MW signal for the R(4) transition was used, together with the conventional formula for static inhomogeneous broadening, to estimate a lower limit for the rotational relaxation time (2 ns). A comparison of the linewidths for the single- and double-resonance spectra provided an estimate of the ratio of the "elastic" to the rotational relaxation times (≥ 10). All of this was based upon a rather crude model: A two-level system described by the rotational relaxation time scale and by the time scale of going in- and out-of-resonance with the MW radiation. Finally, an independent "pulsed microwave" experiment provided an upper limit to the rotational relaxation time (20 ns).

In the course of the present experiment we probed the saturation behavior of the R(2) line of the pure microwave spectrum, and found it to be significantly different from that previously measured for the R(4) line. While trying to interpret these new data, we realized that we needed a model in which the influence of "elastic" relaxation on the saturation behavior was properly accounted for, which was not the case for the static formula of Ref. [29].

The problem of a fluctuating two-level system coupled to a radiation field has been thoroughly discussed in the literature, and a treatment of general validity is available in the framework of the so called "sudden modulation theory" [34]. In particular, we found it possible to express the saturation behavior of both the R(2) and R(4) lines with an analytical formula containing the "elastic" relaxation time as a parameter. A complete description of the model, and how it maps onto our system, is given in Section 6.8; here we only need to introduce, according to the notation of Ref. [34], the "elastic" (τ_0) and rotational (T_1) relaxation times, and the Rabi frequency of the system (χ). The latter is proportional to the MW electric field, hence to the square root of the MW power, P_{MW} (see Eq. 6.17).

Using the present setup, we measured the single microwave resonance signal, as a function of P_{MW}, for the R(2) transition at 9.08 GHz. We then used Equations (6.13) through (6.17), at zero detuning, to estimate the MW-induced population transfer, which we assumed to be proportional to the single-resonance

Table 6.2: Fit parameters for the saturation behavior of the R(2) and R(4) rotational transitions of NCCCH (see Fig. 6.4). Since the exact values of T_1 and T_2 are very sensitive to the value of the ratio τ_0/T_1, the present fit only provides an estimate of their magnitude, which is however consistent with that of Ref. [29]. The value of Δ was fixed by the width of the corresponding line.

Transition	τ_0/T_1	T_1 (ns)	T_2 (ns)	Δ (ns)$^{-1}$
R(2)	1	63	5	1.2
R(2)	0.1	45	45	1.2
R(4)	1	14	14	2.35
R(4)	0.1	17	17	2.35

signal. The same analysis was performed for the data in Fig. 1 of Ref. [29], which concern the R(4) transition. The experimental data and best fits appear in Fig. 6.4. We see that, if the fast modulation condition ($\tau_0 \ll T_1$) is enforced (by setting $\tau_0 = 0.1\,T_1$ in the fit), the fit poorly reproduces the low χ behavior of both the R(2) and R(4) lines. The onset of saturation (roughly where the curve turns from quadratic to linear) occurs at a much higher χ for the model than for the experimental data. The fit improves, however, if one sets $\tau_0 \approx T_1$, or $\tau_0 \gg T_1$, with almost no difference between the two cases. At this level of theory and experimental data available, it is not possible to say if modulation occurs on a similar time scale as rotational relaxation ($\tau_0 \approx T_1$), or if a static picture ($\tau_0 \gg T_1$) should be adopted. On the other hand, the absence of narrow hole burning in the MW-MW DR experiment (see below) rules out the second hypothesis.

In the intermediate condition $\tau_0 \approx T_1$ a double-resonance line should appear as the superposition of the narrow feature expected in the static case and the broad one expected in the fast modulation case. With this in mind, we reinspected our MW-MW DR data at low power, recovering holes as narrow as ≈ 100 MHz on top of a much broader and more intense line (Fig. 6.5). We observe an important difference between "holes" (produced by depletion of the lower of the two levels coupled by the MW probe field) and "peaks" (produced by population transfer to the higher of the two levels coupled by the MW probe field), in that only the former show narrow features, while the latter are always as broad as the corresponding single-resonance peak. In the MW-MW DR scheme there is an inherent difference between "holes" and "peaks" that can be invoked to explain this different behavior: in the "hole" case, the pump and probe fields share the same two manifolds of levels, so, in the static limit, the pump and probe field must be at resonance within the homogeneous linewidth, in order to induce a

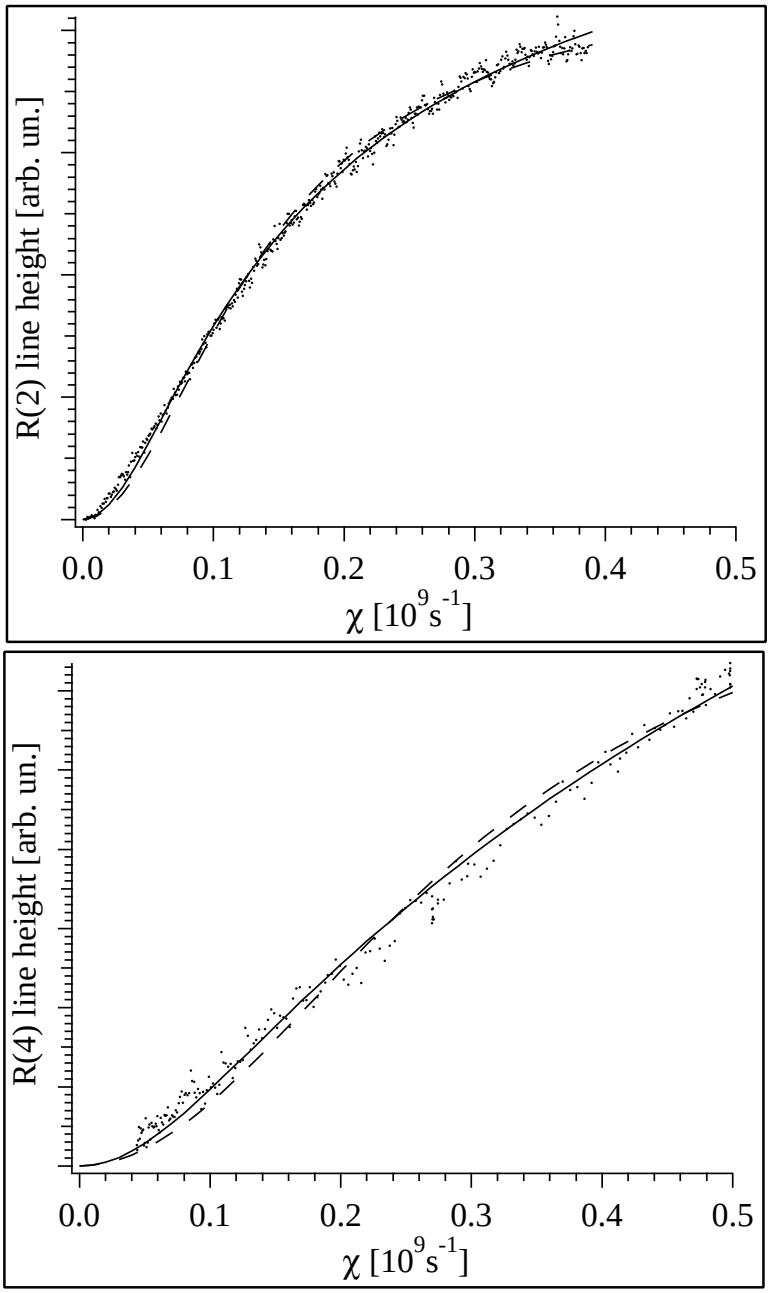

Figure 6.4: Saturation behavior of the R(2) and R(4) purely rotational microwave transitions of NCCCH in He droplets. The solid and dashed lines through the data are the best fits, with $\tau_0 = T_1$ and $\tau_0 = 0.1\,T_1$ respectively, according to the "sudden modulation" model (see Section 6.8). The fit parameters are reported in Tab. 6.2

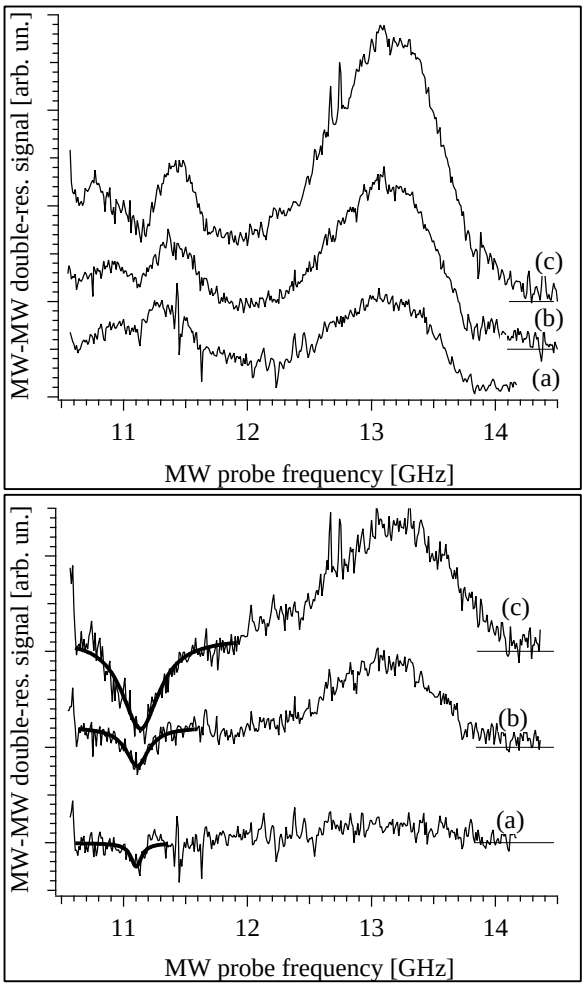

Figure 6.5: MW-MW double-resonance spectra of the R(3) and R(4) transitions of NCCCH. Top panel: as measured. Bottom panel: after subtraction of a suitably scaled reference spectrum, to flatten out the baseline of the R(3) transition and evidence the presence of narrow holes at the pump frequency (11.1 GHz). The experimental apparatus and procedure used to acquire the above spectra differ from those of the present work, and are described in [29]. Experimental conditions are: (a) pump power 0.3 W, probe power 0.8 W; (b) pump power 0.8 W probe power 0.8 W; (c) pump power 0.8 W, probe power 2.4 W. Fitting the hole to a Lorentzian shape (right panel, thick line) gives a FWHM of 105, 220 and 370 MHz respectively.

double-resonance signal. In the "peak" case, three manifolds of levels are involved, because only the intermediate one is shared between the probe and pump field. It is then possible that for a given pump frequency there exists a spread of matching probe frequencies, particularly if more than one broadening mechanism is present, as we confirmed by simple simulations, using the classical formulas presented in Ref. [24].

In summary, based on available data, we are lead to the conclusion that the inhomogeneous broadening of rotational lines of NCCCH in He droplets is dynamic, on a time scale which we tentatively estimate to be similar to that of rotational relaxation.

6.5 MW-IR double-resonance results

Figure 6.6 shows an energy level diagram illustrating the principle of the MW-IR DR experiment. The amplitude-modulated, fixed-frequency MW radiation is in resonance with the $J = 2 \rightarrow 3$ transition, while the IR laser is tuned through the entire spectrum. In the absence of any relaxation processes, this scheme simply transfers population from $J = 2$ to $J = 3$, which would result in the weakening of the R(2) and P(2) transitions in the IR, and an enhancement of the R(3) and P(3) transitions. Figure 6.7 shows a series of MW-IR DR spectra, taken at different source temperatures (droplet sizes), corresponding to the R branch region of the spectrum shown in Figure 6.2. For the large droplets, we observe exactly what is expected, namely the depletion of R(2) and the enhancement of R(3) (although not shown, we see the corresponding changes in the P branch). For smaller droplets however, the double-resonance signals are observed on all IR transitions. Before discussing this phenomenon, it is interesting to examine the

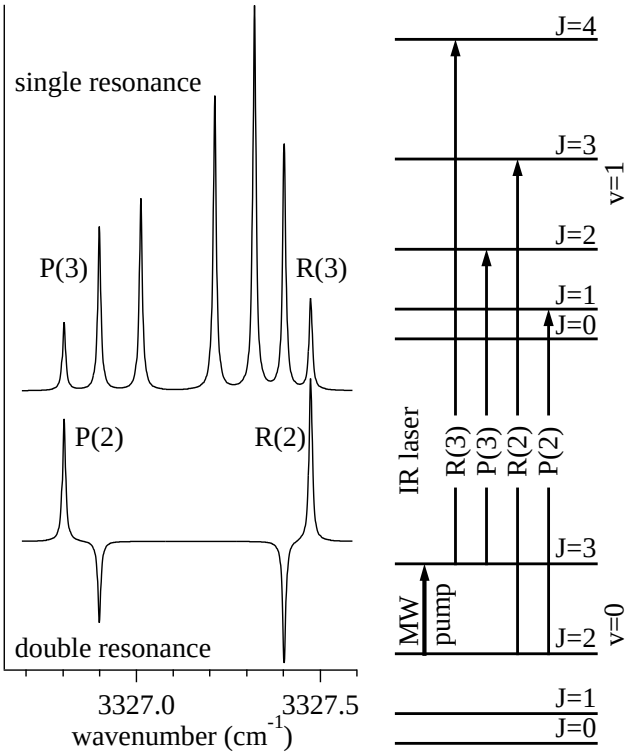

Figure 6.6: Energy level diagram showing the double-resonance scheme used in the present experiment (right) and the idealized single- and double-resonance spectra (left) typically observed when only the populations of the states coupled by the pump radiation are affected (e.g., for free molecules).

line shapes of the "normal" MW-IR DR spectra, which are obtained in the large droplet limit.

In these experiments, both the microwave (100 mW) and the IR power (30 mW) are sufficiently low to exclude power broadening. Furthermore, in a MW-IR double-resonance experiment, because of the change in vibrational quantum number, three manifolds of "hidden" levels are always involved, even when a hole is being detected. Hence, if the argument we gave in the previous section to explain the difference between the width of holes and peaks in the MW-MW DR

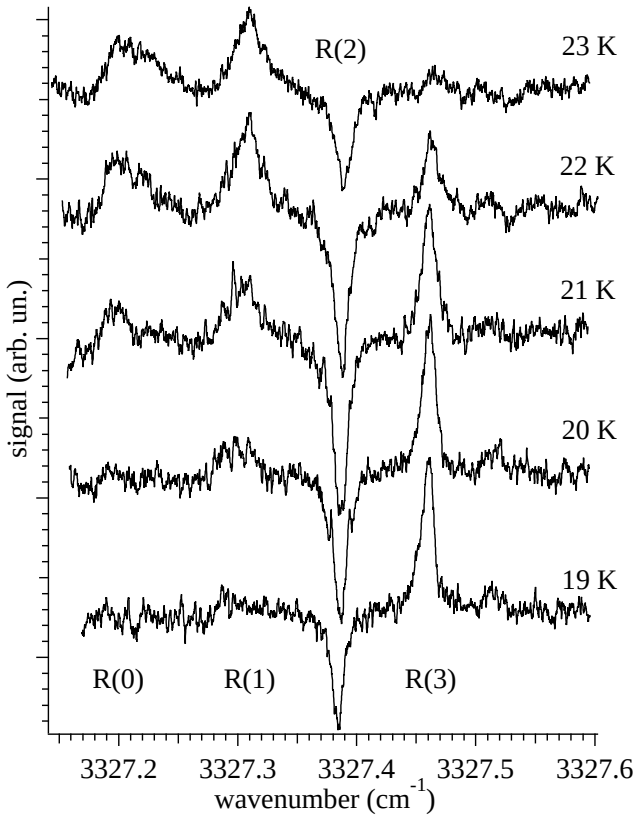

Figure 6.7: Double-resonance spectra of the R branch of the ν_1 band of NCCCH in He droplets for different nozzle temperatures (estimated cluster sizes are, top to bottom: 1900, 2350, 2950, 3650, 4600). The MW pump frequency was set at 9.08 GHz, corresponding to the center of the R(2) transition.

measurements holds, we expect to observe no such differences in MW-IR DR measurements. We also expect the width and shape of the MW-IR DR lines to be very similar to that of the corresponding peaks in the single-resonance IR spectra. In both cases, our expectations correspond just to what we observe.

We return now to the issue of why MW-IR double-resonance signals are observed on rotational transitions that are not directly pumped by the microwaves, showing that the cyanoacetylene molecules are also undergoing rotational relax-

ation on the time scale of the experiment. What is most interesting is the fact that these extra signals (hereafter referred to as "relaxation-induced satellites") disappear for larger droplets (above ≈ 4000 atoms). At first sight, this seems to suggest that, for the larger droplets, the rotational relaxation rate is slow with respect to the time spent in the laser field by the doped droplets (≈ 0.2 ms). However, this is inconsistent with the fact that the molecules are rotationally cold, which means that, even for the larger droplets, there must be rapid rotational relaxation after pickup. The possibility of detecting pure MW spectra [29] also shows that rapid rotational relaxation occurs in the larger droplets as well. Finally, the detailed analysis carried out in Ref. [29], and our estimate (see Table 6.2), place the time scale for rotational relaxation in the 1–10 ns range. We must then look for a mechanism that, for large droplets, can eliminate the "relaxation-induced satellites" in the DR experiment even when rotational relaxation is still occurring. In other words we need to impose that the net rate for population transfer in and out of the rotational levels *not directly pumped by the microwaves* be zero. This seemingly arbitrary condition is routinely assumed in general relaxation problems (not necessarily rotational), and is identified by the terms "noncorrelated" [34], or "strong collision" [36], relaxation. The theoretical formalism that describes this "strong collision" regime is going to be adapted to our problem in the next section.

6.6 Relaxation-induced satellites in the "strong collision" regime

We first define $\mathbf{P}$ as the (column) vector whose components, P_J, are the populations of the rotational level with quantum number J. E_J are the corresponding level energies, k_B is the Boltzmann constant, and $\mathbf{M}$ is the rate matrix defined by:

$$\frac{d\mathbf{P}}{dt} = \mathbf{M}\cdot\mathbf{P} \Leftrightarrow \frac{dP_J}{dt} = \sum_{J'} M_{J,J'}P_{J'} \tag{6.1}$$

With this definition, $M_{J,J'}$ is the population transfer rate **from** level J' **into** level J. A superscript (0) will indicate values at thermal equilibrium, and in the absence of microwaves. We have then:

$$P_J^{(0)} = (2J+1)\exp\left(-\frac{E_J}{k_\mathrm{B}T}\right) \tag{6.2}$$

$$M_{J,J'}^{(0)} = M_{J',J}^{(0)}\frac{2J+1}{2J'+1}\exp\left(-\frac{E_J - E_{J'}}{k_\mathrm{B}T}\right) \qquad (J \neq J') \tag{6.3}$$

$$M_{J,J}^{(0)} = -\sum_{J'\neq J} M_{J',J}^{(0)} \tag{6.4}$$

$$\mathbf{M^{(0)}}\cdot\mathbf{P^{(0)}} = \mathbf{0} \tag{6.5}$$

Equations (6.2–6.4) originate from the Boltzmann distribution and the detailed balance principle. Equation 6.5 corresponds to the equilibrium condition.

When a microwave field coupling $J = 2$ and $J = 3$ is present, a new term k (which is a function of MW power and frequency), appears in the corresponding

elements of the rate matrix, so that:

$$\mathbf{M} = \mathbf{M^{(0)}} + \mathbf{\Delta M} \tag{6.6}$$

$$\mathbf{\Delta M} = \begin{pmatrix} 0 & 0 & 0 & 0 & \cdots \\ 0 & 0 & 0 & 0 & \\ 0 & 0 & -7k & 5k & \\ 0 & 0 & 7k & -5k & \\ \vdots & & & & \end{pmatrix} \tag{6.7}$$

and a new steady state population $\mathbf{P} = \mathbf{P^{(0)}} + \mathbf{\Delta P}$ is established. For the large droplet limit, where we experimentally observe a population transfer from $J = 2$ to $J = 3$ only, we set:

$$\mathbf{\Delta P} = \begin{pmatrix} 0 \\ 0 \\ -\Delta P \\ \Delta P \\ 0 \\ \vdots \end{pmatrix} \tag{6.8}$$

By expanding the new equilibrium condition:

$$\mathbf{0} = \mathbf{M} \cdot \mathbf{P} = \mathbf{M^{(0)}} \cdot \mathbf{P^{(0)}} + \mathbf{M^{(0)}} \cdot \mathbf{\Delta P} + \mathbf{\Delta M} \cdot \mathbf{P} \tag{6.9}$$

and using Eq. 6.5, it is easily seen that for $J \neq 2, 3$ Eq. 6.9 gives $M^{(0)}_{J,2} = M^{(0)}_{J,3}$, i.e., the population transfer rate into a given level J is the same from $J' = 2$ and from $J' = 3$. Since there is nothing special about the coupling between a given J level and either $J' = 2$ or $J' = 3$ (presumably the coupling is unaffected by the presence of a MW field), it is reasonable to assume that, in general, the more restrictive condition $M^{(0)}_{J,J'} = M^{(0)}_{J,J''}$ holds. With this assumption, algebraic manipulation of

Eq. 6.3 gives:

$$M^{(0)}_{J,J'} \propto (2J+1)\exp\left(-\frac{E_J}{k_B T}\right) \quad (J \neq J') \tag{6.10}$$

(For $J = J'$ Eq. 6.4 still holds). Equation 6.10 clearly shows that the rate of population transfer into a given level J is independent of the starting level J' and is only dictated by the fact that the final population of the levels must follow a Boltzmann distribution. This demonstrates the equivalence of our initial requirement on population transfer (Eq. 6.8) and the "strong collision" condition (Eq. 6.10). The latter is commonly assumed to hold in studies of velocity-changing collisions of atoms (see, e.g., [36]), from where the term "strong collision" was borrowed. The underlying assumption is that a single "collision" (or better, relaxation event) is sufficient to completely "erase" the memory of the molecule with regard to its initial (rotational, in our case) state. Incidentally, Eqs. (6.8), and (6.9) also hold for the very special case where $\mathbf{M^{(0)}} = \mathbf{0}$, namely when there is no relaxation (which we know is not the case here).

Assuming the "strong collision" mechanism is responsible for the disappearance of the "relaxation-induced satellites" in the larger droplets, we must now justify their appearance in the small droplets. In particular, why does the molecule retain memory of its initial state after the relaxing "collision". We must first consider the fact that the energies of the phonons and rotons are much larger than the rotational energy of cyanoacetylene for droplets of all sizes. As a result, dissipation of rotational energy into the bulk modes does not seem possible (the lowest such mode in a 10^3 He droplet has been estimated to be 2.6 K [17]). The implication is that the rotational relaxation of cyanoacetylene cannot create such quanta. In addition, these excitations are not thermally populated, so that the corresponding inelastic scattering is not a viable mechanism for rotational relaxation. We are

thus lead to consider the "heat bath" associated with surface excitations, known as ripplons, which are much lower in energy (0.33 and 0.1 K for a 1000 atoms or 10000 atoms droplet, respectively [17]). While the impurity–ripplon coupling has been estimated to be quite small for a molecule located near the center of an average-sized droplet, its magnitude increases rapidly as the impurity approaches the droplet surface [24]. It is therefore reasonable to propose that rotational relaxation occurs primarily when the impurity molecule "collides" with the surface of the droplet. At typical droplet sizes (3–5 nm) and thermal velocities ($\sim$10 m/s) the interval between "collisions" is of the order of 10^{-9} s [24].

Assuming this is the relaxation mechanism, we must now consider why the surface "collisions" would be in the "strong collision" regime for the larger droplets and not for the smaller ones. It is important to note that one of the requirements for the "strong collision" regime is the presence of a "fully statistical" heat bath: in other words, the molecule must be able to transfer any given amount of (rotational) energy and angular momentum to the bath with equal probability. Hence the structure of the bath (in particular its discreteness) must not influence this probability. It is well known that the density of ripplons decreases exponentially with decreasing droplet size, along with a corresponding increase in the level spacing. We therefore postulate that only large droplets provide a sufficiently structureless heat bath to give rise to "strong collision" conditions.

It is interesting to note that in an independent MW-IR DR experiment performed on OCS in helium by Grebenev *et al.* [30], "collisional satellites" of the type discussed above were also observed, at a much larger droplet size ($\approx$ 6000). Taken together with the present results, this might indicate that the nature of the rotational energy transfer processes depends not only on the properties of the helium droplet, such as the density of ripplons at the surface, but also on the de-

tailed nature of the solute–helium interactions. In the case of cyanoacetylene, the large dipole moment of the impurity likely dominates the interactions and may give rise to the behavior discussed above. The smaller dipole moment of OCS may result in a different rotational relaxation mechanism that depends differently on the droplet size.

With regard to the DR spectra associated with the smaller droplets, it should also be noted that the collisional satellites for $J = 0$ and 1 are both positive. The implication is that collisional transfer into these two states, from the MW pumped $J = 3$ level, dominates over the transfer from these states into the hole in $J = 2$ produced by the MW pumping. It is interesting to note that the long range impurity–helium interactions (dipole–induced dipole) are dominated by even Legendre terms [24] so that one would predict that "ΔJ = even" selection rules would apply. Thus depleting the $J = 2$ level by MW pumping would result in a population transfer out of $J = 0$, giving rise to a negative DR signal on the R(0) transition, rather than the enhancement that is observed. Even more curious is the fact that, for the smallest droplets, the positive collisional satellites become even larger than the R(3) signals, the latter arising from direct MW pumping. Unfortunately, a quantitative interpretation based solely on the rates of population transfer is not possible at this point. If population transfer was the sole mechanism responsible for the observed double-resonance spectra, conservation of total population would dictate that the total signal (corrected with appropriate Hönl-London factors) must sum to zero. Instead we observe that the enhancement summed over all J levels is substantially greater than the deficit in the $J = 2$ level. We do not have a good explanation for this behavior, even though it is observed for a wide range of droplet sizes and is very reproducible. Qualitatively, one could think that the microwave pumping may decrease the size of the droplets, and

that this may in turn increase the signal produced by IR absorption. However, a quantitative estimate (assuming that the He evaporation is close to thermal) give far too small an effect to explain this observation. It is interesting to note that similar effects are observable in the OCS IR-MW DR spectra reported in Ref. [30].

6.7 Conclusions

The MW-IR DR experiments presented here firmly establish two important facts about the nature of the interactions between a polar, solvated molecule and its helium nanodroplet host. First, the broadening observed in both the pure IR and the MW-IR DR experiments is confirmed to be inhomogeneous. Second, the broadening mechanism is found to be dynamic, meaning that individual molecules explore the states that contribute to the inhomogeneity on a time scale that, in our best estimate, is comparable to that of rotational relaxation. Pump-probe experiments with suitable pulsed lasers and/or microwave sources should be able to provide more stringent estimates for the various relaxation rates. However, the width of these pulses must be carefully controlled to allow a portion of the inhomogeneous distribution to be pumped, yet allow sufficient time resolution so that elastic and inelastic relaxation could be probed.

The present measurements further demonstrate that there is a dramatic change in the nature of the rotational relaxation with droplet size. The results suggest that rotational relaxation occurs via coupling with the ripplons when the cyanoacetylene molecules "collide" with the surface of the droplet. In large droplets a "strong collision" regime appears to hold, meaning that a single "collision" with the surface is sufficient to completely erase all memory of the molecules' previous history. As a consequence, double-resonance signals are only observed

on transitions involving states that are directly pumped by the microwaves. For smaller droplets, the energy transfer rates deviate from this statistical behavior, resulting in double-resonance signals on all transitions. This qualitatively different behavior is rationalized in terms of the density of ripplons at the surface, which increases dramatically with droplet size, thus making energy conservation less of a restriction for the larger droplets, and hence the relaxation process more statistical. While further work will be necessary to fully clarify this difficult problem, the present work provides a relatively solid basis on which to build future efforts.

6.8 The sudden modulation model

To describe a two-level system, coupled by a radiation field, in a fluctuating environment we will introduce first the model of Ref. [34] and its original notation. Next, we will show how the model maps onto our system. According to the treatment of Ref. [34] the system under investigation is approximated to a two-level system with a time-dependent separation between the two levels, $\epsilon(t)$. The following simplifying assumptions are made: (1) $\epsilon(t)$ is characterized by a Gaussian random distribution around a center frequency ω_0, with variance Δ (FWHM $= 2\Delta\sqrt{2\ln 2} \approx 2\Delta$); (2) $\epsilon(t)$ changes instantaneously (sudden modulation) at random times separated, on average, by a time interval τ_0; (3) the new value of ϵ does not depend on the old one (non-correlated process). Three additional parameters are necessary to complete the model: the population and coherence relaxation times (T_1 and T_2, respectively), and the Rabi frequency of the system (χ). The presence of a radiation field at a frequency ω induces a transfer of population between the two levels, such that at steady state the population

difference between the two levels is given by:

$$\bar{n}_s = \frac{n_0}{1 + 2W_s T_1}. \tag{6.11}$$

n_0 is the population difference in the absence of radiation, and W_s is defined by the following formulas:

$$2\,W_s = \frac{\chi^2 \tau_0 \left[I_0 - (1+w^2) I_0^2 - I_1^2\right]}{(1-I_0)^2 + (1+\alpha w^2) I_1^2 + \alpha w^4 I_0^2 - (1+\alpha) w^2 I_0 (1-I_0)} \tag{6.12}$$

$$I_0 + i I_1 = \frac{1}{q}\sqrt{\frac{\pi}{2}}\left[\frac{\mathrm{Re}(A)}{\sqrt{1+w^2}} - i\,\mathrm{Im}(A)\right] \tag{6.13}$$

$$A = \exp(\xi^2)\left[1 - \mathrm{erf}(\xi)\right] \tag{6.14}$$

$$\xi = \frac{1}{q\sqrt{2}}\left[\alpha\sqrt{1+w^2} + i\,\Delta\omega\,\tau_0\right] \tag{6.15}$$

$$w^2 = \frac{(\chi\tau_0)^2}{\alpha\beta};\ \alpha = 1 + \frac{\tau_0}{T_2};\ \beta = 1 + \frac{\tau_0}{T_1} \tag{6.16}$$

where by definition $\Delta\omega = \omega - \omega_0$, is the detuning between the two level system center frequency and the radiation field, and $q = \Delta \cdot \tau_0$ is called the narrowing parameter. Although the use of the symbol $\Delta\omega$ is ambiguous, we will retain it for sake of consistency. In no case it should be intended as the product of the two quantities Δ and ω.

We will now map the sudden modulation theory onto our system by using the line broadening model for dopant molecules in He droplets proposed in Ref. [24] (according to which the motion of the dopant inside the droplet is quantized into a set of "particle-in-a-box" states). We identify the two level system with the two rotational levels of the NCCCH molecule that are coupled by the MW radiation field, Δ with the (inhomogeneous) linewidth of the corresponding transition (caused by the molecule-droplet interaction, which is a function of the "particle-in-a-box" state the molecule is in), and τ_0 with the average residence time of the dopant molecule in a given "particle-in-a-box" state. Transitions between the latter states require exchange of energy and angular momentum with a "heat bath",

which we identify with the thermally populated surface wave excitations of the droplet (ripplons) [17, 24]. If this attribution is correct, we expect τ_0 to be of the same magnitude as the time scale for the impurity to travel across a droplet at thermal velocities ($\approx 1\,\mathrm{ns}$ in this droplet size range). The Rabi frequency for a given (lower) level, J, is given by [35]:

$$\chi = \frac{\mu E}{\hbar}\sqrt{\frac{J+1}{3(2J+1)}} \tag{6.17}$$

with $\mu = 3.6\,\mathrm{D}$ the permanent dipole moment of NCCCH and E the amplitude of the electric field inside the microwave guide. In the frequency band we worked at, $E = 2.57\sqrt{P_{\mathrm{MW}}}$, if E is measured in kV/m and P_{MW} is the microwave power measured in W.

In closing, we note that the assumption that the process be "non-correlated" is rather drastic. Rather than a random-walk pattern, the trajectory of an NCCCH molecule inside a droplet may instead resemble a well defined orbit, which is only occasionally randomized. In this case a more refined treatment would be necessary to separate the modulation time (roughly 1 ns in this "orbit" picture) from the correlation time of the modulation, which could be much longer.

Bibliography

[1] K. B. Whaley Annu. Rev. Phys. Chem. **13**, 41, (1994).

[2] J. Higgins, C. Callegari, J. Reho, F. Stienkemeier, W. E. Ernst, K. K. Lehmann, M. Gutowski, and G. Scoles, Science **273**, 629 (1996).

[3] J. P. Toennies and A. F. Vilesov, Annu. Rev. Phys. Chem. **49**, 1, (1998).

[4] K. Nauta and R. E. Miller, Science **283**, 1895 (1999).

[5] M. Behrens, R. Fröchtenicht, M. Hartmann, J. G. Siebers, U. Buck, F. C. Hagemeister, J. Chem. Phys. **111**, 2436 (1999).

[6] P. Sindzingre, M. L. Klein, and D. M. Ceperley, Phys. Rev. Lett. **63**, 1601 (1989).

[7] M. Hartmann, F. Mielke, J. P. Toennies, A. F. Vilesov, and G. Benedek, Phys. Rev. Lett. **76**, 4560 (1996).

[8] K. B. Whaley, *Advances in Molecular Vibrations and Collision Dynamics*, edited by J. M. Bowman and Z. Bacic, (JAI Press, Greenwich, CT, 1998), p. 397.

[9] S. Grebenev, J. P. Toennies, and A. F. Vilesov, Science **279**, 2083 (1998).

[10] J. Higgins, C. Callegari, J. Reho, F. Stienkemeier, W. E. Ernst, M. Gutowski, and G. Scoles, J. Phys. Chem. A **102**, 4952 (1998).

[11] K. K. Lehmann and G. Scoles, Science **279**, 2065 (1998).

[12] F. Stienkemeier, F. Meier, A. Hagele, H. O. Lutz, E. Schreiber, C. P. Schulz, and I. V. Hertel, Phys. Rev. Lett. **83**, 2320 (1999).

[13] V. S. Babichenko and Yu. Kagan, Phys. Rev. Lett. **83**, 3458 (1999).

[14] S. Goyal, D. L. Schutt, and G. Scoles, J. Phys. Chem. **97**, 2236 (1993).

[15] M. Hartmann, R. E. Miller, J. P. Toennies, and A. Vilesov, Phys. Rev. Lett. **75**, 1566 (1995).

[16] J. Gspann, in *Physics of electronic and atomic collisions*, edited by S. Datz (North Holland, Amsterdam, 1982), p. 79.

[17] D. M. Brink and S. Stringari, Z. Phys. D **15**, 257 (1990).

[18] F. Stienkemeier, J. Higgins, C. Callegari, S. I. Kanorsky, W. E. Ernst, and G. Scoles, Z. Phys. D **38** 253 (1996).

[19] A. Bartelt, J. D. Close, F. Federmann, N. Quaas, and J. P. Toennies, Phys. Rev. Lett. **77**, 3525 (1996).

[20] M. Hartmann, A. Lindinger, J. P. Toennies, and A. F. Vilesov, Chem. Phys. **239**, 139 (1998).

[21] C. Callegari, A. Conjusteau, I. Reinhard, K. K. Lehmann, G. Scoles, and F. Dalfovo, Phys. Rev. Lett. **83**, 5058 (1999).

[22] K. Nauta and R. E. Miller, Phys. Rev. Lett. **82**, 4480 (1999).

[23] K. Nauta and R. E. Miller, J. Chem. Phys. **111**, 3426 (1999).

[24] K. K. Lehmann, Mol. Phys. **97**, 645 (1999).

[25] M. Hartmann, N. Pörtner, B. Sartakov, J. P. Toennies, and A. F. Vilesov, J. Chem. Phys. **110**, 5109 (1999).

[26] A. Yariv, *Quantum Electronics*, Second edition, J. Wiley & Sons, Inc., New York, 1975.

[27] A. Szabo, and R. Kaarli, Phys. Rev. B **44**, 12307 (1991).

[28] J. P. Toennies and A. F. Vilesov, Chem. Phys. Lett. **235**, 596 (1995).

[29] I. Reinhard, C. Callegari, A. Conjusteau, K. K. Lehmann, and G. Scoles, Phys. Rev. Lett. **82**, 5036 (1999).

[30] S. Grebenev, M. Havenith, F. Madeya, J. P. Toennies, and A. F. Vilesov, preprint.

[31] K. Nauta, D. T. Moore, and R. E. Miller, Faraday Discuss. **113**, 261 (1999).

[32] E. L. Knuth, B. Schilling, and J. P. Toennies, in *International Symposium on Rarefied Gas Dynamics (19^{th} : 1994 University of Oxford)* (Oxford University Press, Oxford, 1995), Vol. 19. With our source parameters,

$\langle N \rangle \approx (119.8\,\mathrm{K}/T_\mathrm{n})^{4.584}$

[33] M. Hartmann, PhD Thesis, University of Göttingen, Germany, 1997.

[34] A. I. Burshtein and V. S. Malinovsky, J. Opt. Soc. Am. B, **8**, 1098 (1991).

[35] C. H. Townes and A. L. Schawlow, *Microwave Spectroscopy* (McGraw-Hill, New York, 1955).

[36] S. G. Rautian and I. I. Sobel'man, Sov. Phys. Usp. **9**, 701 (1967).

[37] F. Winther, S. Klee, G. Mellau, S. Naim, L. Mbosei, and A. Fayt, J. Mol. Spectrosc. **175**, 354 (1996).

Appendix A

He–molecule potentials used in Density Functional calculations of the He density distribution in molecule-doped He clusters

A.1 Notation and basic assumptions

All He–molecule potentials are intended to be a function of $\vec{r} = (\rho, z)$, where ρ and z are cylindrical coordinates centered at the center of mass of the given molecule. Atomic units are used by default, although distances are occasionally given in Å ($1\,\text{a.u.} = 0.529177\,\text{Å}$), and polarizabilities in Å^3 ($1\,\text{a.u.} = 0.529177^3\,\text{Å}^3$).

For a given quantity, A, dependent on the orientation relative to a given axis we will often speak of its Legendre components $(A^{(0)}, A^{(2)})$ or of its parallel and perpendicular components $(A_\parallel, A_\perp)$. The formulas relating them are:

$$A^{(0)} = \frac{1}{3}(A_\parallel + 2A_\perp) \tag{A.1}$$

$$A^{(2)} = \frac{2}{3}(A_\parallel - A_\perp) \tag{A.2}$$

and their inverse:

$$A_{\parallel} = A^{(0)} + A^{(2)} \tag{A.3}$$

$$A_{\perp} = A^{(0)} - \frac{A^{(2)}}{2} \tag{A.4}$$

Subscripts i, j are placeholders for unspecified atoms or bonds in a given molecule, as detailed for individual cases. Subscript n is reserved for the long-range dispersion coefficients. Capital subscripts identify specific atoms, bonds, or the entire molecule (so for example $\alpha^{(0)}_{\mathrm{CH}}$ is the isotropic polarizability of a CH bond).

A.2 He–HCN, He–HCCH, He–OCS

He–HCN [1], He–HCCH [2], and He–OCS [3], potentials were available from the literature and have been used without modifications.

A.3 He–$(HCN)_2$

The He–$(HCN)_2$ potential was generated as the superposition of the potential due to two HCN molecules whose centers of mass are separated by 4.44 Å (the equilibrium distance for the gas phase dimer [4]).

A.4 He–HCCCN

The repulsive part of the He–HCCCN potential was calculated in Ref. [5].

We calculated the induction part (interaction between permanent multipoles of HCCCN and induced multipoles of He) at the dipole–dipole level with the

following formula:

$$E_{\mathrm{ind}}(\vec{r}) = \frac{\alpha_{\mathrm{He}}}{2} \sum_{i,j} \frac{3(\vec{\mu}_i\vec{n}_i)(\vec{\mu}_j\vec{n}_i) - \vec{\mu}_i\vec{\mu}_j - 9(\vec{\mu}_i\vec{n}_i)(\vec{\mu}_j\vec{n}_j)(\vec{n}_i\vec{n}_j) + 3(\vec{\mu}_j\vec{n}_j)(\vec{\mu}_i\vec{n}_j)}{|\vec{r}_i|^3|\vec{r}_j|^3} \tag{A.5}$$

where $\alpha_{\mathrm{He}} = 0.204956\,\text{Å}^3$ is the dipole polarizability of He [6], the indices i, j run over the **chemical bonds** of the HCCCN molecule, $\vec{\mu}_i$ are the permanent dipole moments localized at $\vec{d}_i$, the center of each bond; $\vec{r}_i = \vec{r} - \vec{d}_i$ are the vectors from each bond to the He atom, and $\vec{n}_i = \vec{r}_i/|\vec{r}_i|$ their directions. The values of $\vec{\mu}_i$ were calculated from the charge and dipole distributions given in Ref. [5] (model L) under the simplifying assumption that the charge distribution could be approximated by additional dipoles centered on each bond, and that the dipoles located on the atoms could be re-distributed over the bond centers. The approximation is not too crude, particularly when considering that the induction term contributes to the attractive part of the potential much less than the dispersion term does.

The dispersion part was calculated with the formula suggested in [7] and the concept of distributed interaction proposed in [8]:

$$E_{\mathrm{disp}}(\vec{r}) = -\sum_i \sum_{n=6,8} \frac{C_{n,i}}{(r_i)^n} g_n(\rho_i r_i) f(\rho_i r_i) \tag{A.6}$$

where the sum runs over the **atoms** of the HCCCN molecule, r_i are the distances of each atom from the He atom, $C_{n,i}$ are the usual dispersion coefficients that model the long-range interaction between the He atom and each atom in the HCCCN molecule, $g_n(r) = [1 - \exp(-2.1r/n - 0.109r^2/\sqrt{n})]^n$ are universal damping functions, $f(r) = 1 - r^{1.68}\exp(-0.78r)$ is a short-range universal correction factor, and ρ_i are scaling parameters. The angular dependence of the $C_{n,i}$ is accounted for by expanding them in series of even Legendre polynomials: $C_{n,i} = C^{(0)}_{n,i} + C^{(2)}_{n,i} P_2(\cos\theta_i)$ where θ_i is the angle between $\vec{r}_i$ and the molecular axis.

Since in Ref. [5] the distributed polarizabilities are calculated for each atom in the HCCCN molecule, the $C_{6,i}$ could in principle be estimated from London-type formulas, such as the one proposed in Ref. [5], which can, however, lead to large errors. We find it more reliable to scale the $C_{6,i}$ from the accurately known value for the He–HCCH system: $C_6^{(0)} = 18.73\,\text{a.u.}$ (value used in the FORTRAN code of Ref. [2], also in excellent agreement with [9]). First the $C_6^{(0)}$ coefficient for He–HCN is estimated from:

$$C_{6,\text{HCN}}^{(0)} = C_{6,\text{HCCH}}^{(0)} \frac{\alpha_{\text{HCN}}^{(0)}}{\alpha_{\text{HCCH}}^{(0)}} \tag{A.7}$$

where $\alpha_{\text{HCCH}}^{(0)}$, $\alpha_{\text{HCN}}^{(0)}$ are the isotropic dipole polarizabilities of HCCH and HCN [10]. The value so obtained: $C_{6,\text{HCN}}^{(0)} = 14.5\,\text{a.u.}$ lies between the two values reported in Ref. [1], and very close to the value ($13.067\,\text{a.u.}$) used in Ref. [1] to calculate the He–HCN potential that we will use below. Next, $C_{6,i}$ are calculated for each atom as:

$$C_{6,i}^{(0)} = \frac{\alpha_i^{(0)}}{\sum_j \alpha_j^{(0)}} (C_{6,\text{HCCH}}^{(0)} + C_{6,\text{HCN}}^{(0)})(1 - \frac{2\alpha_{\text{H}}^{(0)}}{\alpha_{\text{HCCH}}^{(0)} + \alpha_{\text{HCN}}^{(0)}}) \tag{A.8}$$

$$C_{6,i}^{(2)} = \frac{\alpha_i^{(2)}}{\sum_j \alpha_j^{(0)}} (C_{6,\text{HCCH}}^{(0)} + C_{6,\text{HCN}}^{(0)})(1 - \frac{2\alpha_{\text{H}}^{(0)}}{\alpha_{\text{HCCH}}^{(0)} + \alpha_{\text{HCN}}^{(0)}}) \tag{A.9}$$

where $\alpha_i^{(0)}$, $\alpha_j^{(0)}$, $\alpha_i^{(2)}$ are the polarizabilities calculated in Ref. [5] (i and j run over the atoms in the molecule) and $(1-\frac{2\alpha_{\text{H}}^{(0)}}{\alpha_{\text{HCCH}}^{(0)}+\alpha_{\text{HCN}}^{(0)}})$ is a correction term accounting for the fact that HCCCN has two H atoms less than the combination HCCH+HCN.

Finally the dispersion part of the He–HCCCN potential is fitted to the sum of the dispersion parts of the He–HCN [1] and He–HCCH [2] potentials in the assumption that the concept of transferability of Ref. [8] holds. ρ_i and $C_{8,i}^{(0)}$ are the free parameters of the fit. The HCCH–HCN center of mass distance is set to $2.54\,\text{Å}$, so as to reproduce the bond lengths of HCCCN [11]. In order to limit the

number of fitting parameters, the values of ρ_i (which are loosely related to the size of the corresponding atom) are constrained to be the same for the three C atom and the N atom; also, it is assumed that $C_{8,i}^{(0)}/C_{6,i}^{(0)} = k$, with the same value of k for all the atoms. In addition the fit is only performed along the molecular axis [$\vec{r} = (0, z)$], and $C_8^{(2)}$ is set to 0. Since it is found that k tends to become negligibly small, we set $C_{8,i}^{(0)} = 0$ and only use ρ_i as free parameters of the fit.

The final values of all the parameters used to generate the He–HCCCN potential are reported in Table A.1.

Table A.1: Parameters used in the fit of the attractive part of the He–HCCCN potential

$\rho_C = \rho_N = 1.82594$	$\rho_H = 1.29158$	$C_{8,i}^{(0)} = 0$	$C_{8,i}^{(2)} = 0$

A.5 He–$HCCCH_3$

The cylindrically averaged He–$HCCCH_3$ interaction potential was generated by superposition of the He–HCCH and He–CH_4 [12] potentials, with the HCCH–CH_4 center of mass distance set to 2.06 Å (as dictated by the bond lengths of propyne [13]); the latter potential was first averaged around the $HCCCH_3$ axis by use of standard spherical harmonics algebra. The concepts of transferability and distributed interaction [8] have again been used to remove the repulsive and attractive contributions due to the two extra H atoms, as detailed below.

The repulsive part of the He–CH_4 potential points calculated in [12] has been fitted to a formula:

$$E_{\text{rep}}(\vec{r}) = \sum_i V_{\text{rep},i}(\vec{r}_i) \tag{A.10}$$

where the sum runs over the **atoms** of the CH_4 molecule, $\vec{r_i} = \vec{r} - \vec{d_i}$ are the vectors from atom i to the He atom ($\vec{d_i}$ are the positions of the atoms relative to the molecule center of mass), and V_i is of the form:

$$V_i(\vec{r_i}) = (a_i^{(0)} + a_i^{(1)} \cos\theta_i) r_i^{(b_i^{(0)} + b_i^{(1)} \cos\theta_i)} \exp(-r_i(c_i^{(0)} + c_i^{(1)} \cos\theta_i)) \tag{A.11}$$

where θ_i is the angle between $\vec{r_i}$ and $\vec{d_i}$. By symmetry, $d_C = 0, a_C^{(1)} = 0, b_C^{(1)} = 0, c_C^{(1)} = 0$. Additionally, we have set $b_C^{(0)} = 0$.

The attractive part of the He–CH_4 potential is calculated using formulae (1) through (5) in Ref. [12], at the same coordinate points for which the repulsive part is given. This set of data is then fitted to a formula:

$$E_{\text{attr}}(\vec{r}) = \sum_i V_{\text{attr},i}(\vec{r_i}) \tag{A.12}$$

where this time the sum runs over the **bonds** of the CH_4 molecule; hence $\vec{r_i}$ are the vectors from the bond centers to the He atom, and V_i is of the same form proposed in [12]:

$$V_i(\vec{r}) = \sum_{n=6,8,10} \frac{C_{n,i}}{(r_i)^n} f(r_i) \tag{A.13}$$

where $f(r_i)$ is the damping function used in Ref. [12] (**different** than the one used in Eq. A.6 above):

$$f(r_i) = \begin{cases} \exp[-0.5(D/r_i - 1)^2] & r_i \le D \\ 1 & r_i > D \end{cases} \tag{A.14}$$

The damping parameter D is a free parameter of the fit.

Again the $C_{n,i}$ are expanded in series of (even) Legendre polynomials: $C_{n,i} = C_{n,i}^{(0)} + C_{n,i}^{(2)} P_2(\cos\theta_i)$ where this time θ_i is the angle between $\vec{r_i}$ and the bond orientation. We assume $C_{6,i}^{(0)} = \frac{C_{6,\text{CH}_4}^{(0)}}{4}$, $C_{6,i}^{(2)} = C_{6,i}^{(0)} \frac{\alpha_{\text{CH}}^{(2)}}{\alpha_{\text{CH}}^{(0)}}$, where the CH bond polarizabilities $\alpha_{\text{CH}}^{(0)}, \alpha_{\text{CH}}^{(2)}$ are taken from Ref. [10]. $C_{8,i}^{(0)}$ and $C_{8,i}^{(2)}$ are free parameters

Table A.2: Parameters used in the fit of the He–CH_4 potential

$a_{\rm C}^{(0)} = 28.0263$	$b_{\rm C}^{(0)} = 0$	$c_{\rm C}^{(0)} = 2.38678$
$a_{\rm C}^{(1)} = 0$	$b_{\rm C}^{(1)} = 0$	$c_{\rm C}^{(1)} = 0$
$a_{\rm H}^{(0)} = 5.13516$	$b_{\rm H}^{(0)} = 1.16372$	$c_{\rm H}^{(0)} = 2.30435$
$a_{\rm H}^{(1)} = -2.49552$	$b_{\rm H}^{(1)} = -0.413963$	$c_{\rm H}^{(1)} = -0.171867$
$C_{8,\rm CH}^{(0)} = 45.6966$	$C_{8,\rm CH}^{(2)} = 4.82994$	
$D = 8.48459$		

in the fit, with the constraint that they are the same for each bond. $C_{10,i}^{(0)}$ and $C_{10,i}^{(2)}$ are expressed as a function of $C_{6,i}^{(0)}, C_{8,i}^{(0)}, C_{6,i}^{(2)}, C_{8,i}^{(2)}$ so that the prescription of Ref. [7]: $C_{10} = \frac{49}{40}\frac{(C_8)^2}{C_6}$ holds both in the direction parallel and in the direction perpendicular to the bond.

The final values of all the parameters used to generate the distributed He–CH_4 potential are reported in Table A.2.

The same exact procedure and formulae have been used to separately fit the attractive and repulsive part of the He–HCCH potential [2]; in this case, two sets of dispersion coefficients have been used: one for the CC bond and one for the CH bonds. The $C_{6,i}$ coefficients were determined via:

$$C_{6,i}^{(0)} = \frac{\alpha_i^{(0)}}{\alpha_{\rm HCCH}^{(0)}} C_{6,\rm HCCH}^{(0)} \tag{A.15}$$

$$C_{6,i}^{(2)} = \frac{\alpha_i^{(2)}}{\alpha_i^{(0)}} C_{6,i}^{(0)} \tag{A.16}$$

Also, for the repulsive part two sets of parameters have been used, one for the C atoms and one for the H atoms, but in this case only the isotropic terms (zeroth-order terms in the Legendre polynomial expansion) were kept. The final values of all the parameters used to generate the distributed He–HCCH potential are reported in table A.3.

Table A.3: Parameters used in the fit of the He–HCCH potential

$a_{\rm C}^{(0)} = 22.528$	$b_{\rm C}^{(0)} = 0.828836$	$c_{\rm C}^{(0)} = 2.02288$
$a_{\rm H}^{(0)} = 6.97493$	$b_{\rm H}^{(0)} = 0.823675$	$c_{\rm H}^{(0)} = 2.67694$
$C_{8,\rm CH}^{(0)} = 43.7667$	$C_{8,\rm CH}^{(2)} = 16.2168$	
$C_{8,\rm CC}^{(0)} = 313.956$	$C_{8,\rm CC}^{(2)} = 192.724$	
$D_{\rm H} = 5.74322$	$D_{\rm C} = 8.87103$	

As mentioned in the beginning of this section, the repulsive contributions of the two extra H atoms (one from CH_4 and one from HCCH) that we just determined, have been subtracted from the sum of the He–CH_4 and He–HCCH potentials. The situation is slightly more complicated for the attractive part (that we have localized on the bonds), because in forming $HCCCH_3$ from CH_4 and HCCH, not only two CH bonds are removed but also one CC bond is added. In view of the fact that the perpendicular polarizability of a CC bond is negligibly small, while the parallel one is roughly twice that of a CH bond [10], we decided to subtract from the sum of the He–CH_4 and He–HCCH potentials only the **perpendicular** contribution to the attraction coming from the two CH bonds that were removed.

Bibliography

[1] K. M. Atkins and J. M. Hutson, J. Chem. Phys. **105**, 440 (1996).
Model 1E8 has been used. Due to a typo in table III of this reference the entry for R_{m1} (model 1E8) should read 0.020 Å rather than 0.200 Å. The correct value of 0.020 Å has been used.

[2] R. Moszynsky, P. E. S. Wormer, and A. van der Avoird, J. Chem. Phys. **102**, 8385 (1995). The sign of parameter C_2 in formula (15) of this reference should be negative, for consistency with the FORTRAN code generating the potential (A. van der Avoird, personal communication).

[3] K. Higgins and W. Klemperer, J. Chem. Phys. **110**, 1383 (1999).
We used the unscaled model (see section V of this reference).

[4] K. W. Jucks and R. E. Miller, J. Chem. Phys. **88**, 6059 (1988).

[5] E. M. Cabaleiro-Lago and M. A. Ríos, J. Chem. Phys. **109**, 8398 (1998).

[6] CRC handbook of Chemistry and Physics, 70^{th} edition. CRC Press, Inc., 1990.

[7] C. Douketis, G. Scoles, S. Marchetti, M. Zen, and A. J. Thakkar, J. Chem. Phys. **76**, 3057 (1982).

[8] R. J. Bemish, R. E. Miller, X. Yang, and G. Scoles, J. Chem. Phys. **105**, 10171 (1996).

[9] T. Slee, R. J. LeRoy, and C. E. Chuaqui, Mol. Phys. **77**, 111 (1992).

[10] J. O. Hirschfelder, C. F. Curtiss, and R. B. Bird, Molecular theory of gases and liquids, Whiley and Sons, New York, 1954.

[11] P. Botschwina, M. Horn, S. Seeger, and J. Flügge, Mol. Phys. **78**, 191 (1992).

[12] U. Buck, K. H. Kohl, A. Kohlhase, M. Faubel, and V. Staemmler, Mol. Phys. **55**, 1255 (1985).

[13] A. Bauer, D. Boucher, J. Burie, J. Demaison, and A. Dubrulle, J. Phys. Chem. Ref. Data **8**, 537 (1979).